THE EFFECT OF INTERFACE STRENGTH ON CRACK INTERACTIONS IN THIN FILM COATED SUBSTRATES

by

Can Özcan

B.S., M.E., Boğaziçi University, 2003

Submitted to the Institute for Graduate Studies in
Science and Engineering in partial fulfillment of
the requirements for the degree of
Master of Science

Graduate Program in Mechanical Engineering

Boğaziçi University

2006

ACKNOWLEDGEMENTS

I want to thank Prof. Günay Anlaş at Boğaziçi University and Assist. Prof. Erdem Alaca at Koç University for their guidance and their invaluable time through out my studies. I want to thank Assist. Prof. Nuri Ersoy at Boğaziçi University for his recommendations which made this study to the point and more readable.

I also want to thank Erhan Turan, who is a Ph.D. candidate at Boğaziçi University, for his invaluable help and efforts in publication of this thesis, and more important then all for his time to discuss several technical issues.

In addition to all, I want to thank Dr. Metin Özen for his tolerance on using computer resources and working time at Ozen Engineering, Inc. for completion of this study. I want to thank my former supervisor Şafak Güneş, M.Sc. at Ford Otosan, again for his tolerance to arrange my working time to attend classes at university. It would not be possible for me to pursue without his understanding. I want to thank Ömür Çeteci, M.Sc. at Ford Otosan, for his help in computational tools and time to discuss technical issues through out my studies.

At last, I want to thank to my mother Dr. Nurhayat Filiz for her endless financial and motivational support. It would be very hard without her.

ABSTRACT

THE EFFECT OF INTERFACE STRENGTH ON CRACK INTERACTIONS IN THIN FILM COATED SUBSTRATES

Crack interactions and propagation paths for thin film and substrate systems are studied by using finite element method. 2D edge crack analysis are performed to validate robustness of the method used; results are compared to analytical results available in literature. A script is developed for 2D crack propagation which is embedded into finite element program. 3D edge cracks in thin films are studied; calculated values of stress intensity factors are compared to analytical results from literature and 2D results. Thin film on an elastic substrate with an edge crack is investigated. During the study, stress intensity factors, crack initiation angles and energy release rates are calculated for each case. Crack front profile determination and its effects on crack propagation paths in thin film-substrate systems are studied. Effect of elastic mismatch is examined by performing analysis using several different material properties for thin film and substrate. Interface effect is studied by crack propagation path comparison of parallel edge cracks and an edge crack on a square plate with a corner cut. Interface strength is modeled by elastic perfectly plastic and cohesive zone material models.

ÖZET

ARAYÜZEY DAYANIMININ İNCE FİLM KAPLANMIŞ ORTAMLARDAKİ ÇATLAK ETKİLEŞİMLERİNE ETKİSİ

İnce film kaplanmış ortamlardaki çatlak etkileşimleri ve ilerleme yolları sonlu elemanlar analizi yöntemi kullanılarak çalışılmıştır. Kullanılan methodun dogrulanması için, 2 boyutlu kenar çatlak analizleri yapılmıştır ve sonuçlar literaturdeki analitik çözümler ile karşılaştırılmıştır. 2 boyutta çatlak ilerleme similasyonu için sonlu elemanlar analizi programı için ek bir kod yazılmıştır. Kenar çatlakları 3 boyutlu ince filmlerde çalışılmış; hesaplanan gerilme yoğunluk faktörleri literatürdeki analitik sonuçlarla ve 2 boyutlu çözümler ile karşılaştırılmıştır. Ortam üzerinde bulunan ince filmdeki kenar çatlağı 3 boyutta araştırılmıştır. Araştırma sırasında, gerilme yoğunluk faktörleri, çatlak başlangıç açıları ve enerji açığa çıkma oranları her değişik durum için hesaplanmıştır. Ortam üzerinde bulunan ince filmlerdeki çatlakların ön yüz profilinin bulunması ve profilin çatlak ilerleme yolları üzerindeki etkileri çalışılmıştır. Film ve ortam arasındaki esneklik katsayısı farkının etkileri değişik film ve ortam malzemeleri kullanılarak yapılan analizler ile incelenmiştir. Ara yüzey etkisi, paralel kenar çatlakları ve köşesi kesik kare plaka üzerindeki çatlak ilerleme yolları karşılaştırılarak çalışılmıştır. Arayüzey dayanımı esnek kusursuz sündürülebilir ve yapışkan bölge malzeme modelleri kullanılarak modellenmiştir.

TABLE OF CONTENTS

LIST OF FIGURES

LIST OF TABLES

LIST OF SYMBOLS/ABBREVIATIONS

A	Arbitrary constant
a	Crack length
a_d	Crack depth
B	Arbitrary constant
C	Tangent modulus
d	Length of uniform pressure applied along plate boundaries
E	Elastic Modulus
E_f	Elastic modulus of thin film
E_s	Elastic modulus of substrate
E^*	Plain strain elastic modulus
f_{ij}	Dimensionless function
F	Normalized stress intensity factor
G	Energy release rate
G_{ave}	Average energy release rate along crack front
G_c	Critical energy release rate
G_{sh}	Shear modulus
$G_{sh,f}$	Shear modulus of thin film
$G_{sh,s}$	Shear modulus of substrate
G_{th}	Threshold energy release rate
H	Height of thin film/plate
$_{I,II,III}$	Subscripts denoting mode of loading
K	Stress intensity factor
K_{Ic},K_{IIc}	Fracture toughness
l	Reference length
O(r)	Terms of order r or higher
P	Uniform pressure applied on plate boundaries
p	Crack spacing
r,θ	Polar co-ordinates at the crack tip
t	Plate thickness

t_f	Thickness of thin film
t_s	Thickness of substrate
u,v,w	Displacement along x, y and z directions
x,y,z	Cartesian co-ordinates at the crack tip
V	Crack tip velocity
V_0	Parameter used to fit experimental data for crack tip velocity function
W	Width of thin film/plate
α	Dundur's parameter of elastic mismatch
β	Crack inclination angle
β_D	Dundur's parameter of elastic mismatch
κ	Arbitrary constant
μ	Ratio of stress intensity factors
ν	Poisson's ratio
ν_f	Poisson's ratio of thin film
ν_s	Poisson's ratio of substrate
σ	Uniform stress applied on boundaries of substrate/plate
σ_{ij}	Stress tensor
σ_{xx}	Normal stress along x-direction
σ_y	Yield strength
σ_{yy}	Normal stress along y-direction
σ_{zz}	Normal stress along z-direction
σ_{xy}	Shear stress on x-plane along y-direction
σ_{rr}	Normal stress along radial direction
$\sigma_{\theta\theta}$	Normal stress along tangential direction
$\sigma_{r\theta}$	Shear stress on r-plane along θ direction
θ_c	Crack initiation angle

BISO	Bilinear isotropic hardening
ERR	Energy Release Rate
FEA	Finite Element Analysis
MEMS	Micro Electro Mechanical Systems

MTS	Maximum Tangential Stress
SIF	Stress Intensity Factor

1. INTRODUCTION

Thin film and substrate systems have found significant application area in today's cutting edge technologies, from electronic packages and Micro Electro Mechanical Systems ($MEMS$) to anticorrosion, heat resistive, optical coatings and solar panels. This makes the thin film and substrate systems worth to study both from manufacturing and design point of view.

Microelectronic device technology relies heavily on the ability to fabricate devices that are made of thin films bonded to substrates. Examples of such systems include Gallium Nitride (GaN) and Aluminum Nitrate (AlN) films on Silicon (Si) substrates [1]. Integrated circuits, $MEMS$ packages are usually constructed using Silicon Dioxide (SiO_2) thin films on Si substrates. Ceramic coatings have been used in stationary and aircraft gas turbine engines for over twenty years to improve thermal efficiency and mechanical durability. In these applications the primary function of the coating has been the protection of metallic substrate against heat and corrosion [2].

Micro-fabrication is used for production of systems with dimensions generally not exceeding micro (μm) level, where conventional (machining) techniques cannot be used. Film growth is usually accomplished on a polished Si wafer substrate using several film deposition techniques. Thin film and substrate system is then subjected to doping, lithography, etching, dicing, packaging and other specific processes for different applications.

Films and coatings bonded to substrates often develop in-plane tensile stresses large enough to cause cracking. Stresses are introduced during fabrication, reliability testing and operation. A film deposited at a high temperature and then cooled, will develop biaxial in-plane tensile stresses if the thermal expansion coefficient of the film exceeds that of the substrate [3]. Stress field concentrates at junctions of dissimilar materials, at corners or if there exists a crack, at crack tip.

Crack growth is driven by the thermal excursions and, in some cases, very small amplitude and high frequency cyclic loading [2, 3]. The problem of mud-flat cracking is frequently encountered in case of ceramic coatings and GaN and AlN films on Si substrates used in the microelectronic devices [4]. Investigation of crack propagation and crack interactions in thin film and substrate systems is crucial at this point not only for application reliability but also as a design parameter of the manufactured systems.

The aim of this study is to analyze quasi-static crack growth and crack interactions in thin film coated substrates. The interface effects are considered with the geometry and elastic mismatch of thin film and substrate as the other contributing parameters. An elastic thin film coating with predefined cracks, bonded to a homogeneous elastic substrate under bi-axial loading will be considered. The study will cover both qualitative and quantitative aspects, such as crack interactions and crack propagation path, the influence of film thickness, substrate material property, interface strength and crack spacing.

2. LITERATURE SURVEY

Cracking in thin films depends on the stresses in the film, the toughness of the interface, film and substrate, and the elastic mismatch between the film and substrate materials. A crack that nucleates from a defect in the film or at the edge may propagate along a direction perpendicular to the interface in the film. Such cracks may stop at the interface, penetrate into the substrate, or bifurcate along the interface depending on the material. Cracks that have stopped at the interface may then channel through the film. Channeling cracks need not be confined to the film but may occur for cracks penetrating into the substrate, if the channel bottom is assumed to be a sharp crack front lying on the interface [5]. Cracking in thin film and substrate systems can be grouped into five main sections as listed below:

A *surface crack* is nucleated from a defect and arrested by the interface. Yet the stress is not high enough for the crack to channel trough the film. Since defects are necessarily isolated, one would see stabilized, unconnected slits.

The *channeling process* is unstable: Once activated, it would never arrest until it encounters another channel or and edge. Consequently, a connected channel network would emerge, surrounding islands of the intact film.

Cracks in a film can propagate further to cause *substrate damage*. Such a crack may be stabilized at a certain depth, since the misfit stress is localized in the film. However, the crack may divert to run parallel to the interface, leading to the next cracking pattern.

Substrate spalling is an intriguing phenomenon: The crack selects a path at a certain depth parallel to the interface, governed by mode-II stress intensity factor, K_{II}, equal to zero. This is not a localized failure pattern in that extensive flakes can be spalled off.

Debonding may initiate from edge defects or channel bottoms. The later can be stable: The driving force for initiation is higher than that for the long debond [6]. Commonly observed crack patterns are presented in figure 2.1.

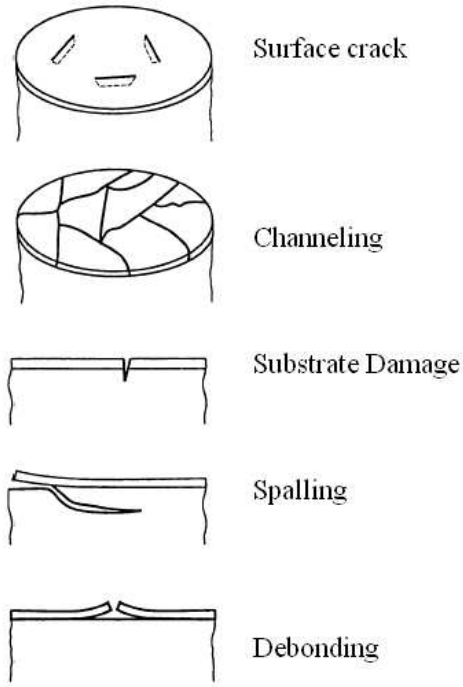

Figure 2.1. Commonly observed crack patterns

The current study is concentrated on channeling cracks of thin film-substrate systems, where the propagating crack path stays in the boundaries of the thin film only, without penetrating into the substrate or interface.

Crack propagation analysis in thin film-substrate systems have been studied by numerous researchers as the topic becomes more important in recently developed electro-mechanical systems. The crack initiation and propagation problem is tried to be solved by using both two dimensional and three dimensional approaches. The techniques include mostly finite element analysis as well as other numerical techniques.

Hutchinson and Suo [6] have contributed to the crack propagation studies by summarizing the previous studies with their own findings. They have restated the crack initiation direction, that cracks in brittle, isotropic, homogeneous materials propagate such that pure mode-I conditions are maintained at the crack tip. And unloaded crack subsequently subject to a combination of mode-I and mode-II will initiate growth by

kinking in a direction such that the advancing tip is in mode-I. A crack in a material with strongly orthotropic fracture properties, or a crack in an interface with a fracture toughness that is distinct from the materials joined across it, can experience either kinking or straight-ahead propagation under mixed mode loading depending on a number of factors, including the relative toughness as associated with the competing directions of advance.

They stated that for all practical purposes, there is no distinction between a criterion for kinking based on maximizing energy release rate or one based on propagation in the direction in which K_{II}=0. Then, Hutchinson and Suo [6] formulated the concept of steady-state cracking: the crack driving force is independent of the crack size in multi layers when the crack grows long compared with the layer thickness. Such a tunneling crack will never be arrested until it meets another crack [7].

The mechanisms and fracture characteristics of cracks in thin film and substrate systems were analyzed by Hutchinson and Suo [6] using mixed mode and interface fracture mechanics. In particular, they considered the energy release rate of straight and kinked cracks, singular crack tip fields for an interfacial crack, crack kinking out of the interface, and the complex interface stress intensity factor as functions of elastic mismatch.

Xia and Hutchinson [3] have studied the crack patterns in thin films by proposing a two-dimensional model of a thin film bonded to a relatively thicker elastic substrate. The effect of an interface is not covered. The study includes simulation of crack propagation paths in thin elastic films. They have presented specific examples for films subject to equal bi-axial residual tensile stress. Single and multiple crack geometries were considered with a view to explain some of the crack patterns which are observed to develop. Tendencies for propagating cracks to remain straight, to attract or repel each other were investigated as a result of crack interaction.

Xia and Hutchinson [3] have studied both straight and curved crack where several geometries were examined to cover most of the crack interaction modes. The straight

crack interactions are of more importance due to its relation to this study. The subsections for the straight crack analysis consider; a single finite crack arrays of parallel semi-infinite cracks; mixed mode interactions among parallel cracks; and interactions between perpendicular cracks.

A pair of aligned film cracks lying side by side a certain distance apart was considered. Stress intensity factors of crack tip were calculated to study the crack interactions. It was shown that there is interaction between cracks when the dimensionless parameter relating the crack spacing to a reference length which is a function of the elastic mismatch is lower than some certain value. Higher values of this dimensionless parameter result in no interaction, where mode-I stress intensity factor, K_I, is nearly identical to the result for the isolated crack and mode-II stress intensity factor is equal to zero. The mode-II stress intensity factor, K_{II}, of the upper, right-hand crack tip is found out to be negative. This implies that a crack advancing from that tip would turn upward. Crack paths evolving from these two starter crack would propagate apart rather than come together. Therefore they have also concluded that, two aligned cracks repel each other [3].

Shenoy et. al. [1] examined the influence of the mismatch in elastic properties on patterns of crack formation in the thin film and substrate systems. Through out their study, the stress intensity factor and crack driving force for growth of a periodic array of cracks in the direction normal to the interface under two-dimensional conditions were determined for any crack depth and any elastic mismatch. It is found that, even for a relatively stiff film material, the stress intensity factor of each crack as a function of crack depth exhibits a local maximum. The driving force for crack extension in the direction parallel to the interface is then determined on the basis of these two-dimensional results, and the equilibrium spacing of crack arrays is estimated for given residual stress.

A descriptive sketch is presented on figure 2.2. As long as the crack depth a_d is less than the film thickness t_f, the stress field at the crack tips is described by the well known square root singularity, the strength of which is called the stress intensity factor

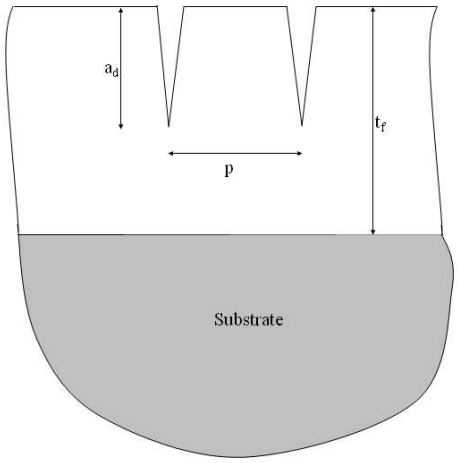

Figure 2.2. Geometry of a periodic array of cracks in a film bonded to a substrate

K. When the crack touches the interface, the singularity is no longer square root but is a more complicated type called the Zak-Williams singularity [8], which depends on the Dundurs parameters[9]. In any case, the Zak-Williams singularity does not affect the calculation of energy release rate right up to $a_d = t_f$ [1].

Shenoy et. al. [1] showed that the driving force for channeling cracks falls with increasing crack density (decreasing crack spacing). For small crack spacing, the driving force for channeling increases initially with crack depth, but attains an almost constant value for greater depth.

The equilibrium crack spacing was found out to be larger for a relatively stiffer film at a given value of the non-dimensional mismatch stress. It is easier to nucleate cracks in a more stiff film (in non-dimensional terms) than in a more compliant film. More compliant films allow for cracks only at larger values of the non-dimensional mismatch stress, with a larger crack density [1].

One of the few fully there-dimensional studies of thin film cracking is that of Nakamura and Kamath [10] who analyzed an isolated finite length through-film crack, including its approach to steady-state propagation wherein conditions at the crack edge become independent of the length of the crack. They have presented the results of a three-dimensional finite element analysis of the mechanics of crack growth and decohesion in a highly compliant film bonded to a rigid substrate.

Their study can be summarized in two main subsections of bonded and debonded thin film analysis. For the bonded film analysis, the film was subjected to residual biaxial tensile stresses induced by the mismatch of thermal expansion coefficients between the film and the substrate during cooling. Initially, the film contains a surface-breaking crack in a plane perpendicular to the film-substrate interface was modeled. In the bonded crack model, further propagation was restricted to occur only along the crack front bounded by the free-surface and the interface. They did not include any nonlinearity in geometry change and material response [10].

The subject thin film was loaded bi-axially with a predefined crack at the edge of the computational model. They have concluded using computational analysis that the stress intensity factor along the leading edge of the crack reaches a steady state value when the crack is about twice the film thickness in the absence of decohesion.

Nakamura and Kamath [10] have found out that there is no difference in crack driving force between long and short cracks in compliant thin films once the crack length is approximately twice the film thickness. This is treated as an equilibrium or steady state crack length. Results show that no further increase in K_I occurs for longer cracks. The crack front shape/profile corresponding to nearly constant K_I across the thickness was determined using an iterative remeshing. This can be generalized to have constant energy release rate G along the crack front. As the crack propagation criteria is based on energy release rate and covers the mixed mode loading case also with three dimensional effects. The steady state crack front shape was determined to be approximately parabolic.

Decohesion was also studied by taking several decohesion region angles (debond opening angle) behind the crack front. These studies showed that the stress intensity factor increases with debond opening angle.

Ambrico and Begley [11] also performed fully three-dimensional finite element analysis to determine energy release rates as a function of defect size for both contained through cracks and edge cracks intersecting free surfaces. The results indicate that

substantially larger defects are required to achieve steady state for edge defects and when the substrate is more compliant than the film. For edge defects, the crack length required to achieve steady state is significantly larger than the film thickness, in contrast to conventional wisdom and of Nakamura and Kamath's study, which assumes steady state is reached when the crack length exceeds only several film thickness.

Ambrico and Begley [11] have used straight crack front in contrast to Nakamura and Kamath. The average energy release rate for straight crack fronts compares favorably with more detailed models that incorporate curved crack fronts. They have concluded that the steady state condition is attained in homogenous elastic systems for center cracks by crack length to film thickness ratio 6 and for edge cracks at ratio of 20. As the compliance of the substrate increases, the crack length required to reach steady state increases. For extremely compliant substrates, steady state for center cracks is reached at crack length to film thickness ratios 40, and even larger lengths for edge cracks [11].

J. Liang et. al. [4] developed the extended finite element method ($XFEM$) to study evolving patterns of multiple cracks, in a brittle thin film bonded to an elastic substrate. The technique has advantage of working with a relatively coarse mesh, and without remeshing during crack propagation. A shear lag model was used to describe the deformation in three dimensions with approximate field equations in two-dimensions. The film is subject to subcritical cracking, obeying a kinematic law that relates the velocity of each crack to its energy release rate, where the relative movement of the propagating cracks is of important.

J. Liang et. al. [4] have studied crack pattern formation in a brittle thin film which is subject to subcritical cracking. The studied thin elastic film was perfectly bonded to an elastic substrate layer of thickness same as that of the film, 1.0 μm. This two layer structure was also bonded to a rigid substrate from the elastic substrate layer. The elastic film was kept at an initial uniform biaxial stress state, where the studied cracks were pre-existing in the thin film. This way the focus of the study falls in between of Nakamura and Kamath, study of thin film fracture on a rigid substrate.

J. Liang et. al.'s study was also different in terms of the modeling, where they have used two dimensional modeling in corporation with an adaptation of a shear lag model to describe the deformation in three dimensions with approximate field equations in two-dimensions. The two-dimensional shear lag model had been studied to study cracks in a thin film bonded to an elastic layer by Xia and Hutchinson [3]. Similar models have been used to study cracking in a brittle film on a viscous underlayer by previous studies of Huang et. al. 2002; Liang et. al., 2003; Lehner et. al., 1981. The film feels a shearing stress on the bottom face from the deformation of the elastic substrate; where the film was modeled as an elastic, isotropic solid under the plane stress conditions [4].

XFEM's advantage is to use discontinuous enrichment functions in the conventional finite element method to account for the presence of cracks, and singular enrichment functions to account for the crack tips. The regular finite element method meshes the geometry of the crack and uses a fine mesh near the crack tip. When the crack grows remeshing is required [4].

Huang et. al. [12] have also applied the extended finite element method ($XFEM$) to compute the steady-state energy release rate of channeling cracks in thin films. The dimensionless driving force for channeling cracks was obtained for different elastic mismatch parameters, crack spacing and thickness ratio between the substrate and the film. The advance in this study over J Liang et. al. is the study of compliant substrates instead of rigid substrates, for which much less information was available from previous studies.

The study by Huang et. al. confined to cracks which are arrested by the film/substrate interface in the direction perpendicular to the interface but advances in the direction parallel to the interface, inside the thin film. In order to maintain equal energy release rate at every point along the crack front, front takes a curved shape. Considering the curved crack front shape, the problem becomes three-dimensional. As it was stated by Nakamura and Kamath, the crack asymptotically reaches the steady state where the entire crack front maintains its shape after the crack length exceeds a

two to three times the film thicknesses. However, this was covering the rigid substrate case only. Just after, Ambrico and Begley [11] showed that the required crack length to achieve the steady state is considerably larger when the substrate is more compliant than the thin film. Huang et. al. did only consider cracks channeling at the steady state, in which case the energy release rate at the channel front can be evaluated using two plane-strain problems, that is, by subtracting the strain energy stored in a unit slice far behind of the front from that far ahead. Both problems can be solved with no knowledge about the shape of the channel front. This study was also different from that of J. Liang et. al. considering finite element modeling. Huang et. al. took two dimensional sections perpendicular to the thin film and substrate system. This is because the substrate is taken to be elastic and as a result needs to be analyzed. However J. Liang et. al. modeled the thin film itself as a two dimensional plain strain computational cell by applying the shear lag model on each node of the film. Substrate was taken to be rigid [12].

For no elastic mismatch, they have showed that a thinner substrate is more compliant and the corresponding energy release rate is larger and the thickness effect becomes indistinguishable for ratios over 20. Thus, in the case of no elastic mismatch, substrate to thin film thickness ratios over 20 is sufficient for a substrate to be considered semi-infinite. It was also shown that for a given thickness ratio, the energy release rate increases as the crack spacing increases and asymptotically approaches the energy release rate for a single channeling crack. Dundurs parameter α is used as a measure of elastic mismatch and is a function of materials stiffness. For the cases with a substrate stiffer than the film ($-1 < \alpha < 0$), the results are similar to that with no elastic mismatch as concluded by Xia and Hutchinson [3] also. For a fixed thickness ratio, the energy release rate increases as the crack spacing increases and asymptotically approaches a value that corresponds to the case with an isolated single crack; the approaching is also slower when the substrate material is more compliant ($\alpha > 0$) [12].

Cracking in thin film systems subject to residual tension was examined by Chakravarthy et. al. [5]. They have modified the solution for the case of a crack tip in the substrate for higher accuracy. The influence of external tensile loads on thin film and

substrate cracking was studied with presence of residual stresses. The solution to the problem of thin film/substrate system under both residual stress and tensile stress due to external loading was mainly based on the approximate superposition scheme. Crack arrest was examined and parameters for determining the possibility of crack arrest were presented.

The energy release rate for a system with an external load can be determined by replacing residual stress value with external load stress value using the energy relation presented by Beuth [9]. This implies that the only effect of the external loading on the energy release rate is to increase the stress in the film. Therefore Chakravarthy et. al. concluded that the behavior of the cracks channeling through the film will be identical to those predicted by Beuth [9] that is the case of thin bonded films in residual tension. This conclusion is important from modeling the cracking in thin film and substrate systems as external loading can be used to model residual stresses also [5].

3. THEORY

3.1. Objective

Main objective of this study is to predict the crack initiation angle; through the crack initiation angle, path of a propagating edge crack in both 2D and 3D media under mixed-mode loading. The effect of the elastic mismatch and interface will be studied by comparing crack propagation paths.

Crack initiation criteria, available in literature can be as: energy based, stress based and strain based criteria. A comprehensive study of crack initiation criteria had been performed by Copur [13].

For the determination of the crack initiation angle in this study, Maximum Tangential Stress (MTS) criterion is used. As it can be deduced from its name, MTS criterion is a stress based crack initiation criteria. The MTS criterion is presented by Erdogan and Sih [14] and used by Liang et. al. [4] through out their study in prediction of the crack interactions on thin film-substrate systems. The criterion will be discussed in the next sections in detail.

Stress intensity factors are needed to determine crack initiation angle via MTS criterion. Therefore accurate calculation of stress intensity factors is essential.

Energy release rate for the crack tip is another important parameter for crack analysis in thin film-substrate systems. The crack propagation path, crack front profile and relative movement of the interacting cracks are effected by the energy release rate. Calculation of the energy release rate will be covered in the proceeding sections with its effects on cracking.

3.2. Calculation of the Stress Intensity Factor

Stress intensity factor is a measure of intensity of near tip stress and strain field under linear elastic conditions. Basically three stress intensity factors can be defined for a three dimensional crack. K_I for opening mode, K_{II} for shearing mode and K_{III} for tearing mode as presented in figure 3.1. Westergaard [15] and Williams [16] were first derived set of solutions for near crack tip stress distributions which would satisfy equilibrium and compatibility equations. They have presented the stress field around a crack tip in 2D with the following equation:

$$\sigma_{ij} = \frac{K}{\sqrt{2\pi r}} f_{ij}(\theta) + ... \tag{3.1}$$

where σ_{ij} is the stress tensor, θ and r are as defined in 3.2, f_{ij} is a dimensionless function and K is the stress intensity factor.

In non-dimensional form the stress intensity factor can be written as;

$$F_I = \frac{K_I}{P\sqrt{\pi a}} \tag{3.2}$$

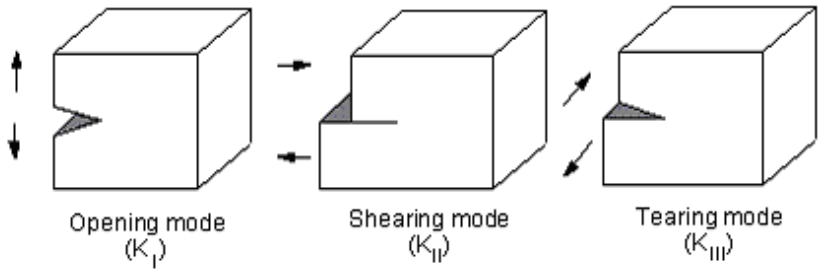

Figure 3.1. The three basic modes of fracture

Computation of the SIFs using finite element analysis requires either a refined mesh around the crack tip or the use of special elements with embedded stress singularity near the crack tip. Finite element analysis with conventional elements near the crack tip always underestimate the sharply rising stress-displacement gradients [17].

Instead of trying to capture the well-known $1/\sqrt{r}$ singular behavior with smaller and smaller elements, Henshell and Shaw [18] and Barsoum [19, 20] introduced a direct method by shifting the mid-side node of an 8-noded isoparametric quadrilateral element to the one-quarter point from the crack tip node. Relocating the mid-side nodes to the one-quarter point achieves the desired $1/\sqrt{r}$ singular behavior.

Stress intensity factors at a crack tip for a linear elastic fracture mechanics analysis are computed using the KCALC command of Ansys [21]. The analysis uses a fit of the nodal displacements in the vicinity of the crack. Including crack tip node, a total of 5 nodes (3 nodes for 2D analysis) are required for stress intensity factor calculation. The nodes around crack tip is shown in figure 3.3. Elements with mid-side nodes are chosen in both 2D (8-noded quadrilateral) and 3D (20-noded brick) analysis and mid-side nodes are located to the one-quarter point achieving the desired square root singularity at the crack tip. Nodes I and J in figure 3.3 are chosen from the quarter-point shifted nodes.

The actual displacements at and near a crack for linear elastic materials are given by Paris and Sih [22]:

$$u = \frac{K_I}{4G_{sh}}\sqrt{\frac{r}{2\pi}}\left((2\kappa-1)cos\frac{\theta}{2} - cos\frac{3\theta}{2}\right) - \frac{K_{II}}{4G_{sh}}\sqrt{\frac{r}{2\pi}}\left((2\kappa+3)sin\frac{\theta}{2} + sin\frac{3\theta}{2}\right) + O(r) \tag{3.3}$$

$$v = \frac{K_I}{4G_{sh}}\sqrt{\frac{r}{2\pi}}\left((2\kappa-1)sin\frac{\theta}{2} - sin\frac{3\theta}{2}\right) - \frac{K_{II}}{4G_{sh}}\sqrt{\frac{r}{2\pi}}\left((2\kappa+3)cos\frac{\theta}{2} + cos\frac{3\theta}{2}\right) + O(r) \tag{3.4}$$

$$w = \frac{2K_{III}}{4G_{sh}}\sqrt{\frac{r}{2\pi}}sin\frac{\theta}{2} + O(r) \tag{3.5}$$

where:

u, v, w : displacements in a local Cartesian coordinate system (as shown in figure 3.2)

r, θ : coordinates in a local cylindrical coordinate system (as shown in figure 3.2)

G_{sh} : shear modulus

K_I, K_{II}, K_{III} : stress intensity factors relating to deformation shapes

$\kappa = 3 - 4\nu$ for plane strain

$\kappa = \frac{3\nu}{1+\nu}$ for plane stress

ν : Poisson's ratio

$0(r)$: = terms of order r or higher

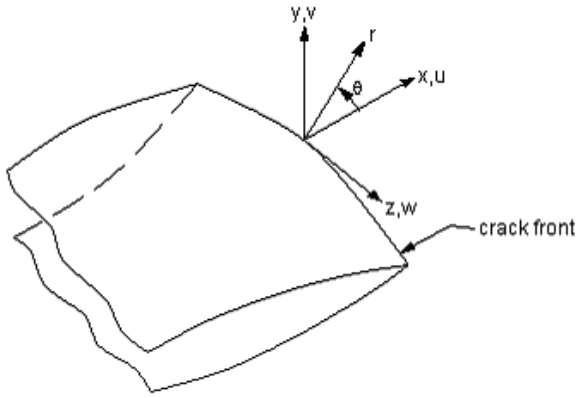

Figure 3.2. Local coordinates measured from a three dimensional crack front

Evaluating displacement equations 3.3 through 3.5 at $\theta = \pm 180.0^o$ and dropping the higher order terms yields:

$$u = \frac{K_{II}}{2G_{sh}}\sqrt{\frac{r}{2\pi}}(1+\kappa) \tag{3.6}$$

$$v = \frac{K_I}{2G_{sh}}\sqrt{\frac{r}{2\pi}}(1+\kappa) \tag{3.7}$$

$$w = \frac{2K_{III}}{G_{sh}}\sqrt{\frac{r}{2\pi}} \tag{3.8}$$

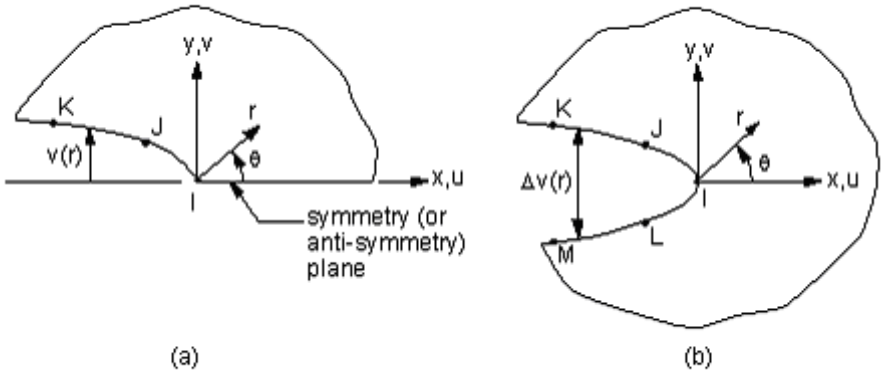

Figure 3.3. Nodes used for the approximate crack tip displacements; (a) Half model, (b) Full model

For models symmetric about the crack plane (half-crack model, (a)), equations 3.6 to 3.8 can be reorganized to give:

$$K_I = \sqrt{2\pi}\frac{2G_{sh}}{1+\kappa}\frac{|v|}{\sqrt{r}} \tag{3.9}$$

$$K_{II} = \sqrt{2\pi}\frac{2G_{sh}}{1+\kappa}\frac{|u|}{\sqrt{r}} \tag{3.10}$$

$$K_{III} = \sqrt{2\pi}2G_{sh}\frac{|v|}{\sqrt{r}} \tag{3.11}$$

and for the case of no symmetry (full-crack model, (b)):

$$K_I = \sqrt{2\pi}\frac{G_{sh}}{1+\kappa}\frac{|\Delta v|}{\sqrt{r}} \tag{3.12}$$

$$K_{II} = \sqrt{2\pi}\frac{G_{sh}}{1+\kappa}\frac{|\Delta u|}{\sqrt{r}} \tag{3.13}$$

$$K_{III} = \sqrt{2\pi}\frac{G_{sh}}{1+\kappa}\frac{|\Delta w|}{\sqrt{r}} \tag{3.14}$$

where Δv,Δu, and Δw are the motions of one crack face with respect to the other.

As the above six equations are similar, one can consider only the first one further. The final factor is $|v|/\sqrt{r}$; which needs to be evaluated based on the nodal displacements and locations. As shown in figure 3.3(a), three points are available. v is normalized so that v at node I is zero. Then A and B can be determined so that;

$$\frac{|v|}{\sqrt{r}} = A + Br \tag{3.15}$$

at points J and K. Next, let r approach 0.0:

$$\lim_{r\to 0}\frac{|v|}{\sqrt{r}} = A \tag{3.16}$$

Thus, equation 3.7 becomes:

$$K_I = \sqrt{2\pi}\frac{2G_{sh}A}{1+\kappa} \tag{3.17}$$

Equations 3.10 through 3.14 are also fit in the same manner.

3.3. Crack Initiation Criteria

3.3.1. MTS Criterion

The MTS criterion, which is proposed by Erdogan and Sih [14], is used to predict the crack initiation angle through out this study. Erdogan and Sih stated that there are two frequently accepted hypotheses for the extension of cracks in a brittle material under slowly applied plane loads:

i. The crack extension starts at its tip in radial direction,
ii. The crack starts in the plane perpendicular to the direction of greatest tension.

These hypotheses entail that the crack will start to grow from the tip in the direction along which the tangential stress $\sigma_{\theta\theta}$ is maximum. The tangential stress $\sigma_{\theta\theta}$ near the crack tip for two dimensional mixed-mode problems, including only the singular term is:

$$\sigma_{\theta\theta} = \frac{1}{\sqrt{2\pi r}} cos\frac{\theta}{2}\left[K_I cos^2\frac{\theta}{2} - \frac{3}{2}K_{II} sin\theta\right] \tag{3.18}$$

Based on these hypotheses that crack propagation initiates along the direction, which corresponds to the maximum tangential stress around the crack tip, we have;

$$\begin{aligned} \frac{\partial\sigma_{\theta\theta}}{\partial\theta} &= 0 \\ \frac{\partial^2\sigma_{\theta\theta}}{\partial\theta^2} &< 0 \end{aligned} \tag{3.19}$$

Taking the derivative of $\sigma_{\theta\theta}$ with respect to θ;

$$\frac{\partial \sigma_{\theta\theta}}{\partial \theta} = \frac{1}{\sqrt{2\pi r}} \left(-\frac{3}{4} cos\frac{\theta}{2} \right) (K_I sin\theta + K_{II}(3cos\theta - 1)) \tag{3.20}$$

Taking the second derivative $\sigma_{\theta\theta}$ with respect to θ;

$$\frac{\partial^2 \sigma_{\theta\theta}}{\partial \theta^2} = \frac{1}{\sqrt{2\pi r}} \left[\left(-\frac{3}{8}(3cos\theta - 1) \right) \left(K_I cos\frac{\theta}{2} - K_{II} sin\frac{\theta}{2} \right) + \frac{9}{4} K_{II}(1 + cos\theta) sin\frac{\theta}{2} \right] \tag{3.21}$$

Using equations 3.19 through 3.21, one can obtain;

$$\left(cos\frac{\theta_c}{2} \right) (K_I sin\theta_c + K_{II}(3cos\theta_c - 1)) = 0 \tag{3.22}$$

$$\frac{3}{8}(1 - 3cos\theta_c) \left(K_I cos\frac{\theta_c}{2} - K_{II} sin\frac{\theta_c}{2} \right) + \frac{9}{4} K_{II}(1 + cos\theta_c) sin\frac{\theta_c}{2} < 0 \tag{3.23}$$

Equation 3.22 has a trivial solution, for which corresponds to the free surface conditions of the crack and a non-trivial solution which corresponds to the angles of maximum tangential stress. The non-trial solution can be found by solving the following equation which is known in the literature as a classical Erdogan and Sih directional criterion.

$$K_I sin\theta_c + K_{II}(3cos\theta_c - 1) = 0 \tag{3.24}$$

Equation 3.24 implies that the crack initiation angle is;

for mode-I, $K_{II} = 0$,

$$K_I sin\theta_c = 0 \Rightarrow \theta_c = 0^0 \tag{3.25}$$

for mode-II, $K_I = 0$,

$$K_{II}(3cos\theta_c - 1) = 0 \Rightarrow \theta_c = 70.5^0 \tag{3.26}$$

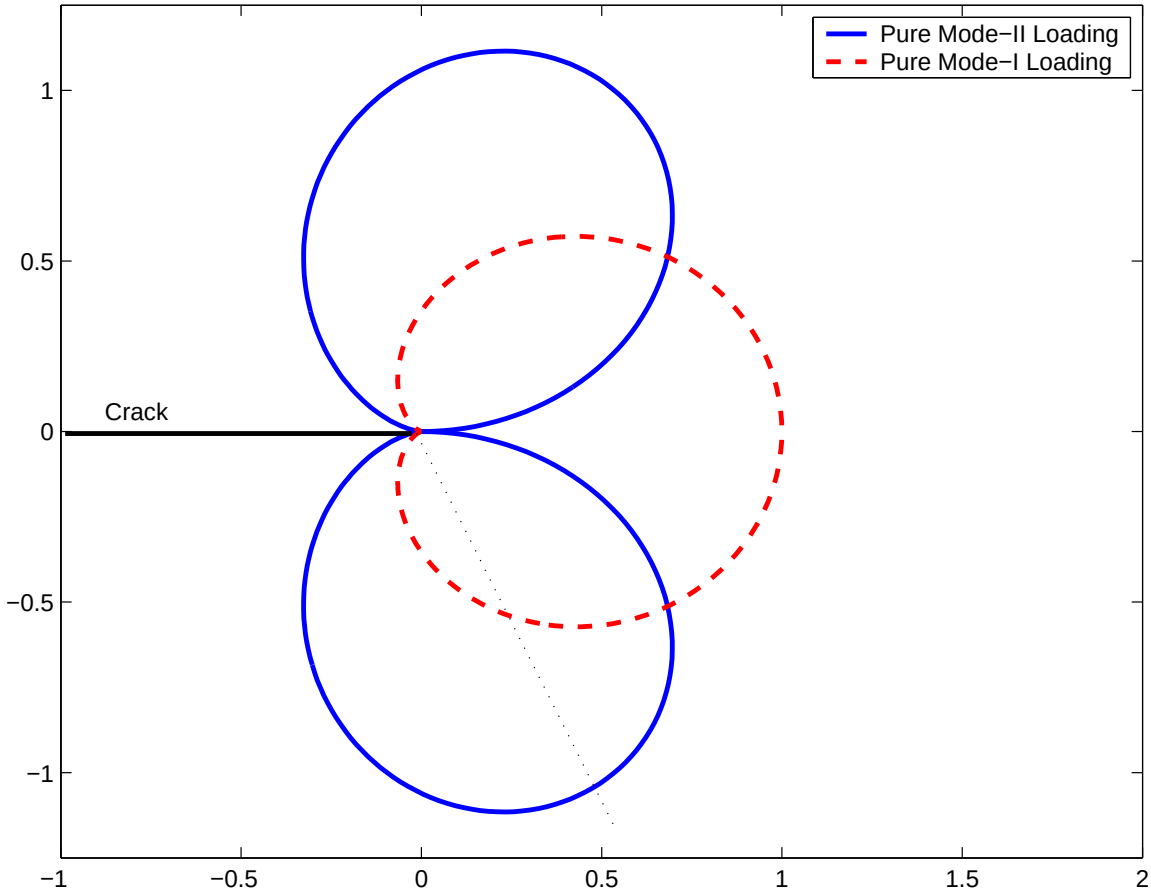

Figure 3.4. Polar plot of tangential stress near the crack tip for mode-I and mode-II

In Figure 3.4, polar plots of dimensionless tangential stresses are given around the crack tip for the two special cases as a function of θ. It can be seen that for pure mode-I ($K_{II} = 0$), the tangential stress has a relative maximum at 0^o. For pure mode-II ($K_I = 0$), tangential stress has two extreme at $\theta = \pm 70.5^o$. The positive one, $\theta = +70.5^o$, is a relative minimum and the negative one, $\theta = -70.5^o$, is a relative maximum.

These extremes can also be observed in Figure 3.5. These angles are the extreme θ_c values of the crack propagation angles.

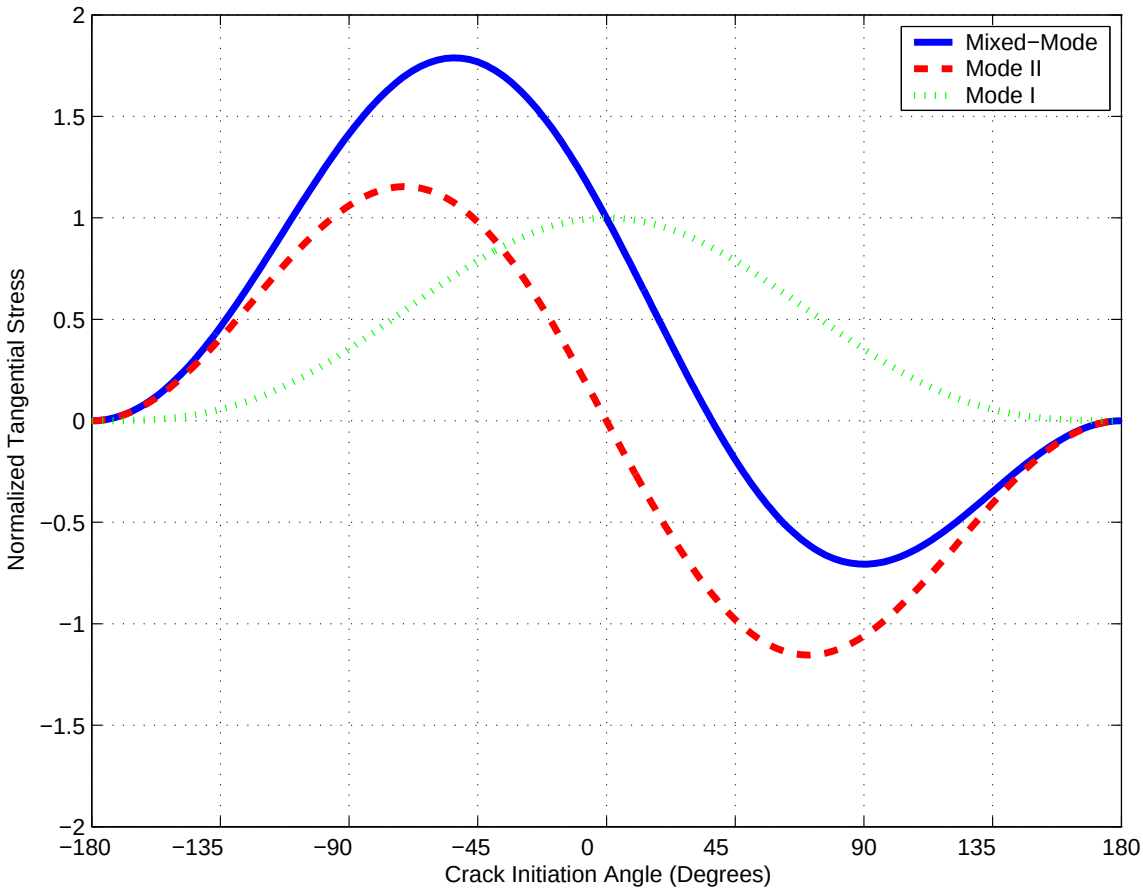

Figure 3.5. Dimensionless tangential stresses versus θ_c for pure mode-I ($K_{II} = 0$), pure mode-II ($K_I = 0$) and mixed-mode ($K_I/K_{II} = 1$)

The mixed mode intermediary values can be found by solving Equation 3.24 for θ_c after some simple trigonometric transformation as;

$$\begin{aligned} K_I sin\theta_c + K_{II}(3cos\theta_c - 1) = 0 \\ 2\left(tan\frac{\theta_c}{2}\right)^2 - \mu\left(tan\frac{\theta_c}{2}\right) = 0 \end{aligned} \tag{3.27}$$

where $\mu = \frac{K_I}{K_{II}}$. Therefore, the crack initiation angle, θ_c, as a function of μ is:

$$\theta_c = 2arctan\left[\frac{\mu}{4} - \frac{1}{4}\sqrt{\mu^2 + 8}\right] \tag{3.28}$$

Erdogan and Sih did also some experiments to check their results. First, they did tensile tests with specimens with inclined central crack. They obtained eight different crack initiation angles, for each crack angle. Secondly, they did eight tests for mode-II loading, and again obtained eight different crack initiation angles. The average results of the experiments were found to be inline with the theoretical values.

3.3.2. Crack Initiation Angle - Determination of the Sign

Sign of the crack initiation angle has vital importance through out this study as it will be used in determining the crack interactions. Based on the calculated values, the propagation paths will be constructed and the fracture parameters will be calculated from to the computational models.

Ansys command KCALC, which calculates the stress intensity factors from crack tip displacements always return positive values. This is because the crack tip displacements and displacement differences respectively for half and full crack models are taken in absolute values through equations 3.9 to 3.14.

As stated in the previous section, the MTS criterion is used to determine the crack initiation, specifically by applying equation 3.28. For every positive value of the stress intensity factors, the parameter μ takes positive values and therefore the θ_c. This condition may lead to erroneous calculations and has to be corrected by calculating the crack initiation angle separately from direct investigation of the tangential stress distribution.

A plate with an ($\beta = 75^o$) degrees inclined edge crack is loaded uniaxially as a test case and the tangential stress($\sigma_{\theta\theta}$) values are plotted in figure 3.6. The crack initiation angle calculated from the MTS criterion is found out to be 6.99^o. Due to finite element modeling the nodes around the crack tip are located at equal and specific positions. This condition does not allow the analyst to check the tangential stress value at calculated crack initiation direction. Instead of calculating tangential stress at crack initiation direction the nearest node values are read and compared to

find the correct sign. The tangential stresses at two angle values which are taken to be the boundary points of an interval including $\pm\theta_c$ are calculated. For the specific test case, 32 elements are present around the crack tip and are 11.25^o apart from each other. The interval $\theta = \pm 11.25^o$ contains both $\theta_c = \pm 6.99^o$. The greater value of tangential stress is found at $\theta_c = -11.25^o$ and due to sinusoidal distribution it can be concluded that the maximum tangential stress is at $\theta_c = -6.99^o$.

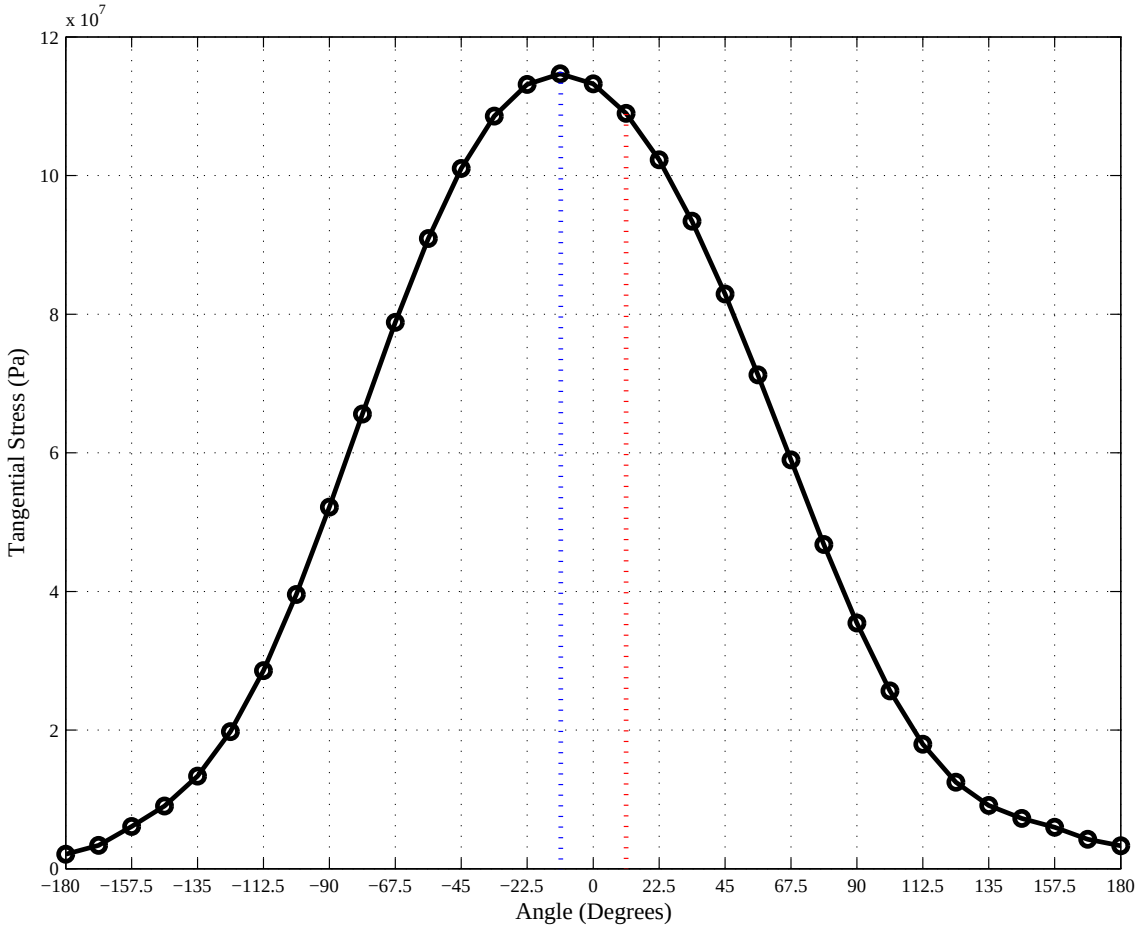

Figure 3.6. Determination of crack initiation angle sign from $\sigma_{\theta\theta}$ distribution

The process is applied for all two dimensional and three dimensional problems. For three dimensional problems, the crack initiation angle is calculated at each element layer with the corresponding sign. Averaged values of crack initiation angle are used for three dimensional models.

3.4. Calculation and Importance of Energy Release Rate

The cracking energy release rate can influence thin film crack interactions and the propagation paths that cracks follow. There are instances, for example, in which a propagating film crack induces an interface debond on one side of the crack tip, causing the crack to follow a curved trajectory [3].

In applying the model to predict a crack propagation path under quasi-static conditions, the path is required to evolve such that pure mode-I conditions ($K_{II} = 0$) are maintained at the tip with the cracking energy release rate is equal to its critical value, $G = G_c$. A preexisting film crack subject to increasing pre-stress may experience combined mode-I and mode-II conditions at its tip. The crack will initiate growth by kinking in the direction for which K_{II} of the putative crack increment vanishes. Once growth has been initiated, however, the path is expected to evolve smoothly such that $K_{II} = 0$ [3].

Quasi-static crack propagation is chosen for determination of the cracking path through out this study. At this point it is necessary to mention about definition of subcritical cracking which most of the brittle solids are subject to. Subcritical cracking, by definition refers to a crack which propagates at a value of energy release rate, G, smaller than the critical mechanical energy release rate, G_c for fast crack growth. The crack remains stationary if G is smaller than the threshold value, G_{th}.

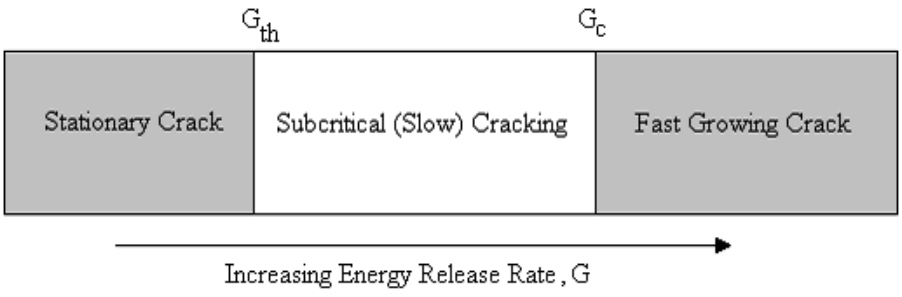

Figure 3.7. Subcritical Cracking

Subcritical cracking is usually due to environmental molecules supporting failure of the atomic bonds at the crack tip. The corrosive molecules lower the surface tension and promote crack growth. This mechanism is generally observed in the failure of optical fibers and in micro electronic devices [4].

The energy release rate G of a steady-state channeling crack can be obtained from a two-dimensional plane strain analysis, even though the process itself is three-dimensional. By considering the energy difference between sections of the film/substrate system far ahead and far behind the crack edge, one can achieve results for the energy release rate averaged over the crack edge in terms of plane strain solutions for cracked films. Solutions for steady-state channeling in films have been presented by Beuth [9], and further relevant mechanics and results are summarized in the review article by Hutchinson and Suo [3].

Beuth's [9] result for the energy release rate averaged over the advancing front of a semi-infinite isolated crack is

$$G = \frac{\pi}{2}\frac{(1-\nu_f^2)t_f\sigma^2}{E_f}g(\alpha,\beta) \tag{3.29}$$

where t_f is the film thickness, E and ν are the Young's modulus and Poisson's ratio of the film, respectively. The Dundur's parameters, α and β_D, characterizing the elastic mismatch between the film and the substrate are

$$\alpha = \frac{E_f^* - E_s^*}{E_f^* + E_s^*} \tag{3.30}$$

$$\beta_D = \frac{1}{2}\frac{G_{sh,f}(1-2\nu_s) - G_{sh,s}(1-2\nu_f)}{G_{sh,f}(1-\nu_s) + G_{sh,s}(1-\nu_f)} \tag{3.31}$$

where E_s and ν_s are the elastic constants of the substrate, respectively, $G_{sh} = \frac{E}{(2(1+\nu))}$ denotes a shear modulus, and $E^* = \frac{E}{(1-\nu^2)}$ is a plane strain tensile modulus. Equation 3.29 applies for cracks extending down to the film/substrate interface with σ as the

uniform pre-stress in the film acting normal to the crack line. The pre-stress has no shear component acting parallel to the crack, and thus mode-I conditions hold on the crack edge. The function $g(\alpha, \beta)$ is presented in figure 3.8 [3].

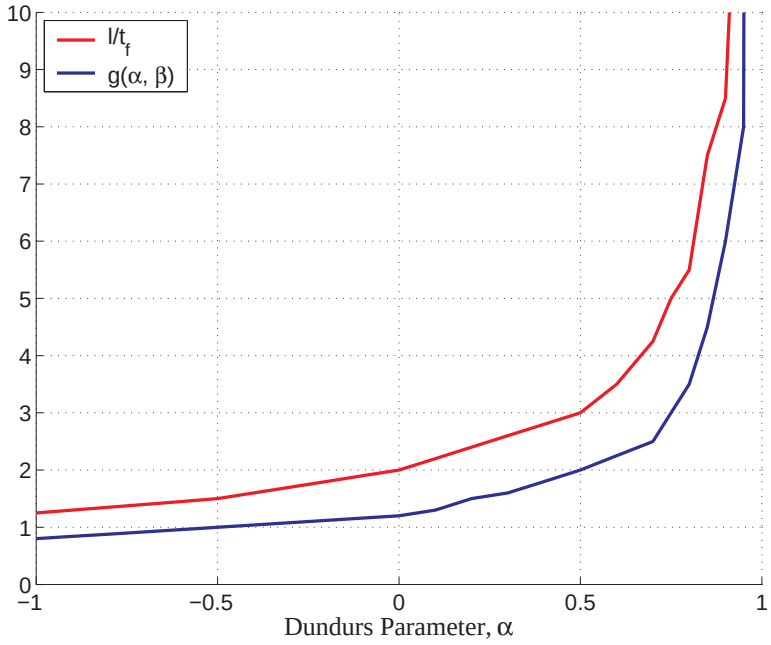

Figure 3.8. Steady state channeling crack in a thin film

With G_c as the mode-I fracture toughness of the film measured in units of energy per unit area, the condition for propagation of an isolated crack across a brittle film is:

$$G = G_c$$

This condition provides a robust condition to design against extensive film cracking because short cracks and crack-like defects will have energy release rates which fall below the steady-state rate. When only small defects are present, film cracks will not begin to propagate until the pre-stress and/or film thickness exceeds the steady-state requirement. On the other hand, the Nakamura and Kamath's study [10] showed that any crack-like defects must be small compared to the film thickness if crack spreading is likely to be postponed to stress/thickness levels significantly above the steady-state requirement. Film cracking is frequently influenced by environmental factors, producing some degree of time-dependence of crack growth. Humidity affects the propagation

of cracks in glasses, and curing and drying are inherently time-dependent [3].

Energy release rate of the crack (energy release per unit of crack advance per unit thickness of film) is related to the stress intensity factors by the classical plane stress relation $G = \frac{(K_I^2+K_{II}^2)}{E}$.

For a general two-dimensional mixed mode problem, the relationship between the energy release rate and the stress intensity factors (SIF) is;

$$G = \frac{K_I^2}{E^*} + \frac{K_{II}^2}{E^*} \tag{3.32}$$

where $E^* = E$ for plane stress problems and $E^* = \frac{E}{(1-\nu^2)}$ for plane strain problems [4].

For mixed-mode general problems, one can use the modified three dimensional version of the energy release rate related to stress intensity factors relation given by Griffith;

$$G = \frac{B}{E}K_I^2 + \frac{B}{E}K_{II}^2 + \frac{(1+\nu)}{E}K_{III}^2 \tag{3.33}$$

where

$B = 1$ for plane strain

$B = 1 - \nu^2$ for plane stress

We will be using the two dimensional plane strain energy release rate equation for 2-D edge crack analysis. The 3-D energy release rate equation for the plane stress will be used for the analysis of edge cracks in thin film-substrate systems as the thin film is more subject to plane stress conditions because of its relative thickness with respect to elastic substrate.

Energy release rate plays a vital role in the crack interactions of more than one propagating cracks. Liang et. al. [4] have considered the time effect in their study by introducing it into the problem by prescribing a crack growth law which is related to energy release rate. A representative relation between the crack tip velocity V and the energy release rate G takes the form:

$$V = V_0 \sinh \left[B \left(\frac{G}{G_{th}} - 1 \right) \right] \tag{3.34}$$

where V_0 and B are parameters to fit experimental data. When $G < G_{th}$, the crack is assumed to be stationary; when $G > G_{th}$ the crack moves with a velocity according to above mentioned crack velocity equation. The time concept was used on a relative basis where quasi-static analysis were carried out without considering the dynamic effects. It is more on a relative basis to determine the relative movement of several crack tips through out an analysis. We will not be investigating two or more cracks propagating at a time, but rather sequential crack propagation [4].

4. 2D EDGE CRACK ANALYSIS

4.1. Background & Analysis

2D analysis of an inclined edge crack on a plate, shown in figure 4.1, is studied in this chapter. Uniaxial loading on top and bottom edges are defined as the only boundary conditions. Crack root is taken at the mid-point of vertical edge. Plain strain assumption is used for element formulation and stress intensity factor calculation. Finite element model is constructed using quadrilaterals with mid-side nodes (8-noded). Crack tip elements are forced to have mid-side nodes located at quarter point location to attain square root singularity. Results are compared to study's of Sih [23], Fett [24, 25] and finite element analysis performed by Copur [13] using FEA package $Marc$.

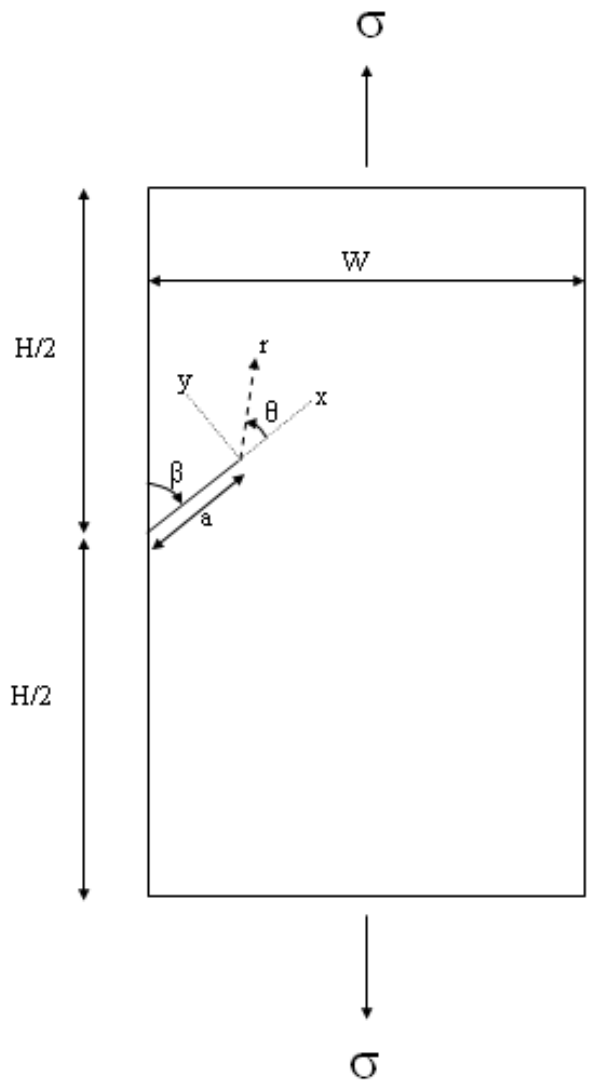

Figure 4.1. 2D edge cracked plate

4.2. Crack Tip Element Size Effect

Initial analysis revealed that the element shape and size around the crack tip plays an important role on the SIF calculations. The number of elements around the crack tip is varied up to 64 for edge crack with $\beta = 90^o$. 16 and 32 element around crack tip models are presented in figure 4.2. FEA analysis are performed. Calculated SIF values are then compared to Franc-2D value to get the effect of the number of elements around the crack tip.

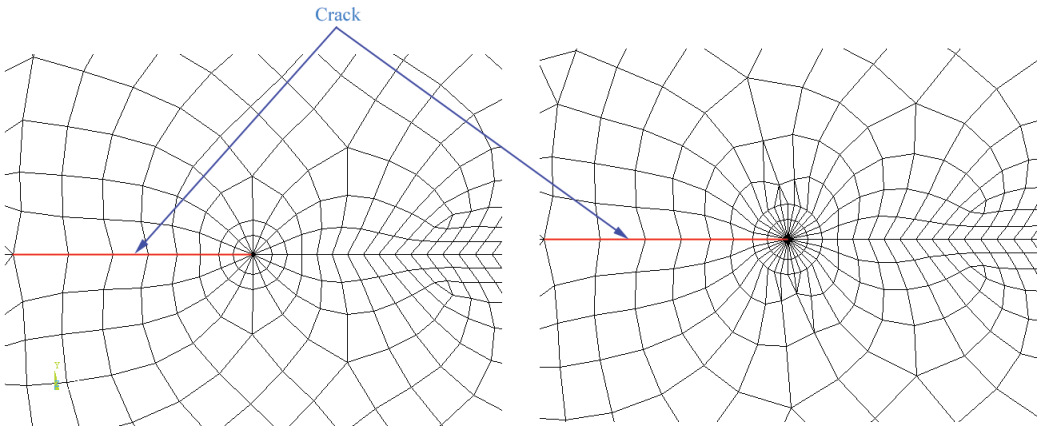

Figure 4.2. Crack tip element number, 16-32 elements around crack tip

Figure 4.3 shows the effect of the element size around the crack tip. The effect is more dominant on mode-II SIF calculations, therefore the crack initiation angle value, which is a function of both K_I and K_{II} is studied. Based on this study the crack tip element number is set to 32 for the following analysis.

4.3. Flat Crack Stress Intensity Factors

Stress intensity factors are calculated for several crack lengths and plate geometry, varying H/W and a/W ratios, in order to compare finite element results with available literature data.

Non-dimensional stress intensity factors calculated using Marc and Ansys are presented in table 4.2. Percentage error values are given with respect to theoretical values of Sih [23]. Error values are found out to be less then 1 percent.

Table 4.1. Effect of crack tip element number on SIF

elements around crack tip	**Ansys (@ 60 deg)**			**Error % wrt. Franc Results**		
	θ	**F - I**	**F - II**	**Tetha**	**F - I**	**F - II**
8	29,97	1,260	0,393	1,59	0,35	2,60
12	30,22	1,262	0,399	0,76	0,14	1,24
16	30,32	1,262	0,401	0,41	0,16	0,78
20	30,38	1,262	0,402	0,23	0,19	0,56
24	30,41	1,261	0,402	0,14	0,21	0,45
28	30,43	1,261	0,402	0,08	0,23	0,38
32	30,44	1,261	0,403	0,05	0,24	0,34
36	30,44	1,261	0,403	0,02	0,24	0,31
40	30,45	1,261	0,403	0,00	0,25	0,29
44	30,45	1,261	0,403	0,01	0,25	0,27
48	30,46	1,261	0,403	0,02	0,25	0,26
52	30,46	1,261	0,403	0,03	0,26	0,25
56	30,46	1,261	0,403	0,04	0,26	0,25
60	30,46	1,261	0,403	0,05	0,26	0,23
64	30,47	1,261	0,403	0,05	0,26	0,23

Table 4.2. Normalized SIF comparison for a 2D plate flat edge crack, for H/W=1 & 2;$\beta = 90^o$

Flat Crack (0 angle)						Ansys				Marc			
Geometry				F - Analytical		F - Numerical		Error %		F - Numerical		Error %	
H/W	a	W	a/W	F - A	F - B	P. Strs	P. Strn	P. Strs	P. Strn	P. Strs	P. Strn	P. Strs	P. Strn
2	15	150	0,1	11,932	11,916	11,900	11,892	0,14%	0,21%	11,870	11,873	0,39%	0,36%
	15	75	0,2	13,755	13,693	13,688	13,677	0,04%	0,12%	13,644	13,646	0,36%	0,34%
	15	50	0,3	16,692	16,612	16,621	16,598	0,05%	0,08%	16,553	16,556	0,36%	0,34%
	20	50	0,4	21,224	21,127	21,140	21,097	0,06%	0,14%	21,053	21,057	0,35%	0,33%
	15	30	0,5	28,341	28,253	28,269	28,248	0,06%	0,02%	28,086	28,096	0,59%	0,56%
	30	50	0,6	40,351	40,335	40,351	40,320	0,04%	0,04%	40,152	40,159	0,46%	0,44%
	35	50	0,7	63,536	63,542	63,564	63,513	0,03%	0,04%	63,210	63,229	0,53%	0,50%
	80	100	0,8	119,473	11,944	119,414	119,309	0,02%	0,11%	119,068	119,088	0,31%	0,30%
Geometry				F - Analytical		F - Numerical		Error %		F - Numerical		Error %	
H/W	a	W	a/W	F - A	F - B	P. Strs	P. Strn	P. Strs	P. Strn	P. Strs	P. Strn	P. Strs	P. Strn
1	15	150	0,1	-	12,218	12,299	12,289	0,66%	0,58%	12,265	12,267	0,38%	0,40%
	15	75	0,2	-	14,882	14,878	14,866	0,03%	0,10%	14,765	14,766	0,79%	0,79%
	15	50	0,3	-	18,477	18,486	18,472	0,05%	0,02%	18,410	18,413	0,36%	0,35%
	20	50	0,4	-	23,279	23,248	23,230	0,13%	0,21%	23,157	23,161	0,53%	0,51%
	15	30	0,5	-	3,012	30,100	30,077	0,07%	0,14%	-	-	-	-
	30	50	0,6	-	41,489	41,506	41,474	0,04%	0,04%	41,312	41,319	0,43%	0,41%
	35	50	0,7	-	64,035	63,954	63,903	0,13%	0,21%	63,604	63,622	0,68%	0,65%
	80	100	0,8	-	119,529	119,424	119,323	0,09%	0,17%	118,996	119,016	0,45%	0,43%

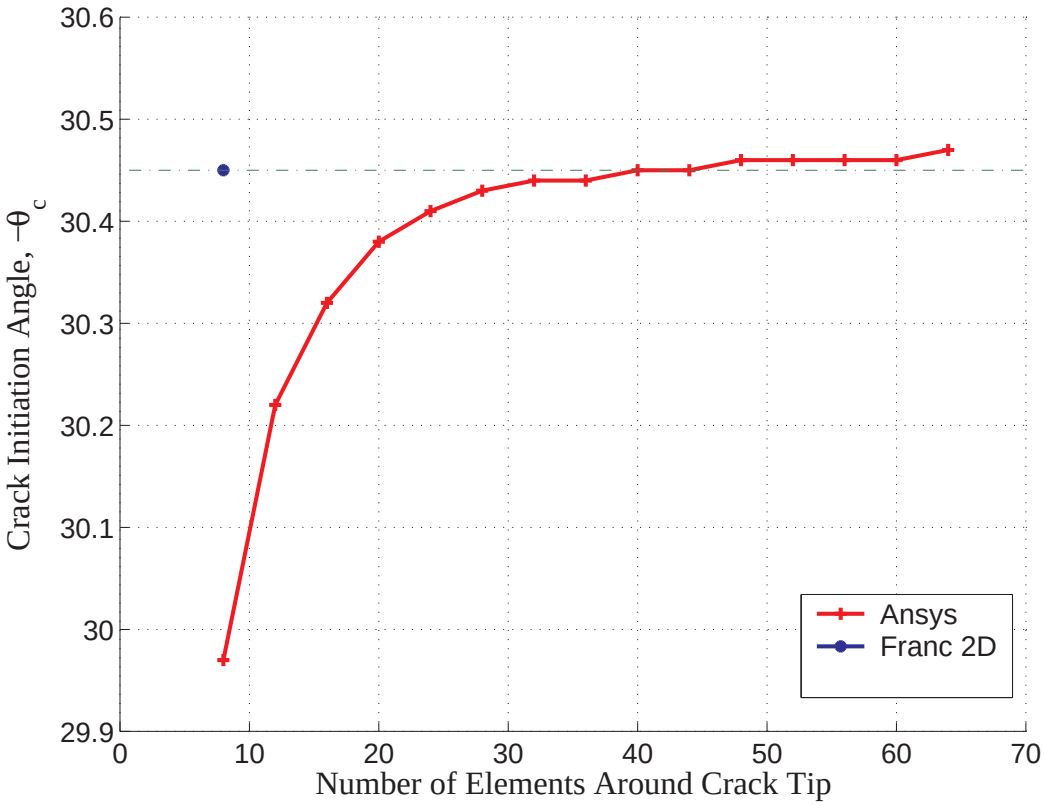

Figure 4.3. Effect of crack tip element number on crack initiation angle, $\theta = 60^o$

4.4. Inclined Crack Stress Intensity Factors

Stress intensity factors for the inclined edge crack is collected for various crack angles (β) and crack lengths (a/W). The calculated results are compared to studies of Fett [24, 25] and Marc. Errors are presented in tables 4.3 and 4.4.

4.5. Crack Initiation Angles

Crack initiation angles for different crack lengths are calculated using MTS criterion, equation 3.28. Calculated values are compared to results presented by Fett [24, 25], and analysis performed using Franc2D and Marc. Tables 4.5 and 4.6 shows the crack initiation angles and the related stress intensity factors.

Table 4.3. Normalized SIF comparison for a 2D plate flat edge crack

a/W	Crack Angle, β	Fett		Ansys		Ansys Error % wrt Fett		Marc		Marc Error % wrt Fett	
		F - I	F - II	F - I	F - II	F - I	F - II	F - I	F - II	F - I	F - II
0,1	90	1,180	0,000	1,187	0,000	0,592%	-	1,185	0,000	0,422%	-
	75	1,120	-	1,127	0,178	0,644%	-	1,127	0,186	0,621%	-
	60	0,970	0,330	0,963	0,319	0,734%	3,399%	0,965	0,330	0,518%	0,000%
	45	0,720	0,385	0,727	0,375	0,995%	2,538%	0,734	0,392	1,907%	1,786%
0,2	90	1,370	0,000	1,366	0,000	0,278%	-	1,366	0,000	0,293%	-
	75	1,290	-	1,287	0,201	0,221%	-	1,287	0,207	0,233%	-
	60	1,180	0,365	1,076	0,353	8,799%	3,306%	1,076	0,357	-	-
	45	0,790	0,410	0,789	0,404	0,181%	1,493%	0,791	0,412	0,126%	0,485%
0,3	90	1,660	0,000	1,660	0,000	0,016%	-	1,658	0,000	0,121%	-
	75	1,550	-	1,548	0,235	0,131%	-	1,548	0,239	0,129%	-
	60	1,260	0,420	1,261	0,403	0,054%	4,033%	1,259	0,415	0,079%	1,205%
	45	0,880	0,450	0,888	0,446	0,964%	0,801%	0,889	0,450	1,012%	0,000%

Table 4.4. Normalized SIF comparison for a 2D plate flat edge crack, Ansys vs Marc

Crack Angle, β	a/W=0.1				a/W=0.2				a/W=0.3			
	Ansys		Marc		Ansys		Marc		Ansys		Marc	
	F - I	F - II	F - I	F - II	F - I	F - II	F - I	F - II	F - I	F - II	F - I	F - II
90^o	1,187	0,000	1,185	0,000	1,366	0,000	1,366	0,000	1,660	0,000	1,658	0
80^o	1,161	0,122	1,160	0,127	1,332	0,137	1,330	0,140	1,610	0,161	1,608	0,162
75^o	1,127	0,178	1,127	0,186	1,287	0,201	1,287	0,207	1,548	0,235	1,548	0,239
70^o	1,082	0,229	1,083	0,242	1,229	0,258	1,229	0,266	1,468	0,299	1,467	0,306
60^o	0,963	0,319	0,965	0,330	1,076	0,353	1,076	0,357	1,261	0,403	1,259	0,416
50^o	0,809	0,357	0,816	0,381	0,887	0,388	0,890	0,405	1,014	0,434	1,015	0,449
45^o	0,727	0,375	0,734	0,392	0,789	0,404	0,791	0,412	0,888	0,446	0,889	0,45
40^o	0,641	0,364	0,649	0,391	0,687	0,388	0,691	0,407	0,763	0,424	0,765	0,44
30^o	0,469	0,331	0,478	0,362	0,492	0,347	0,484	0,367	0,530	0,370	0,532	0,386
20^o	0,307	0,264	0,312	0,295	0,315	0,272	0,305	0,291	0,328	0,283	0,331	0,297
15^o	0,230	0,220	0,229	0,240	0,235	0,225	0,224	0,242	0,242	0,231	0,244	0,244
10^o	0,156	0,171	-	-	0,160	0,172	0,149	0,188	0,164	0,175	0,165	0,186
0^o	-	-	-	-	-	-	-	-	-	-	-	-

Table 4.5. Crack initiation angle for edge crack, Ansys vs Marc

	Marc			Ansys			Difference %		
Crack Angle, β	$\frac{a}{W} = 0.1$	$\frac{a}{W} = 0.2$	$\frac{a}{W} = 0.3$	$\frac{a}{W} = 0.1$	$\frac{a}{W} = 0.2$	$\frac{a}{W} = 0.3$	$\frac{a}{W} = 0.1$	$\frac{a}{W} = 0.2$	$\frac{a}{W} = 0.3$
90^o	0,00	0,00	0,00	0,02	0,03	0,00	-	-	-
80^o	12,25	11,80	11,27	11,78	11,62	11,28	3,84%	1,54%	0,09%
75^o	17,87	17,41	16,81	17,22	16,98	16,55	3,62%	2,49%	1,56%
70^o	23,17	22,53	21,85	22,19	21,94	21,44	4,24%	2,62%	1,89%
60^o	31,90	31,25	31,16	30,73	30,48	29,95	3,66%	2,45%	3,89%
50^o	38,73	38,16	37,54	37,52	37,32	36,86	3,13%	2,19%	1,80%
45^o	41,60	41,05	40,49	40,42	40,20	39,81	2,84%	2,06%	1,69%
40^o	44,06	43,63	43,15	42,84	42,78	42,45	2,76%	1,95%	1,61%
30^o	48,48	48,47	47,68	47,19	47,18	46,97	2,66%	2,66%	1,49%
20^o	52,30	52,37	51,43	50,99	50,83	50,73	2,51%	2,94%	1,37%
15^o	53,79	54,27	53,19	52,54	52,49	52,43	2,32%	3,28%	1,43%
10^o	-	56,34	54,86	54,73	54,87	54,07	-	2,60%	1,45%
0^o	-	-	-	-	-	-	-	-	-

Table 4.6. Crack initiation angle for edge crack, a/W=0.3

Crack Angle, β	**Franc Results**			**Ansys Results**			**Error % wrt. Franc Results**		
	Tetha	**F - I**	**F - II**	**Tetha**	**F - I**	**F - II**	**Tetha**	**F - I**	**F - II**
90^o	0,00	1,639	0,000	0,00	1,661	0,000	-	-	-
80^o	11,59	1,613	0,167	11,54	1,611	0,166	0,43%	0,12%	0,48%
75^o	16,90	1,554	0,242	16,91	1,551	0,241	0,07%	0,22%	0,34%
70^o	21,92	1,472	0,308	21,87	1,470	0,307	0,21%	0,17%	0,37%
60^o	30,45	1,264	0,404	30,47	1,261	0,403	0,05%	0,26%	0,23%
50^o	37,38	1,016	0,446	37,38	1,015	0,445	0,00%	0,08%	0,15%
45^o	40,30	0,890	0,447	40,31	0,888	0,446	0,03%	0,17%	0,14%
40^o	42,96	0,765	0,436	42,94	0,764	0,435	0,04%	0,19%	0,25%
30^o	47,45	0,531	0,380	47,43	0,530	0,379	0,04%	0,19%	0,23%
20^o	51,12	0,329	0,290	51,11	0,329	0,290	0,02%	0,09%	0,04%
15^o	52,75	0,243	0,237	52,72	0,243	0,237	0,05%	0,03%	0,12%
10^o	54,25	0,165	0,178	54,18	0,166	0,178	0,14%	0,53%	0,04%
0^o	-	-	-	-	-	-	-	-	-
Crack Angle, β				**Marc Results**			**Error % wrt. Franc Results**		
				Tetha	**F - I**	**F - II**	**Tetha**	**F - I**	**F - II**
90^o				0,00	1,658	0,000	-	-	-
80^o				11,27	1,605	0,162	2,76%	0,50%	2,99%
75^o				16,81	1,548	0,239	0,53%	0,39%	1,24%
70^o				21,85	1,467	0,306	0,32%	0,34%	0,65%
60^o				31,16	1,259	0,404	2,33%	0,40%	0,00%
50^o				37,54	1,015	0,449	0,43%	0,10%	0,67%
45^o				40,49	0,889	0,450	0,47%	0,11%	0,67%
40^o				43,15	0,765	0,440	0,44%	0,00%	0,92%
30^o				47,68	0,532	0,386	0,48%	0,19%	1,58%
20^o				51,43	0,331	0,297	0,61%	0,61%	2,41%
15^o				53,19	0,244	0,244	0,83%	0,41%	2,95%
10^o				54,86	0,165	0,186	1,12%	0,00%	4,49%
0^o				-	-	-	-	-	-

It is found out that both stress intensity factors and crack initiation angles calculated using *Ansys* well match with available literature of Sih [23] and Fett [24, 25]. Analysis parameters such as mesh density and crack tip element number are taken as in this chapter in following chapters, to guarantee validity of analysis.

4.6. 2D Edge Crack Propagation

Quasi-static, 2D crack propagation analysis of a rectangular plate with edge crack is studied in this section for homogeneous materials. Rectangular plate is loaded uniaxially, in pure mode-I condition. The finite element model is updated at each analysis step by moving crack tip at constant increments. The update process is handled by an automatic script written in *Ansys*.

An edge crack is modeled with 32 singular elements around the crack tip. 8-node quadrilateral elements are used for modeling rectangular plate. Crack initiation direction is determined by using the MTS criterion, as presented by Erdogan and Sih [14].

$$\theta_c = 2arctan\left[\frac{\mu}{4} - \frac{1}{4}\sqrt{\mu^2 + 8}\right] \tag{4.1}$$

θ_c always take negative values as can be seen from the formula for positive μ values ($K_I > 0$ and $K_{II} > 0$). Based on the orientation of the crack angle, the maximum hoop stress direction is determined by checking the stress state on nodes around the crack tip. Using this procedure one can get a reasonable crack propagation path as can be seen in the following figures 4.4 to 4.15.

For all crack inclination angle, β, it is found out that crack follows a straight path, which is perpendicular to loading direction. Therefore, it can be concluded that crack follows path to attain pure mode-I conditions at the crack tip. It is also observed that mode-I stress intensity factor increases exponentially as crack length increases at each propagation step. This reveals that cracking in rectangular plate with an edge crack is an unsteady process. An edge crack which exceeds critical energy release rate or critical SIF propagates until it reaches far free edge.

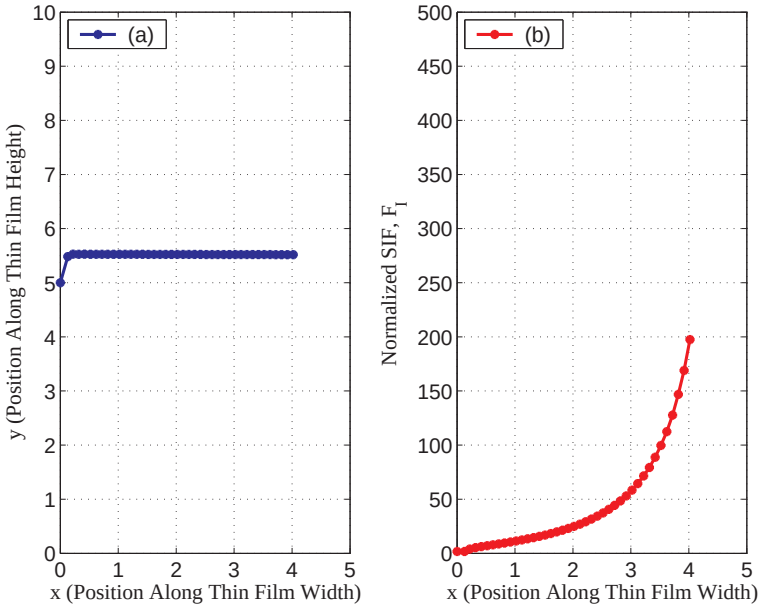

Figure 4.4. (a) Crack propagation path, (b) Stress intensity factor $\beta = 15^o$

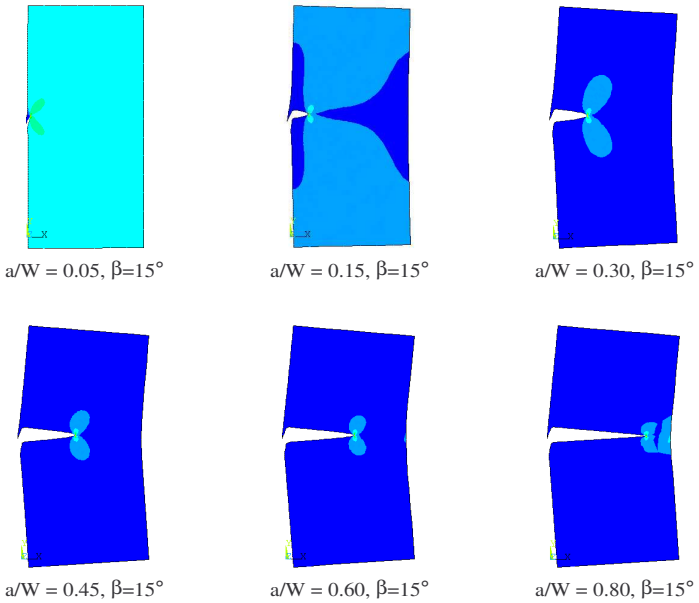

Figure 4.5. Crack propagation steps for Mode - I loading, $\beta = 15^o$

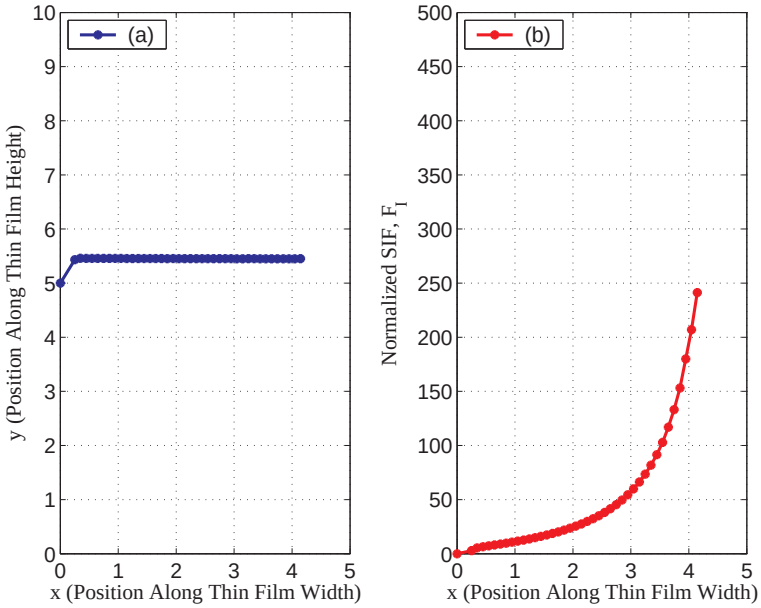

Figure 4.6. (a) Crack propagation path, (b) Stress intensity factor $\beta = 30^o$

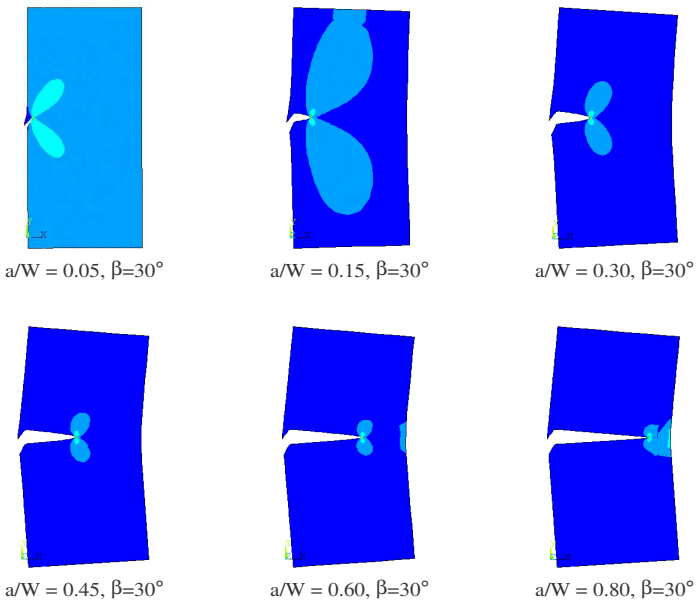

Figure 4.7. Crack propagation steps for Mode - I loading, $\beta = 30^o$

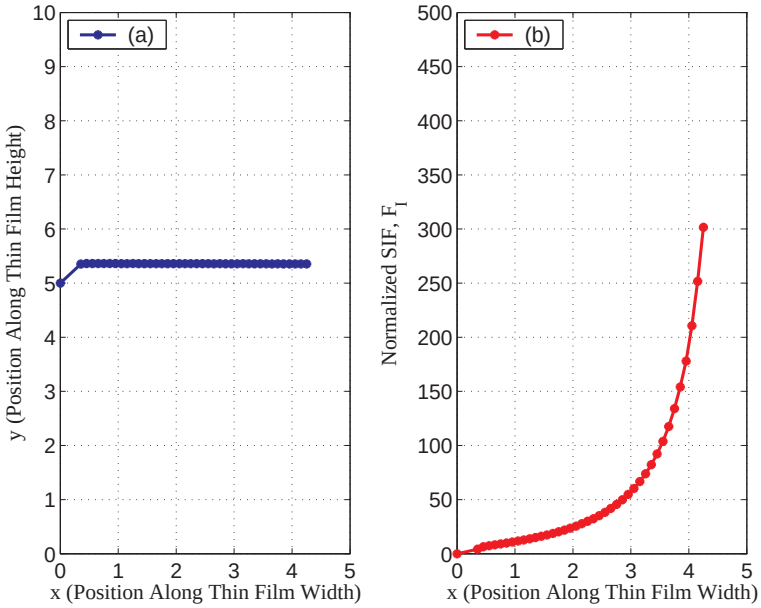

Figure 4.8. (a) Crack propagation path, (b) Stress intensity factor $\beta = 45^o$

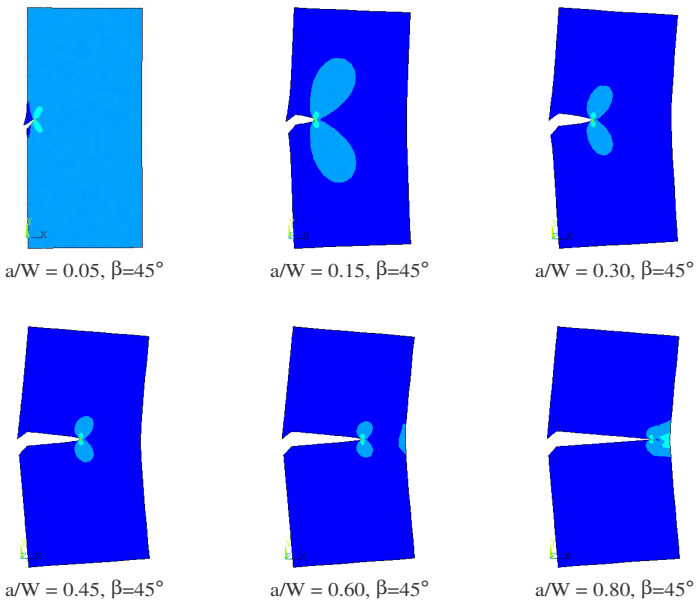

Figure 4.9. Crack propagation steps for Mode - I loading, $\beta = 45^o$

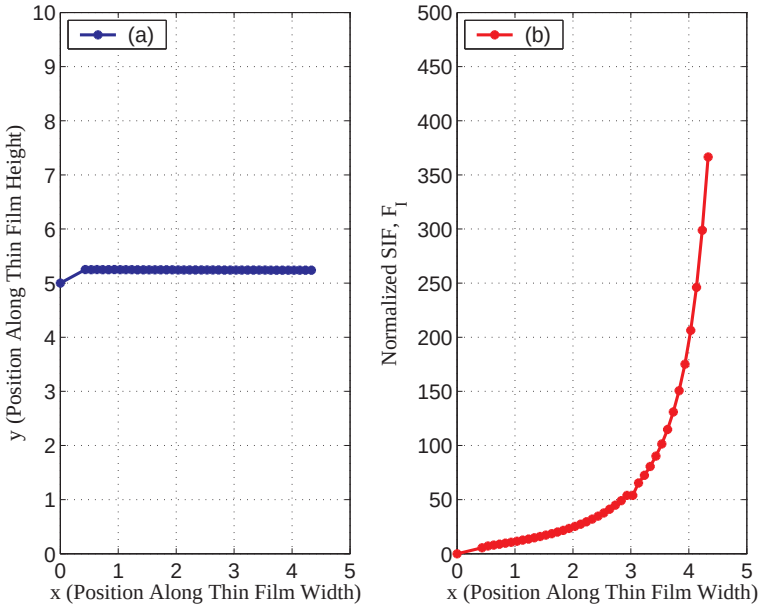

Figure 4.10. (a) Crack propagation path, (b) Stress intensity factor $\beta = 60^o$

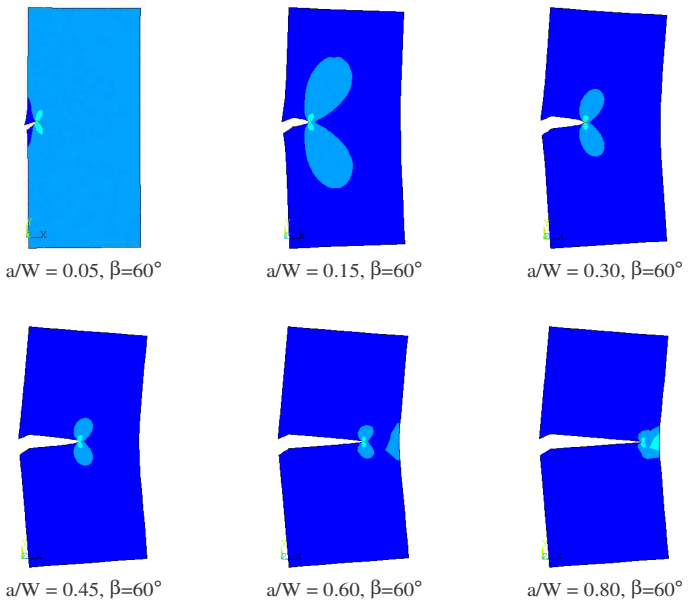

Figure 4.11. Crack propagation steps for Mode - I loading, $\beta = 60^o$

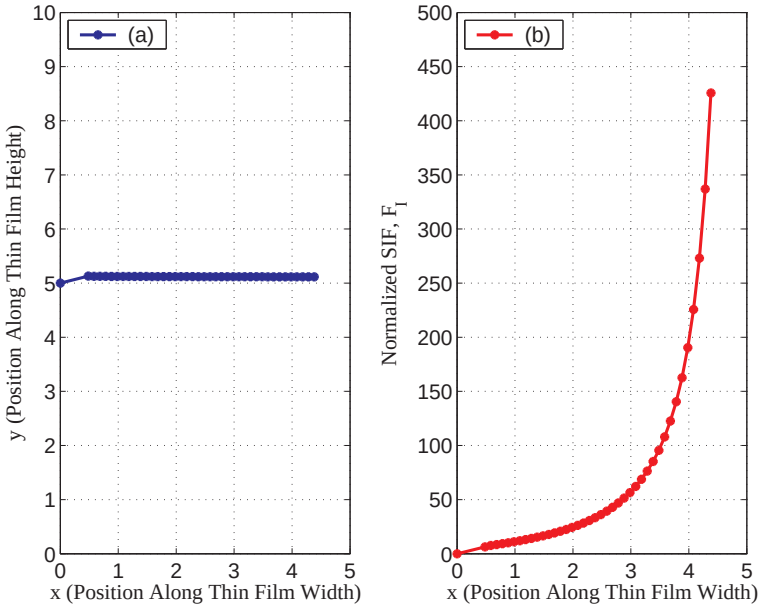

Figure 4.12. (a) Crack propagation path, (b) Stress intensity factor $\beta = 75^o$

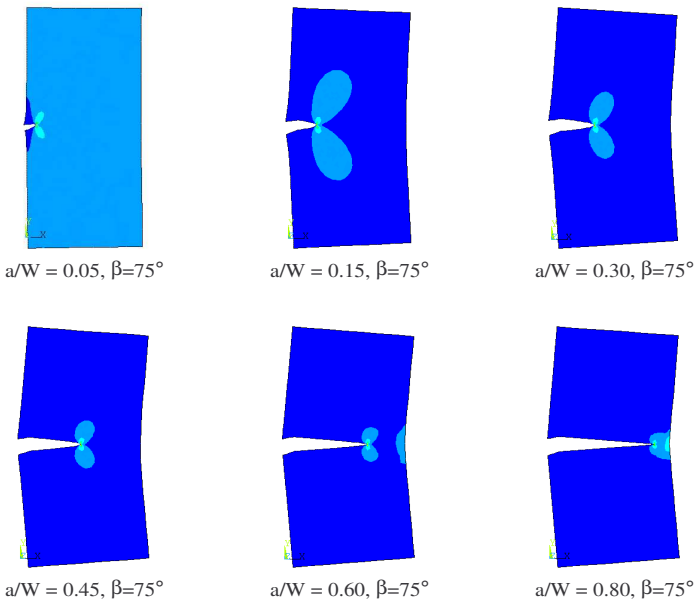

Figure 4.13. Crack propagation steps for Mode - I loading, $\beta = 75^o$

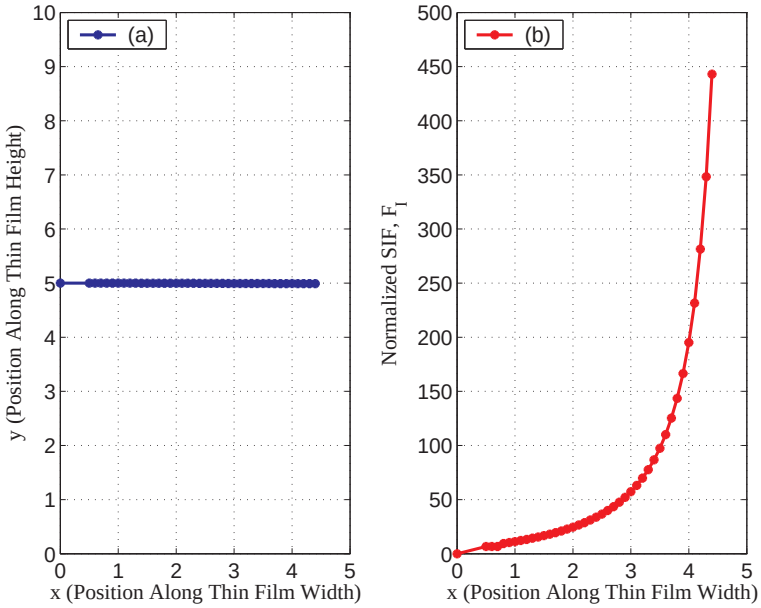

Figure 4.14. (a) Crack propagation path, (b) Stress intensity factor $\beta = 90^o$

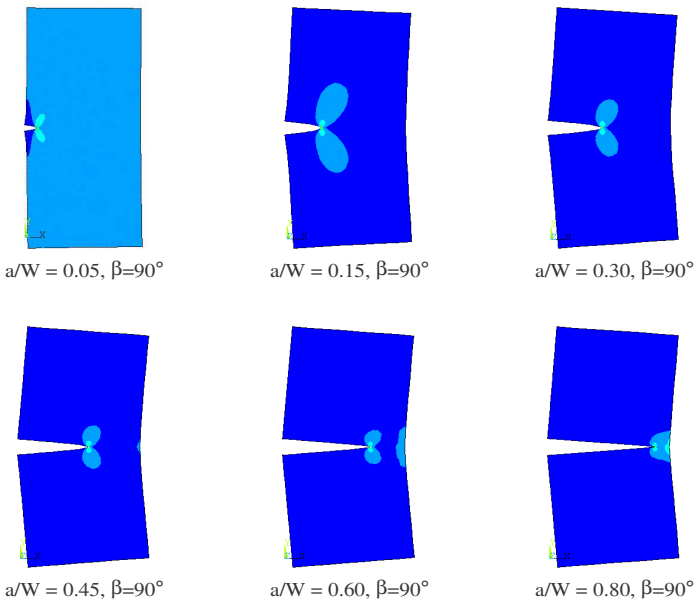

Figure 4.15. Crack propagation steps for Mode - I loading, $\beta = 90^o$

5. 3D EDGE CRACK ANALYSIS IN A THIN FILM

5.1. Background & Analysis

Edge crack in a rectangular plate is studied with 3D modeling, assuming straight crack front in this chapter. Geometry is presented in figure 5.1. Edge crack root is positioned at mid-point of vertical face. Constant pressure load is defined on top and bottom faces as only boundary conditions. Stress intensity factors, crack initiation angles are calculated at each element layer through thickness direction. Results are compared to available literature by Murakami [26] and 2D values presented by Fett [24, 25].

All the numerical analysis in this chapter are performed with 8 elements along film thickness direction of the 3D rectangular plate. The mesh density around the crack tip is chosen as in the case of the formerly performed 2D analysis, where finite element model was confirmed with the literature values. For 3D analysis 20 node, brick elements with mid-side nodes were used with the same pattern at each thickness level. Plain strain conditions is assumed when stress intensity factors are calculated. Validity of plain strain assumption is discussed at the end of this chapter.

5.2. Straight Crack Analysis

An edge cracked plate with $\beta = 90^o$, is loaded in tension and fracture parameters are calculated in this section. Straight crack front is assumed at each analysis stage and plain strain assumption is employed for stress intensity factor calculations. The stress intensity factors along crack front for straight crack ($\beta = 0^o$) shows a self-similar trend for all cases. The mode-I stress intensity factor, F_I, makes a peak at the mid-point of the plate, where it drops sharply on the edges. This phenomenon is seen more drastically in relatively thin plates as expected where the plane stress effects are more dominant. Same phenomenon is also presented by Liu et. al. [27] for straight crack fronts using Zencrack software.

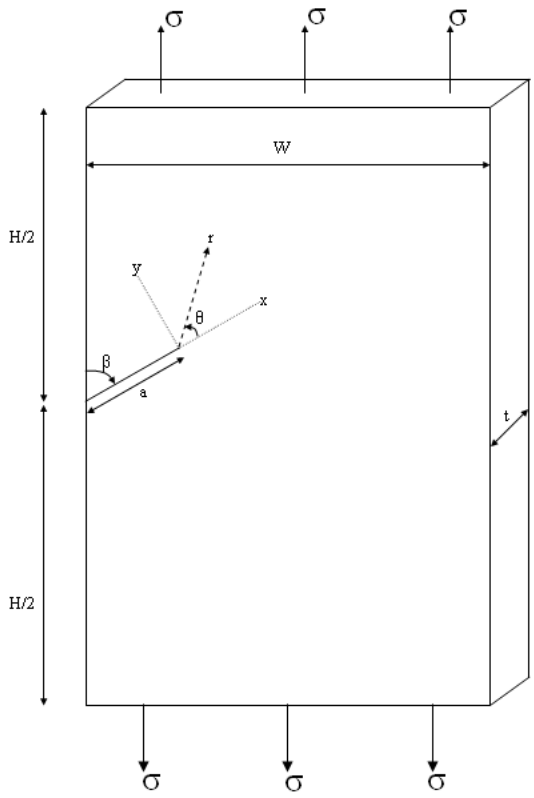

Figure 5.1. 3D edge cracked thin film

This phenomenon can be explained by edge effects and plain strain assumption validity around crack edges near to free surfaces. High longitudinal stresses set up at a distance r ahead of the crack root cause the material there to extend elastically and consequently to contract because of the Poisson effect. This contraction is greatest near the crack root (figure 5.2) where longitudinal stresses are highest. Crack faces does not want to contract because there are no longitudinal stresses acting across it; all of these are concentrated ahead of the root [28]. Therefore the crack opening at the edges are slightly smaller than in the middle of the crack front due to contraction at the edges. As mode-I stress intensity factor is calculated from the crack opening displacement, it decreases at the edges. All the related analysis data are presented in figures 5.3 through 5.6.

The average stress intensity factors asymptotically approaches the plane strain values for increased film thicknesses as expected. Behavior of the stress intensity factor can be seen in figure 5.7.

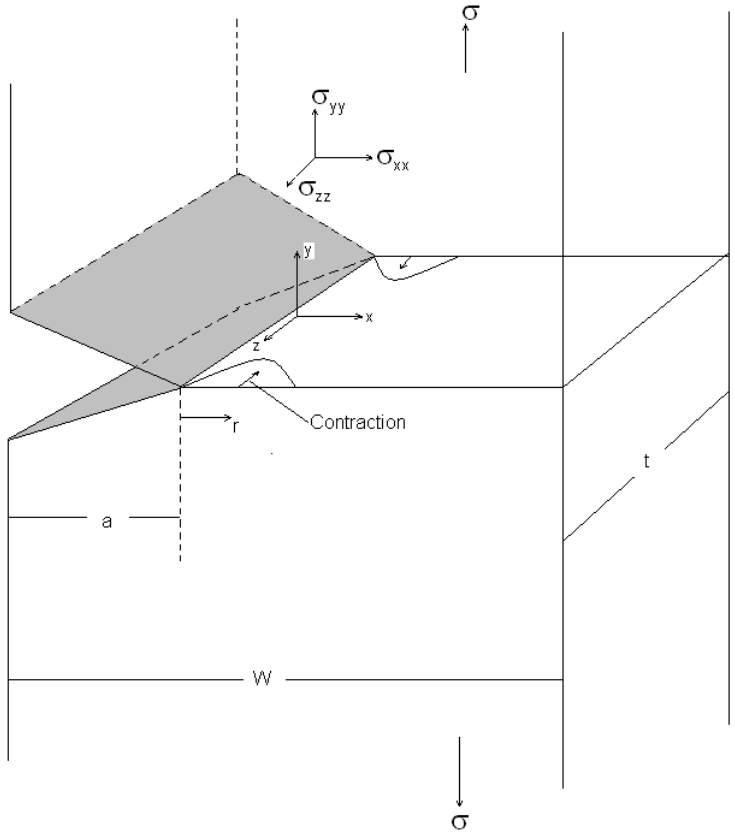

Figure 5.2. Transverse contractions that occur near the tip of a notch in a thick plate

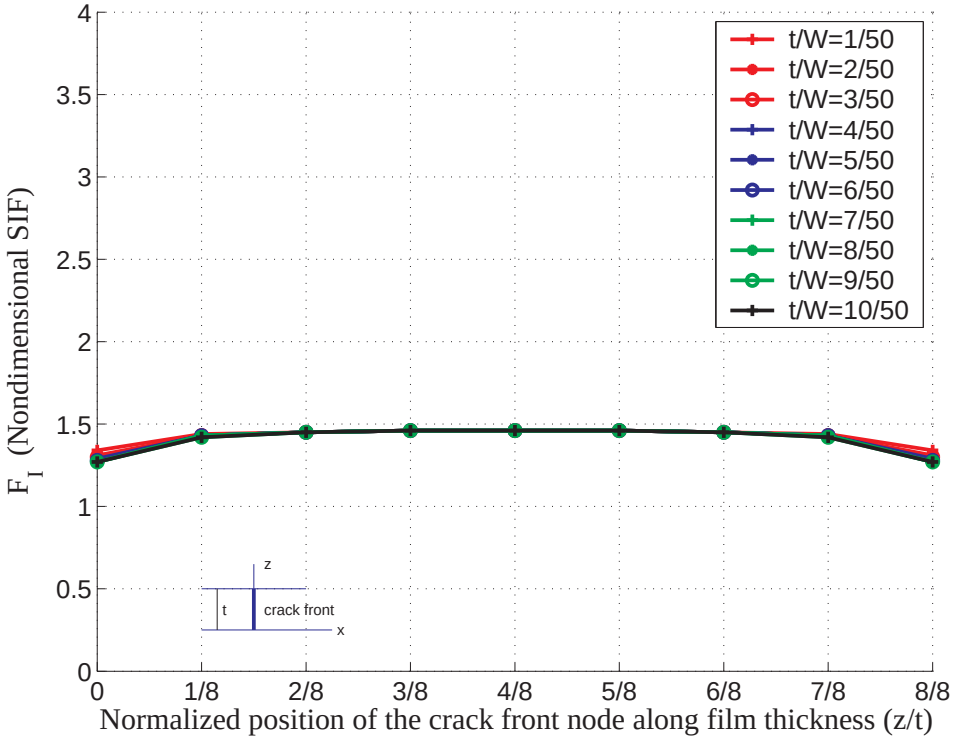

Figure 5.3. Non-dimensional SIF along film thickness, a/W=0.2

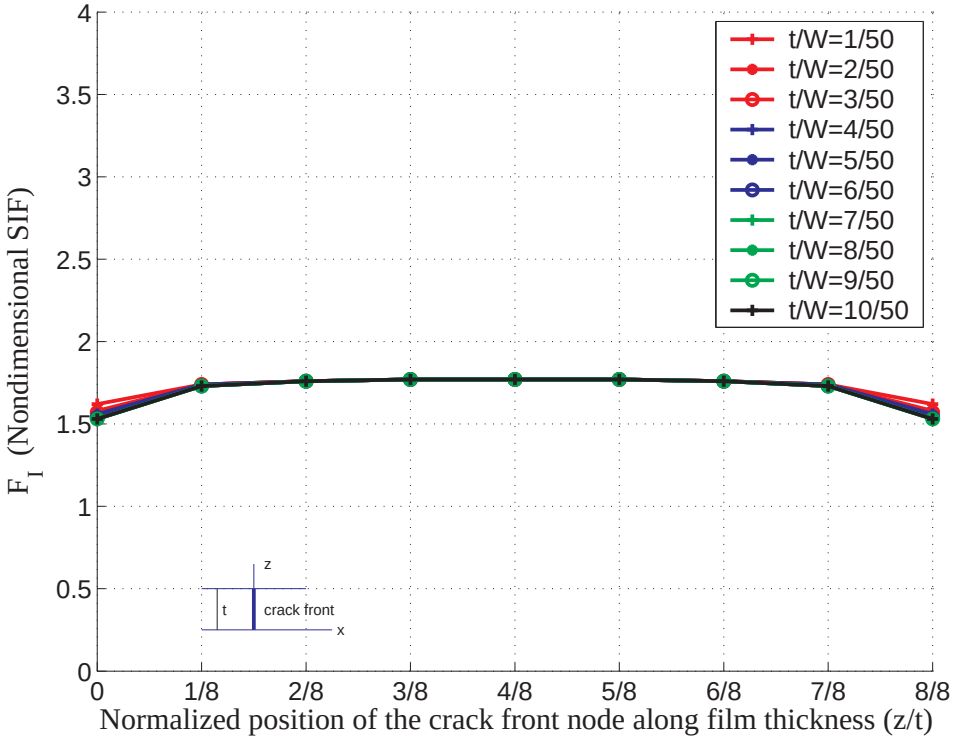

Figure 5.4. Non-dimensional SIF along film thickness, a/W=0.3

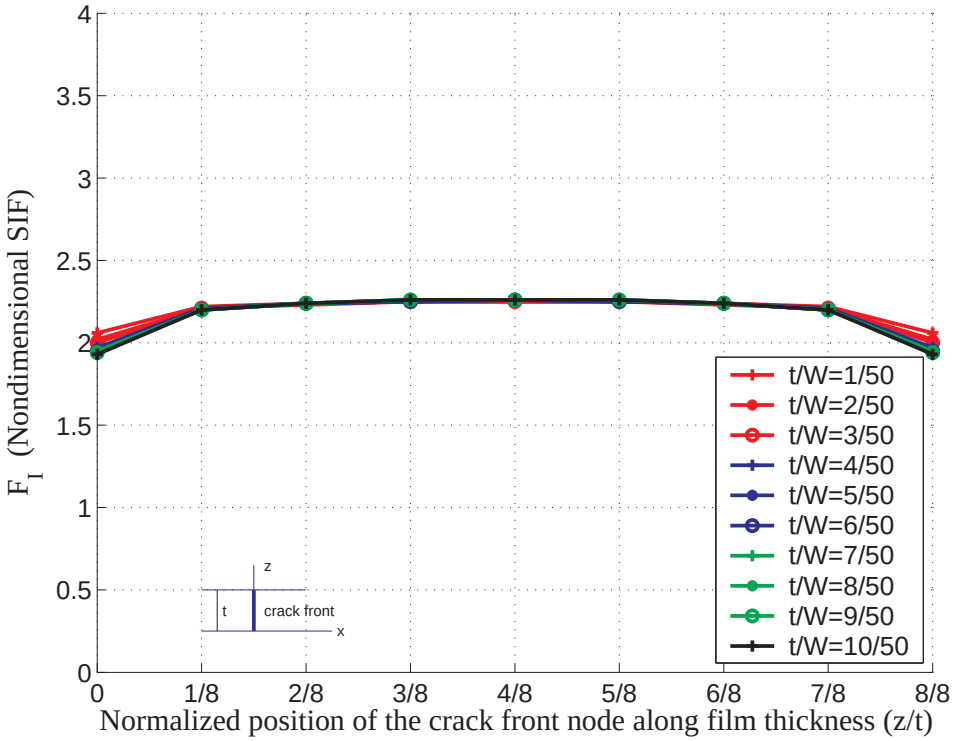

Figure 5.5. Non-dimensional SIF along film thickness, a/W=0.4

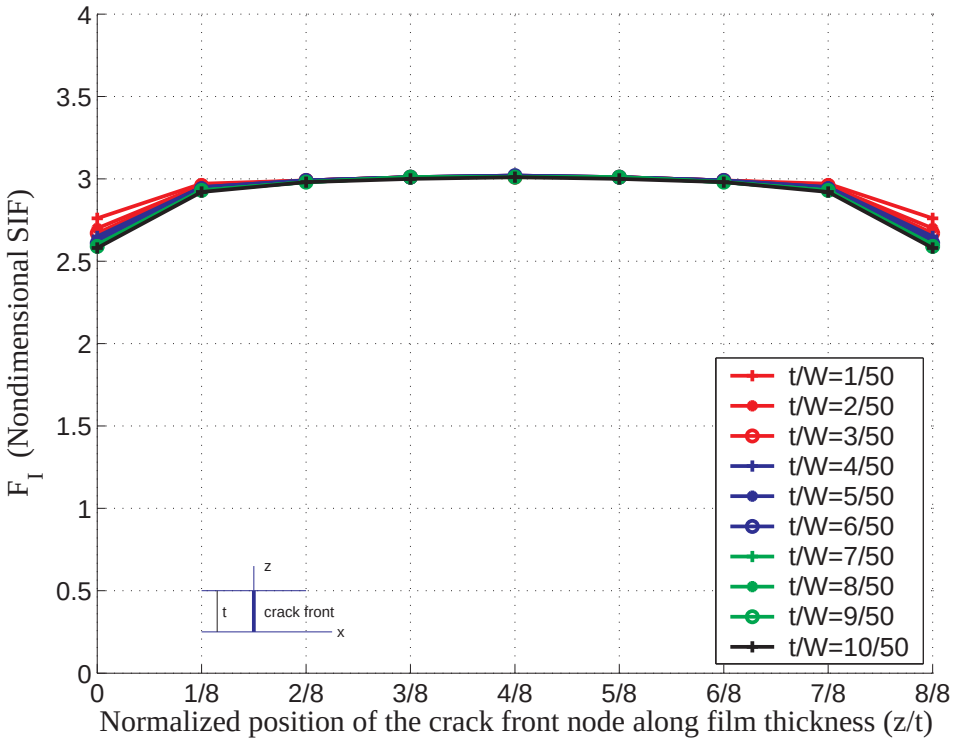

Figure 5.6. Non-dimensional SIF along film thickness, a/W=0.5

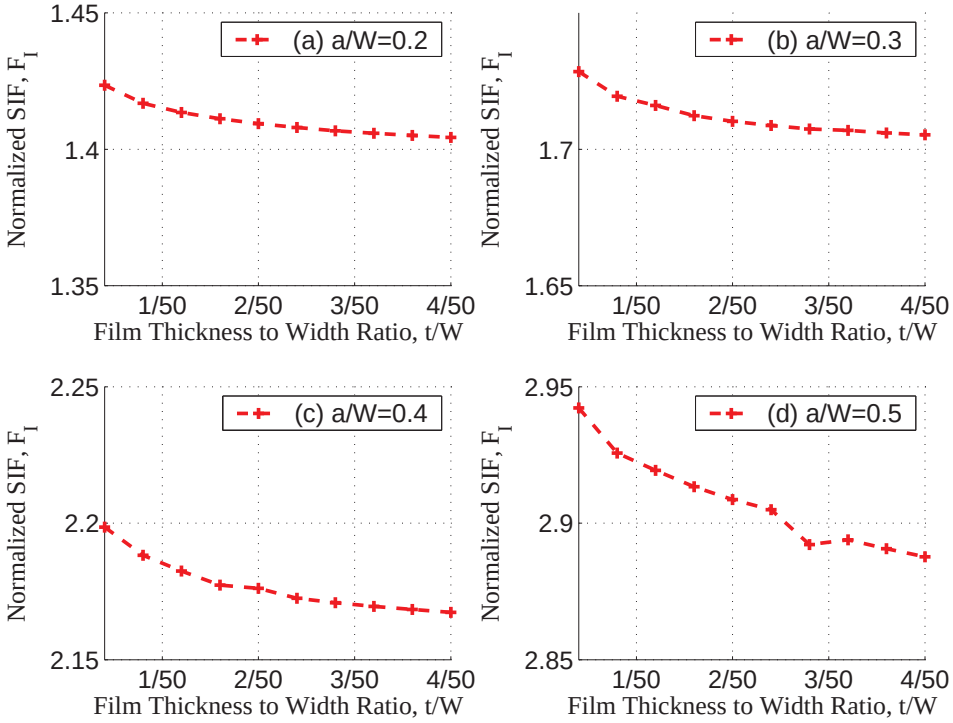

Figure 5.7. Non dimensional SIF (F_I) vs film thickness

2D calculated values match well with the 3D in increased thickness values, where the 2D plain strain value and the 3D value cross at t/W=50/50=1 value as can be checked from the fitted logarithmic function. Numerical calculations are carried out for 4 different crack lengths, namely a/W=0.2, 0.3, 0.4 and 0.5 where the height to width ratio is kept constant at H/W=2. Thickness of the plate is varied from t/W=1/50 to t/W=10/50 in 10 increments. Average stress intensity factors for varying film thicknesses are presented in figures 5.8 to 5.11.

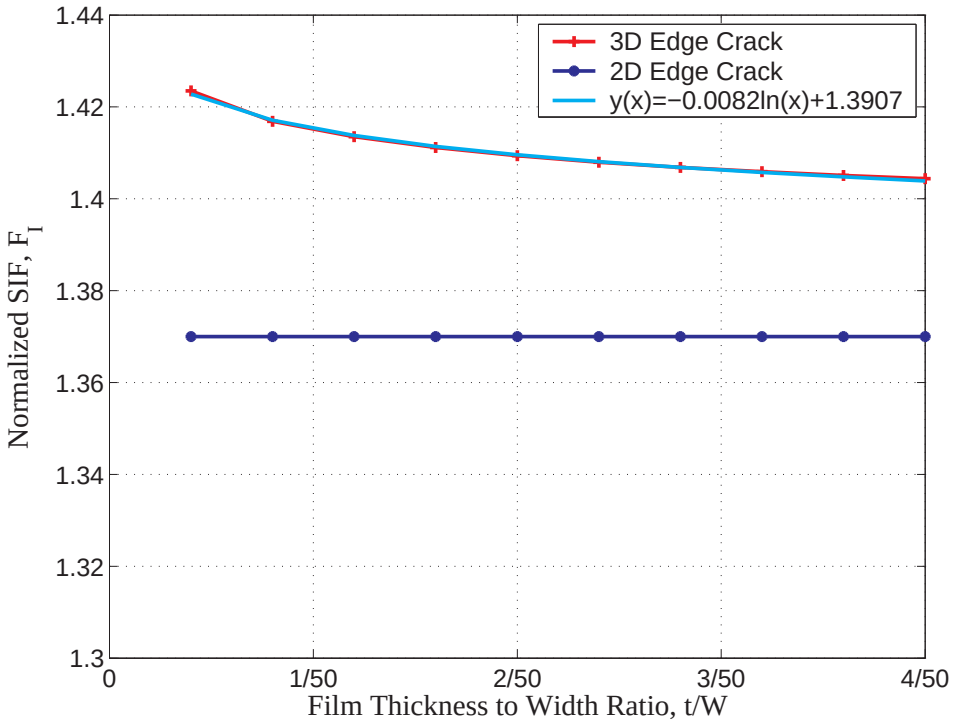

Figure 5.8. Average F_I vs film thickness, a/W=0.2

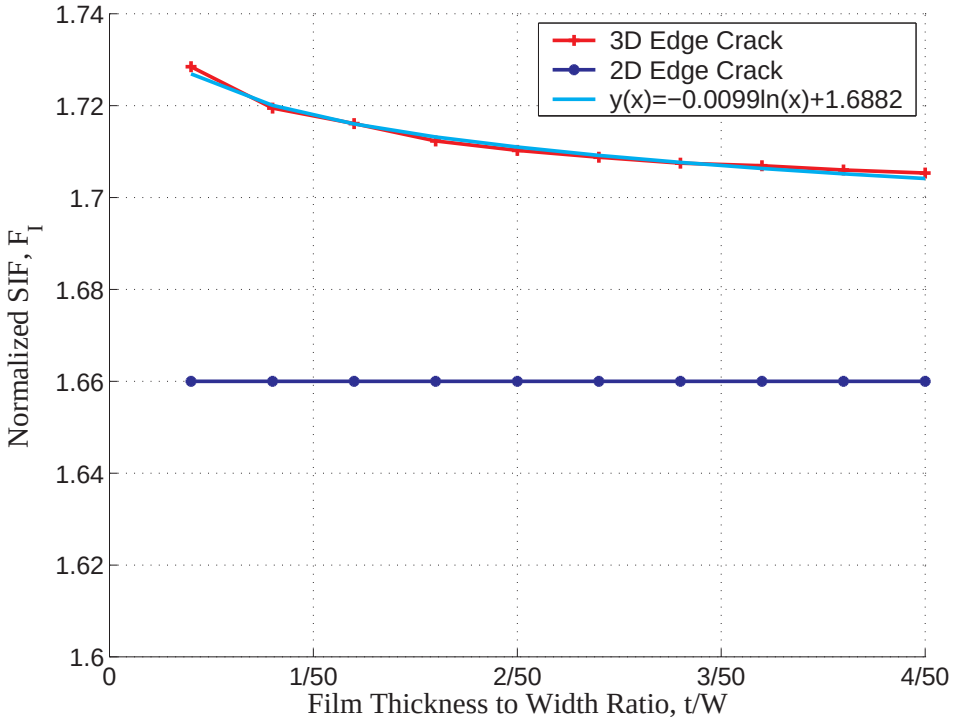

Figure 5.9. Average F_I vs film thickness, a/W=0.3

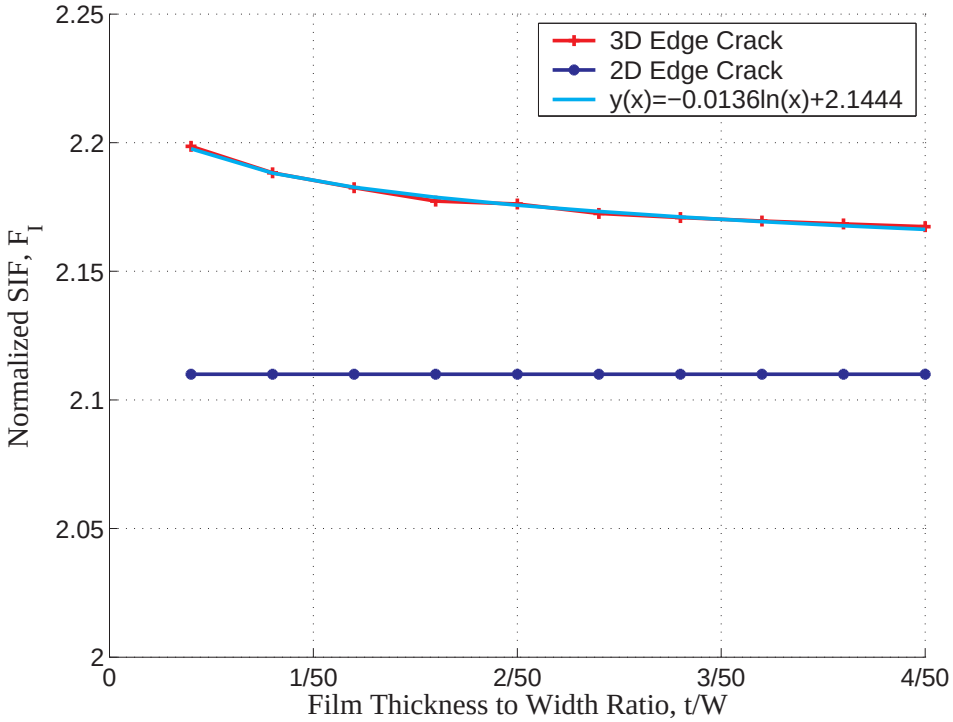

Figure 5.10. Average F_I vs film thickness, a/W=0.4

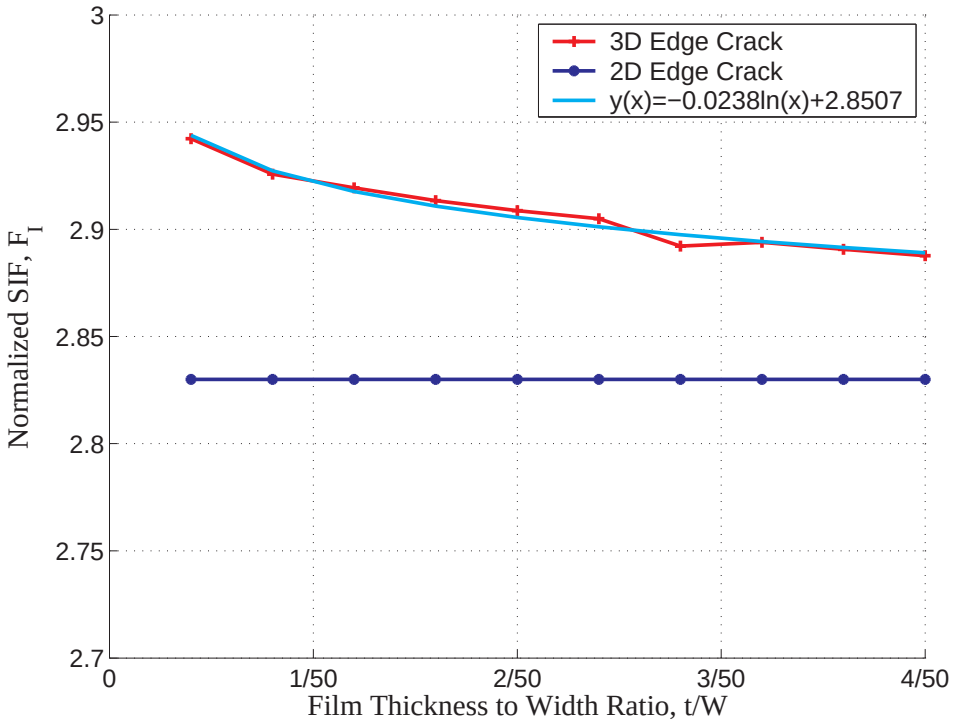

Figure 5.11. Average F_I vs film thickness, a/W=0.5

5.3. Energy Release Rate

At each instant of the growth, the channel crack front self-adjusts to a curved shape, such that energy release rate (ERR) at every point along film thickness is same. After the length exceeds a few times the film thickness, the channel asymptotically approaches a steady-state: the entire front maintains its shape as it advances; the cross-section profile in the wake, which attains the shape of a plane strain through-crack [6]. Therefore it is essential to calculate energy release rate and plot profile along crack front. Crack front profile can be deduced from energy release rate profile as each crack front node propagates relatively based on their relative energy release rates.

For a general two-dimensional mixed mode problem, the relationship between the energy release rate and the stress intensity factors(SIF) is;

$$G = \frac{K_I^2}{E^*} + \frac{K_I^2}{E^*}$$

where $E^* = E$ for plane stress problems and $E^* = E/(1-\nu^2)$ for plane strain problems [4].

For mixed-mode general problems, one can use the $ERR - SIF$ relation given by Griffith;

$$G = \frac{B}{E}K_I^2 + \frac{B}{E}K_{II}^2 + \frac{1+\nu}{E}K_{III}^2$$

where

$B = 1$ for plane strain

$B = 1 - \nu^2$ for plane stress

Plane strain assumption is employed when energy release rate along the crack front is calculated. It is observed that energy release rate along crack front is almost equally distributed near middle points of the film, where it drops at the edges. This phenomenon is identical to mode-I stress intensity factor distribution and again can be explained by the edge contraction effect. As equation 5.3 is used for energy release rate calculations, there is a direct relation between energy release rate and stress intensity factors and thus the crack tip displacements. Relative larger displacements at crack faces results in larger stress intensity factors. As there is contraction at edges, near crack root (figure 5.2) mode-I stress intensity factor drops. Also mode-III stress intensity factor does not rise as the contraction effect result in equal deformation in z-direction at the crack edges. Therefore energy release rate decrease in total at the edges and the energy difference between mid-points and edges is used in compression at the edges. The energy release rate along crack front nodes are presented in figures 5.12 to 5.15.

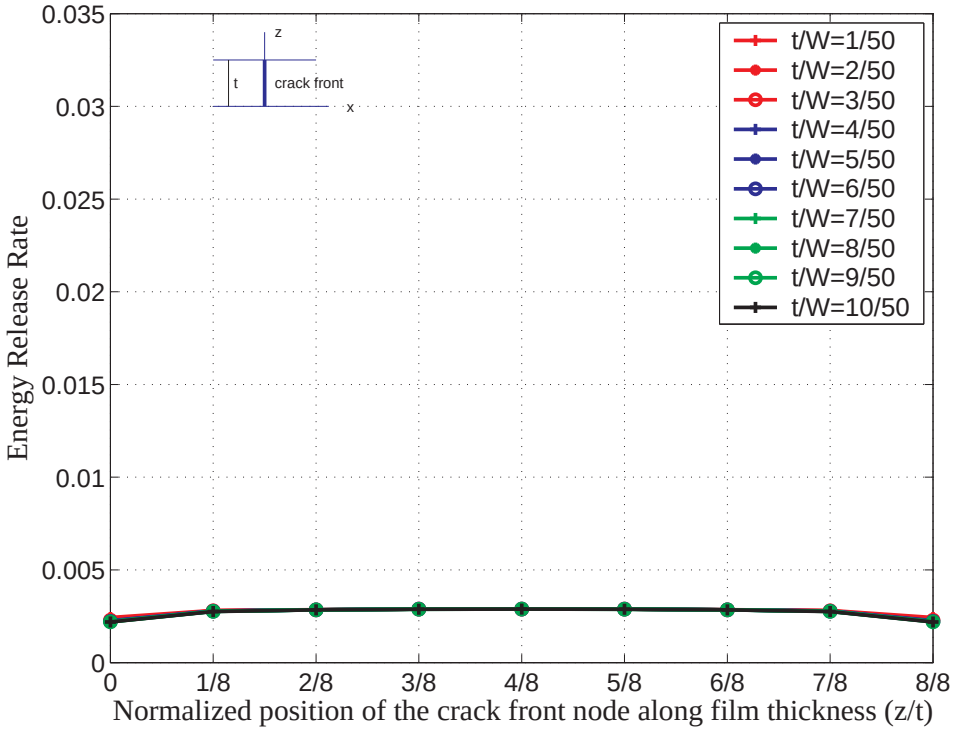

Figure 5.12. Average ERR vs crack front node position along film thickness, $a/W = 0.2$

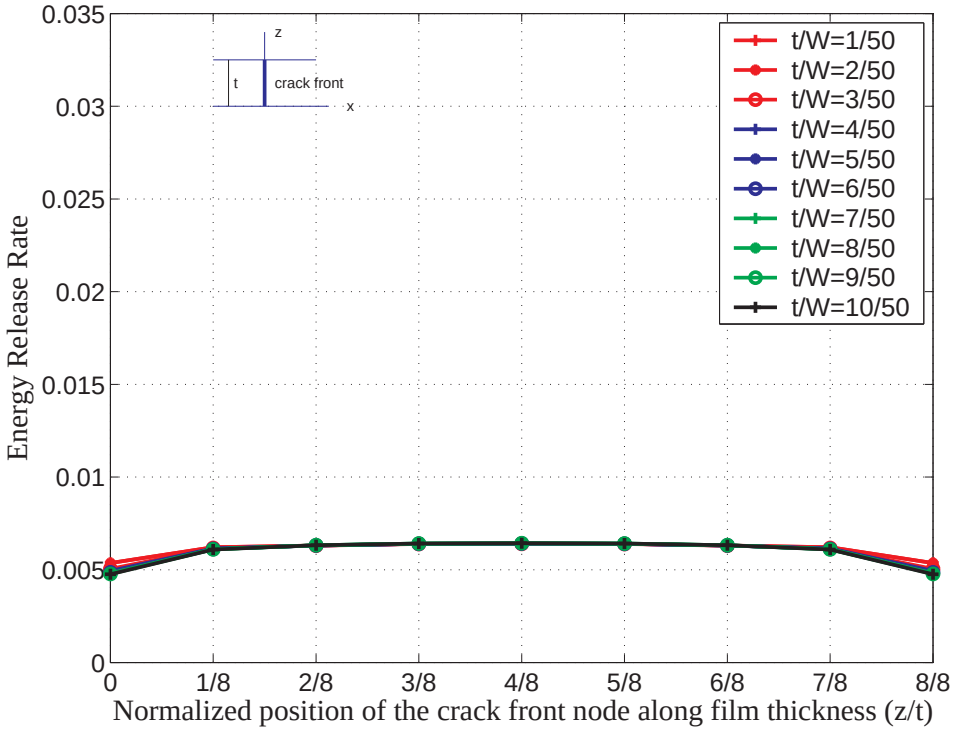

Figure 5.13. Average ERR vs crack front node position along film thickness, $a/W = 0.3$

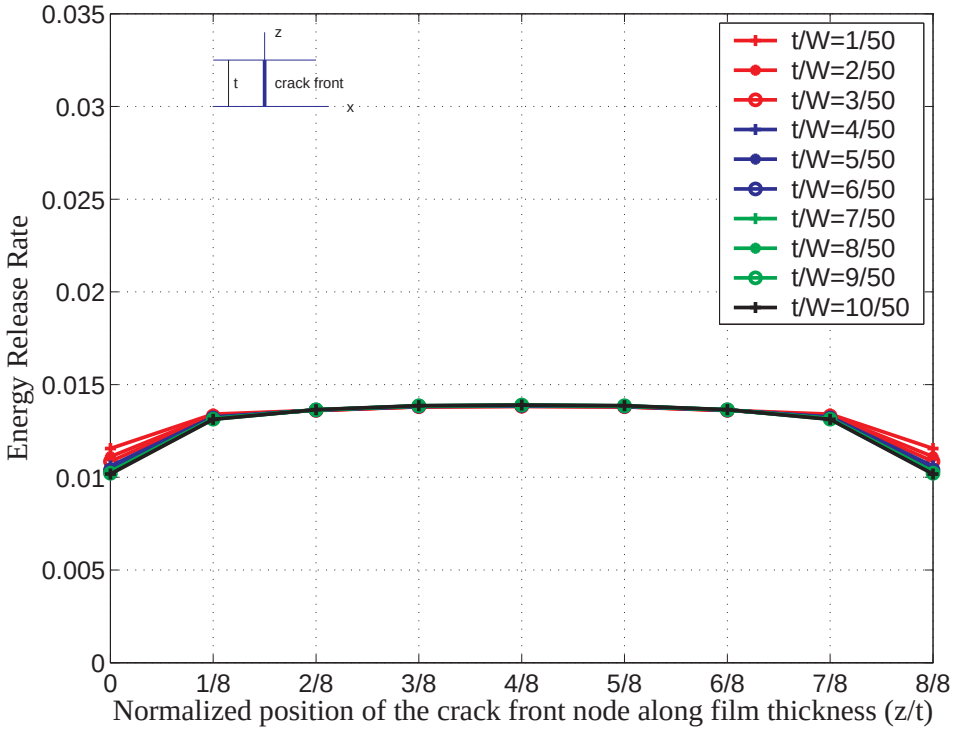

Figure 5.14. Average ERR vs crack front node position along film thickness, $a/W = 0.4$

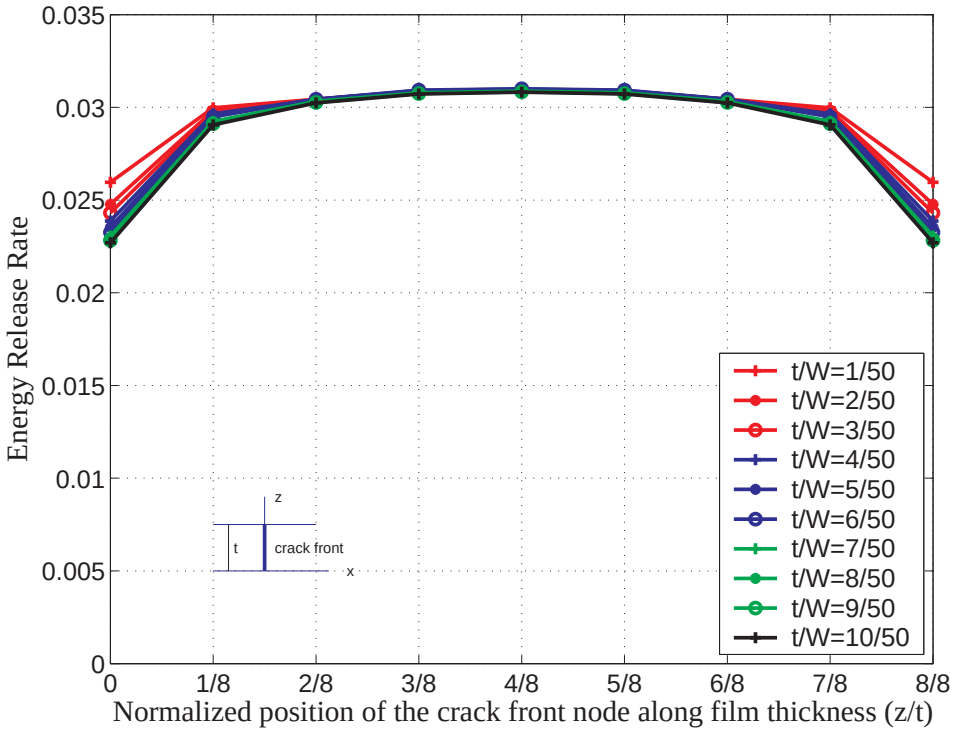

Figure 5.15. Average ERR vs crack front node position along film thickness, $a/W = 0.5$

5.4. 3-D Analysis Verification with Literature

There is not much theoretically or experimentally proven data available in the literature especially for 3-D cracks. However, verification of the 3-D crack analysis with the available straight crack data is essential in the research of crack propagation in several media.

For "Single Edge Crack in a Rectangular Panel", literature data is given by Murakami [26] for width(W)/height(H) ratio of 1.0.

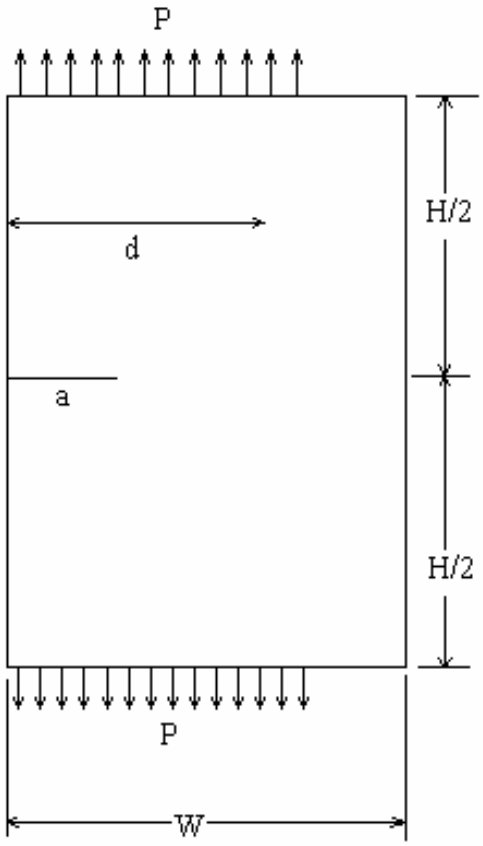

Figure 5.16. Single edge crack in a rectangular panel

In the table provided by Murakami, there is no specific thickness region is mentioned. Numerical analysis are carried out for 4 different plate thicknesses as t/W = 0.1/50, 1/50, 10/50 and 50/50. Analysis are performed for P/W equal to 1.

Table 5.1. Edge crack data from literature

F_I, Murakami [26]	a/w=0.2	a/w=0.3	a/w=0.4	a/w=0.5
Single Edge Crack in a Rectangular Panel (W/H=1.0)	1.49	1.85	2.32	3.01

Table 5.2. SIF for literature verification

a/W=0.2		t/W=0.1/50	t/W=1/50	t/W=10/50	t/W=50/50
	Average K_I	28033.53	27425.22	26951.57	26369.28
	F_I	1.58	1.55	1.52	1.49
	Error %	6.15%	3.85%	2.05%	0.15%
a/W=0.3		t/W=0.1/50	t/W=1/50	t/W=10/50	t/W=50/50
	Average K_I	42649.31	41775.32	41023.70	39973.58
	F_I	1.96	1.92	1.89	1.84
	Error %	6.20%	4.02%	2.15%	0.46%
a/W=0.4		t/W=0.1/50	t/W=1/50	t/W=10/50	t/W=50/50
	Average K_I	62082.35	60632.22	59513.49	57799.39
	F_I	2.48	2.42	2.37	2.31
	Error %	6.76%	4.26%	2.34%	0.61%
a/W=0.5		t/W=0.1/50	t/W=1/50	t/W=10/50	t/W=50/50
	Average K_I	89871.86	87764.00	86056.66	83317.94
	F_I	3.21	3.13	3.07	2.97
	Error %	6.54%	4.04%	2.02%	1.23%

Error is minimized in the case of $t/W = 50/50$ for the case of equal width and thickness of the plate. The numerical values presented by Murakami and calculated values can be found respectively in the tables 5.1 and 5.2. Error values decrease with increasing film thickness as shown in figure 5.17.

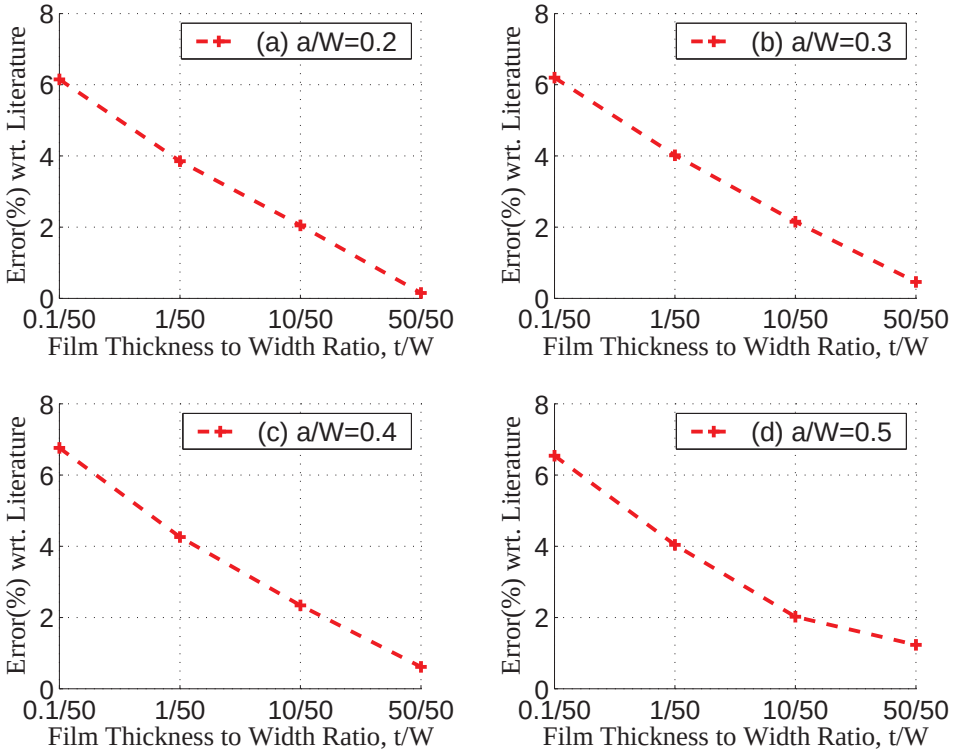

Figure 5.17. *FEA* error for single edge crack in a rectangular panel

5.5. Inclined Crack Analysis

Inclined crack stress intensity factors shows a self-similar behavior as in the case of straight crack. The mode-I stress intensity factor tends to decrease on the edges where as both mode II and mode-III stress intensity factors increase. This condition results in high crack initiation angles on the edges of the plate as the crack initiation angle is a function of K_I/K_{II}.

The average values stress intensity factors are found out to be very near to corresponding plane strain solutions. The results can be seen in the below figures 5.18 to 5.22.

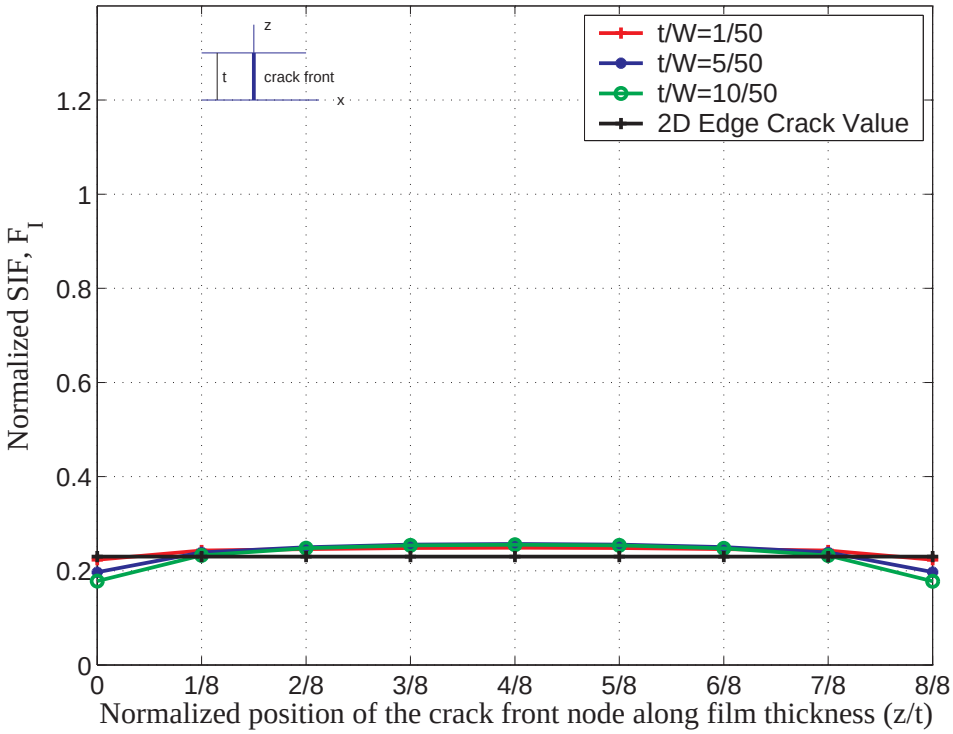

Figure 5.18. Non dimensional SIF along film thickness, $a/W = 0.2$, $\beta = 15^o$

The mode-I stress intensity factor plots are skipped for crack length to plate width ratios $a/W = 0.3, 0.4$ and 0.5 in order not to disturb the reader. The behavior is found out to be similar with $a/W = 0.2$ case.

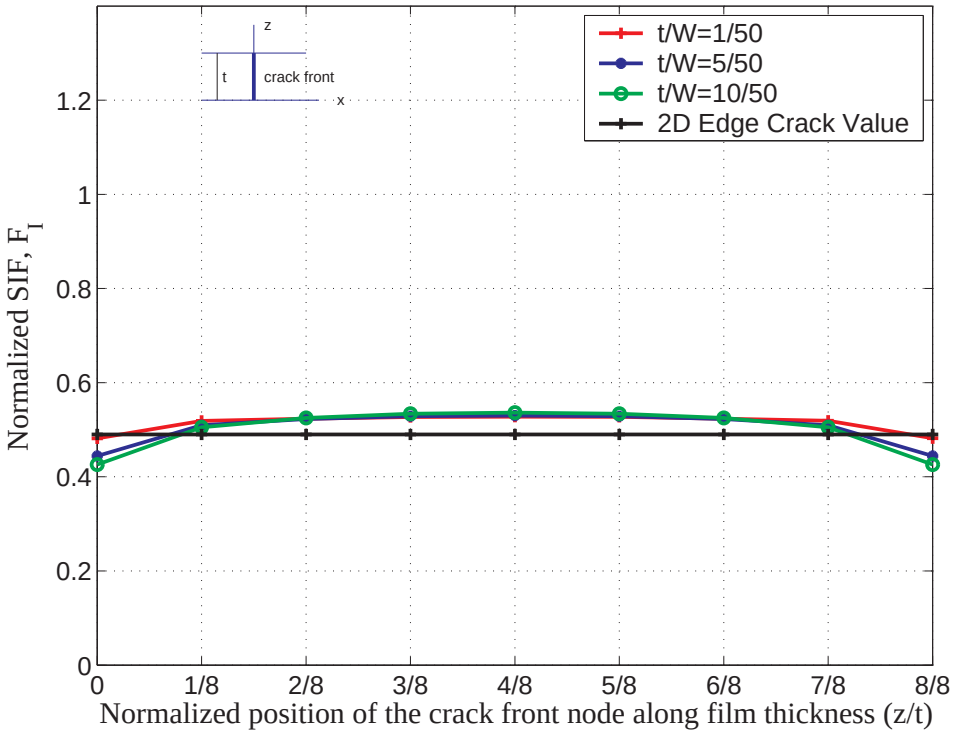

Figure 5.19. Non dimensional SIF along film thickness, $a/W = 0.2$, $\beta = 30^o$

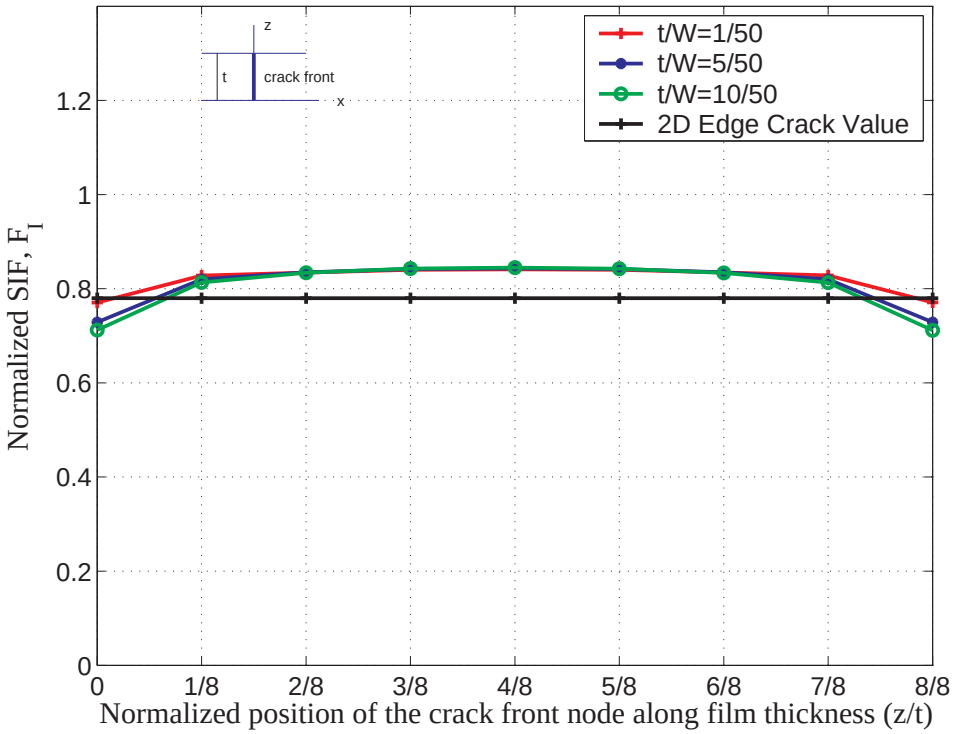

Figure 5.20. Non dimensional SIF along film thickness, $a/W = 0.2$, $\beta = 45^o$

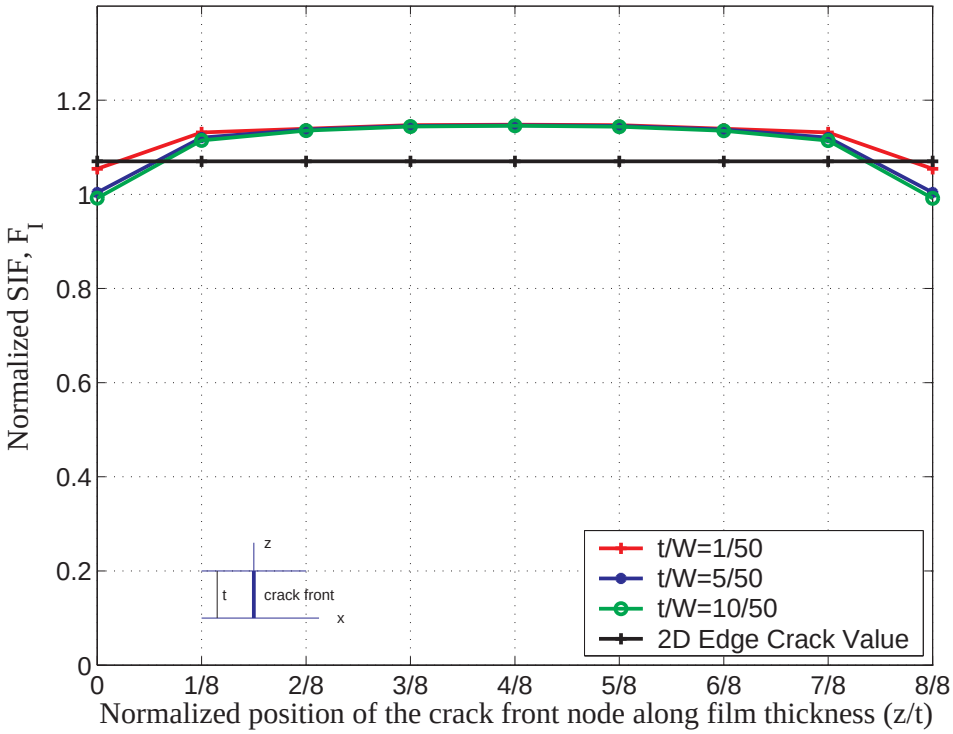

Figure 5.21. Non dimensional SIF along film thickness, $a/W = 0.2$, $\beta = 60^o$

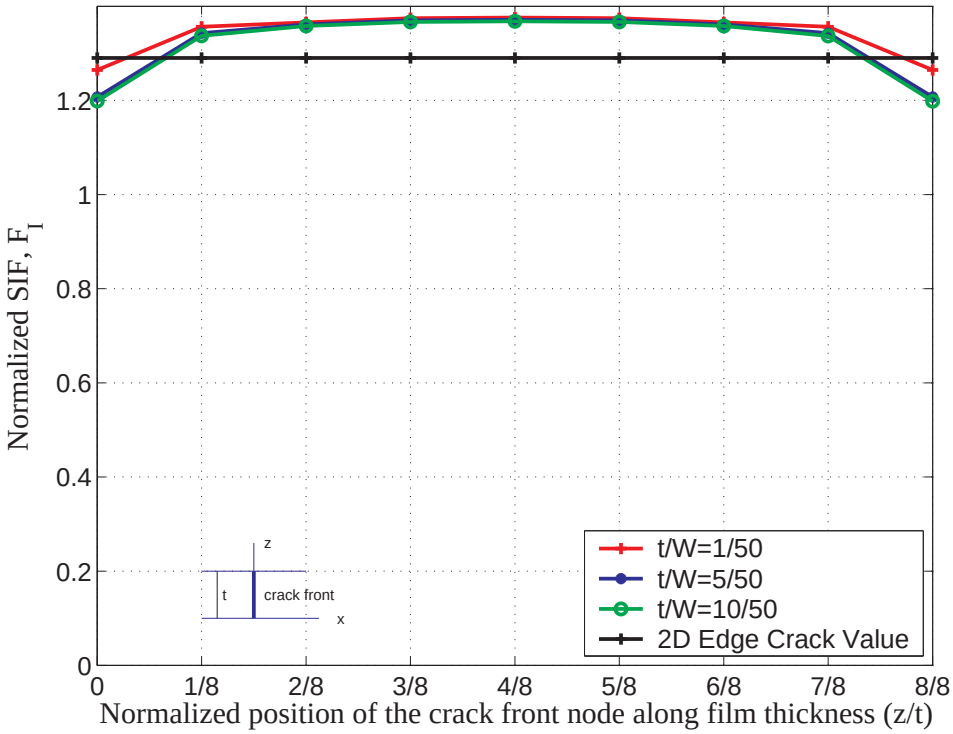

Figure 5.22. Non dimensional SIF along film thickness, $a/W = 0.2$, $\beta = 75^o$

Stress intensity factors are averaged and plotted for each initial crack angle β in figure 5.23 for crack length to plate width ratio of $a/W = 0.2$. Three different plate thickness to width ratios are studied by keeping width at a constant value. It is observed that mode-I stress intensity factor tend to decrease with decreasing initial crack angle (β). Mode-II stress intensity factor reaches its maximum value around initial crack angle, β equal to 45^o. Mode-III stress intensity factor does not vary as much as the remaining SIFs, but attains its minimum value at $\beta = 90^o$ and reach a constant value. Same phenomenon is showed for 2D cases by Fett [24, 25] and recalculated by Copur [13] using finite element method. Effect of plate thickness is found out to be minimal. Results for crack length to plate width ratios of $a/W = 0.3, 0.4$ and 0.5 are not presented but show similar behavior of $a/W = 0.2$; except that all stress intensity factors tend to increase with increasing crack length to width ratio.

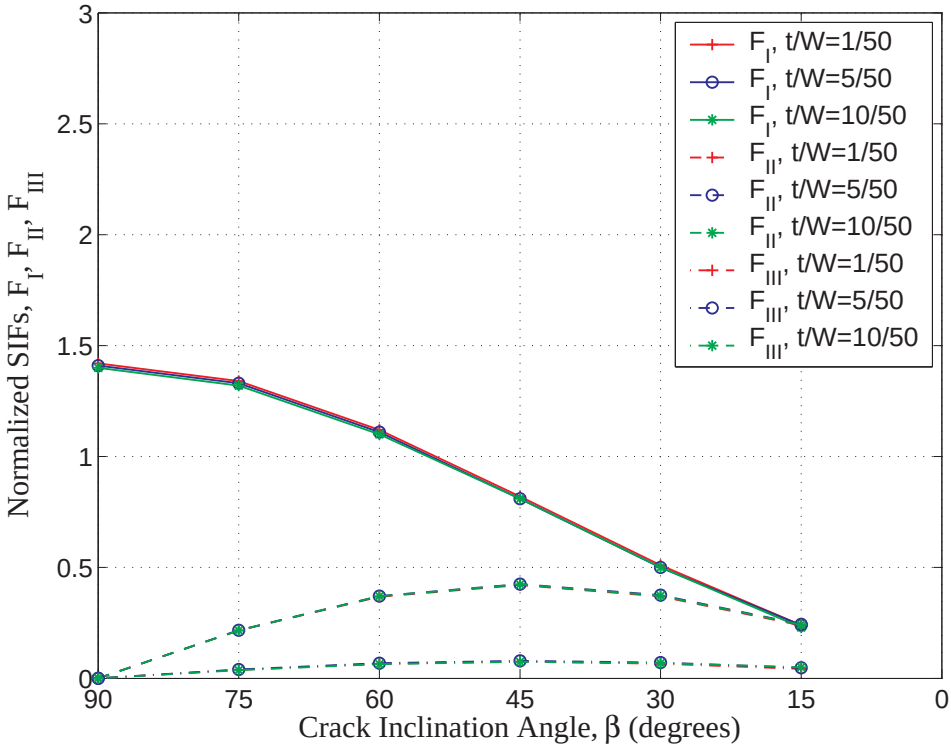

Figure 5.23. SIF versus initial crack angle, $a/W = 0.2$

Crack initiation angles θ_c along crack front for crack length to plate width ratio $a/W = 0.2$ is presented in figure 5.24. Distribution is almost equal except on the free edges where edge effects become dominant. However the difference is at most 5%, where it affects the averaged value around 1% which is an acceptable level. The effect

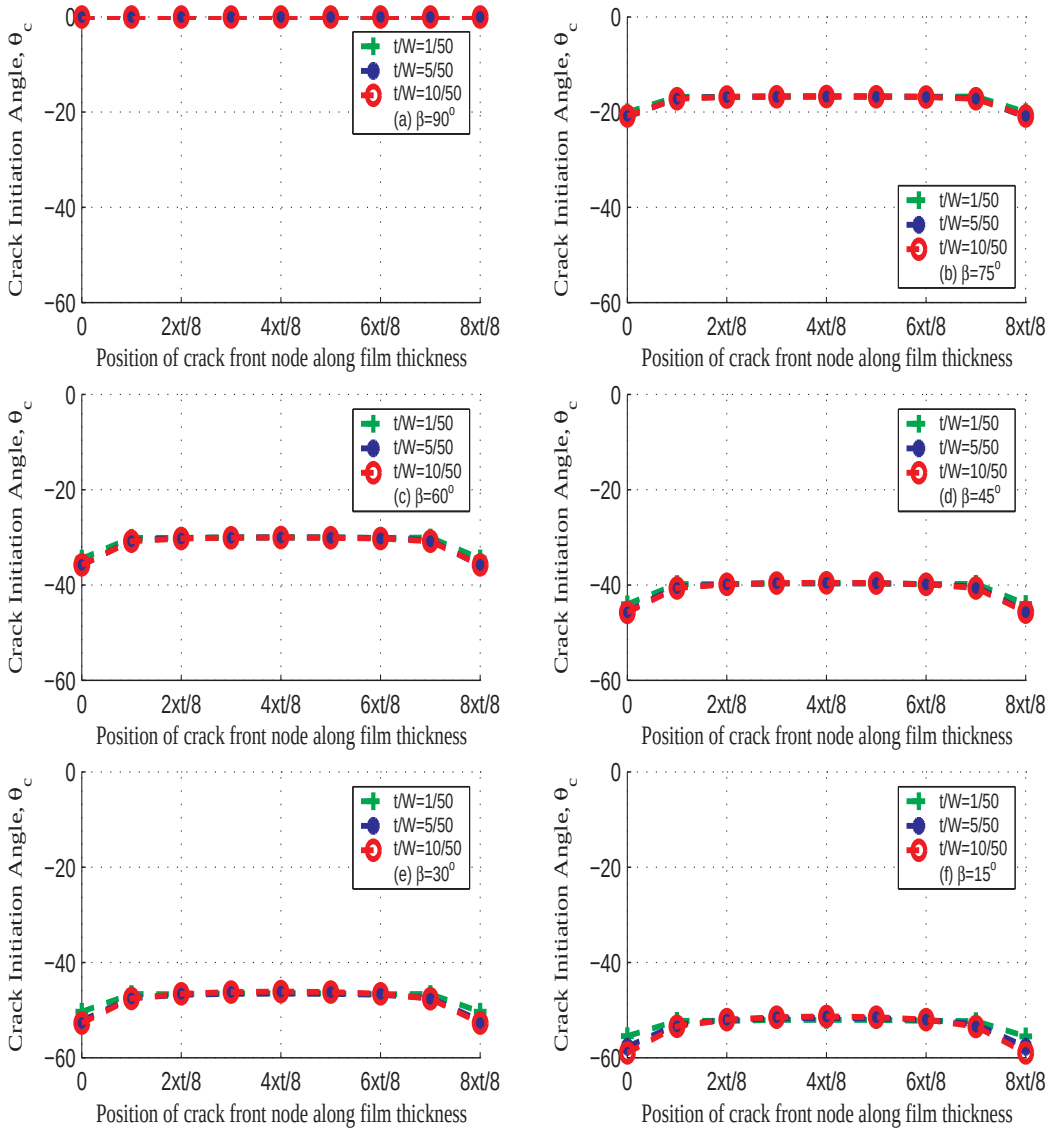

Figure 5.24. Crack initiation angles for $a/W = 0.2$

of plate thickness is again found out to be of minimal contribution. Crack initiation angles θ_c, tend to increase with decreasing initial crack angle β, as expected.

Energy release rate for inclined cracks shows similar behavior as of straight crack. As it can be observed in figure 5.25 that energy release rate decrease with decreasing initial crack angle β. Distribution along crack front is almost equal expect at the edges, again due to edge compression effect as described in previous sections. Results for crack length to plate width ratios $a/W = 0.3, 0.4$ and 0.5 are not presented but is found out to be similar except that the energy release rate increase with increasing crack length.

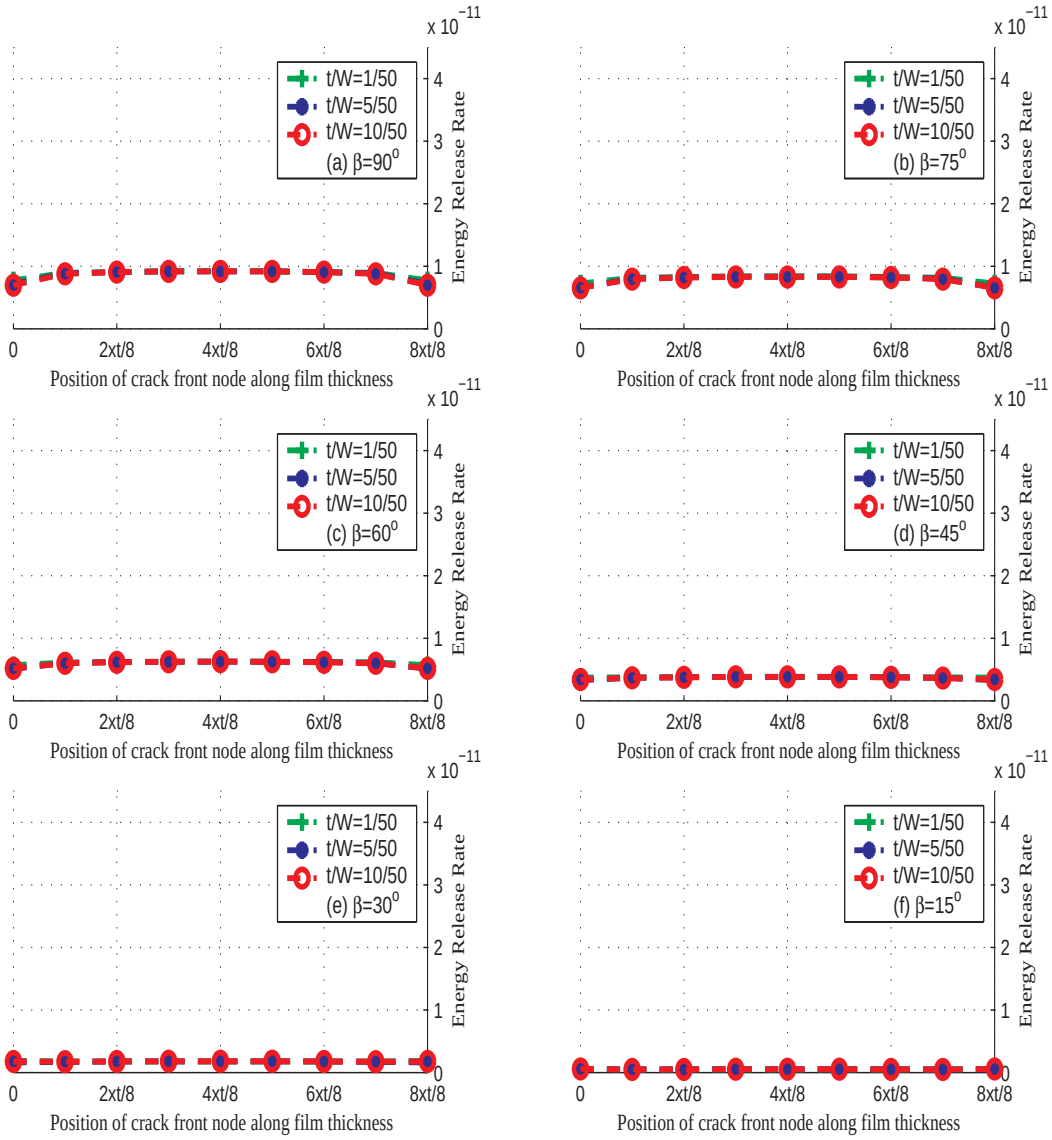

Figure 5.25. Energy release rate along thickness, $a/W = 0.2$

6. 3D EDGE CRACK ANALYSIS IN THIN FILM-SUBSTRATE SYSTEMS

6.1. Background & Analysis

A thin film on an elastic substrate with an edge crack is studied under mixed mode loading through out this chapter. There is not any analytical result available in the literature for this problem; therefore results of this chapter are discussed more on a qualitative basis. The geometry of the problem is shown in figure 6.1, where equal amount of pressure is applied only on substrate vertical walls in the outward normal direction.

The problem is modeled in 3-D by assuming straight crack front and results are examined in detail to consider the effect of material mismatch of substrate and film. Two different film-substrate systems are studied: Two different materials are considered as thin film materials, namely Gallium Nitride (GaN) and Aluminum Nitrate (AlN). Si is used as elastic substrate material. The material properties are summarized in table 6.1.

Thin film is modeled with 20-noded brick elements to get accurate results around the crack tip whereas the substrate is modeled with 10-noded tetrahedral elements. Pyramid elements are used for transition from quadrilateral elements to tetrahedrons. A 3D volume mesh is created from a 2D area mesh. Sweep command is employed with equal element size on each layer along film thickness. The interface between the thin film and the elastic substrate is modeled as a perfect bond by using common nodes for thin film and substrate meshes on the interface (i.e. continuous media). No further interface properties are studied in this chapter.

During the analysis only substrate is loaded bi-axially from vertical walls as shown in figure 6.2, where there is no direct load applied to thin film. Bottom face of the substrate is constrained in z direction. A bottom corner node of the substrate is fully

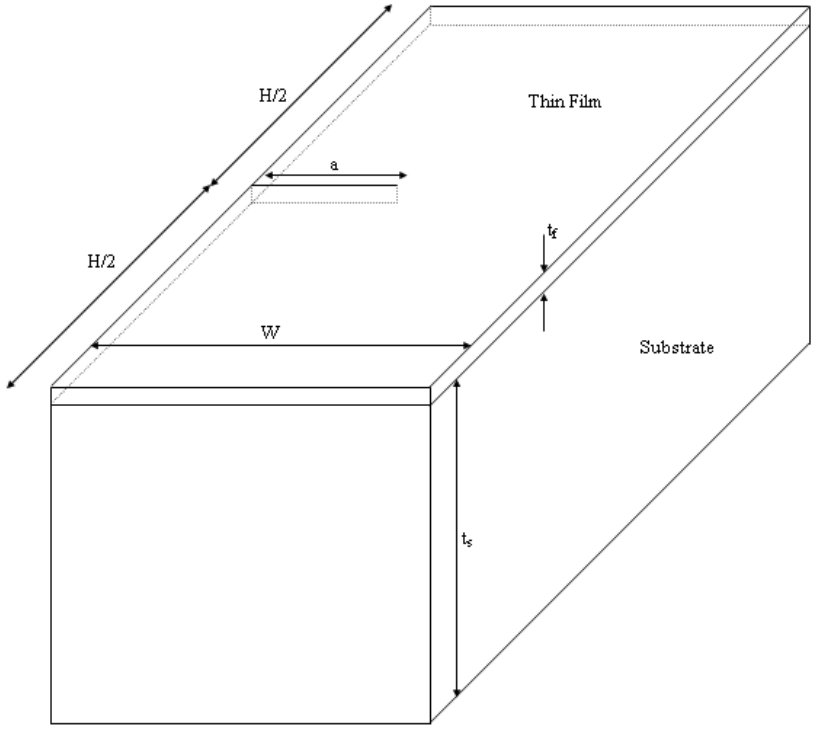

Figure 6.1. Thin film on elastic substrate with an edge crack, Isometric

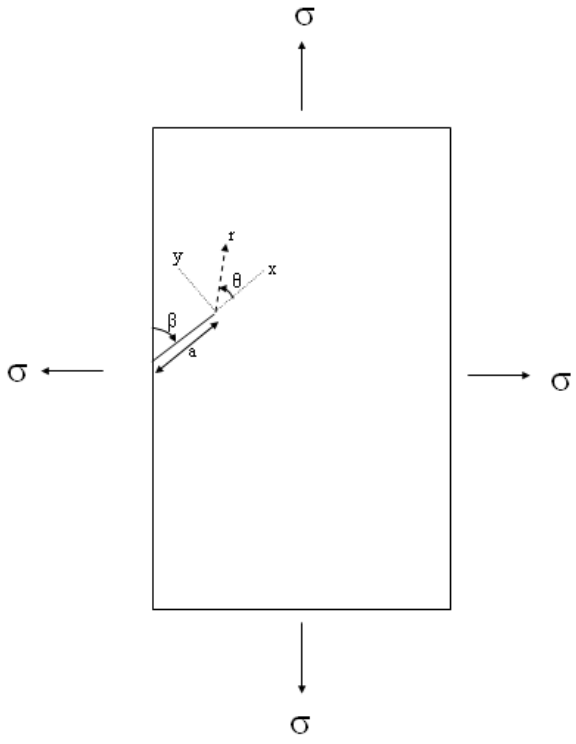

Figure 6.2. Thin film on elastic substrate with an edge crack, Top

Table 6.1. Material properties of thin film-elastic substrate systems

Material	E (Young's Modulus)	ν (Poisson's Ratio)
Gallium Nitride (GaN)	181 GPa	0.352
Aluminum Nitrate (AlN)	308 GPa	0.287
Silicon (Si)	131 GPa	0.266

constrained(i.e. reference point) to prevent rigid body motion resulting in divergence during analysis. Four different ratios of a/W are considered, namely 0.2, 0.3, 0.4 and 0.5. 6 different crack inclination angles, β, are used namely 90, 75, 60, 45, 30 and 15 degrees. Thin film thickness is taken as 1/80 of substrate thickness through out the analysis.

Crack initiation angles, stress intensity factors, energy release rates are plotted for each case. The normal and shear stress distributions along specific paths are also plotted to present the general response of the system to biaxial loading.

Mesh density and substrate geometry effects are studied in the first two sub sections. Using the outcome of this comparative study, broader analysis are carried out and presented at following sections.

6.1.1. Effect of Mesh Density on SIF Calculations

The number of elements used is changed between 10,000 and 30,000 elements to get a general understanding of the effect of mesh size on stress intensity factor calculations. The refinement box element density is doubled while holding the outer edge element size constant. This way the refinement around crack tip is examined also. The finite element mesh is shown in figure 6.3.

An analysis is carried out for comparison purposes where GaN is used as film material with a Si substrate and $a/W = 0.3$, $H/W = 1$ and straight crack.

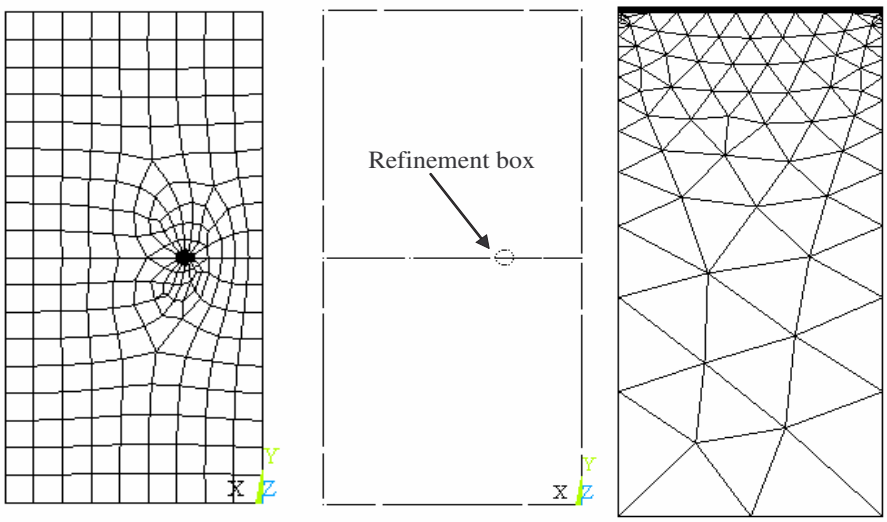

(a) 2D film mesh (b) Refinement box (c) Substrate mesh

Figure 6.3. Mesh density effect on thin film - substrate edge crack analysis

Mode-I SIF plot in figure 6.4 along film thickness direction shows that for calculated values, 9000 element coarse mesh, is satisfactory for further crack analysis. This is the case also for mode-II and mode-III stress intensity factors as it can be seen from figures 6.5 and 6.7. There is very little variation in crack initiation angle, figure 6.6 for different mesh densities. Energy release rate is plotted in figure 6.8. Trend is similar to F_I as mode-I is dominant over mode-II and mode-III for straight crack case. Based on the comparative analysis for mesh density it was decided to use a refined-box type of mesh with 32 elements around the crack tip. This way both accuracy and computation time is optimized.

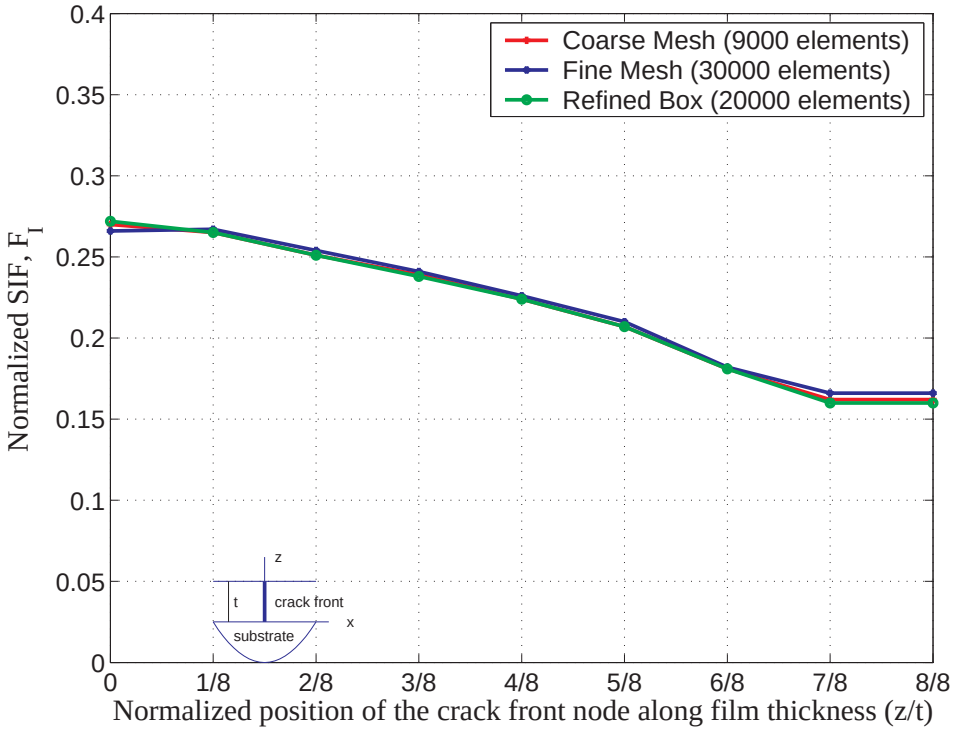

Figure 6.4. Mode-I stress intensity factor for $a/W = 0.3$, $H/W = 1$, $\beta = 90^o$ (Straight Crack)

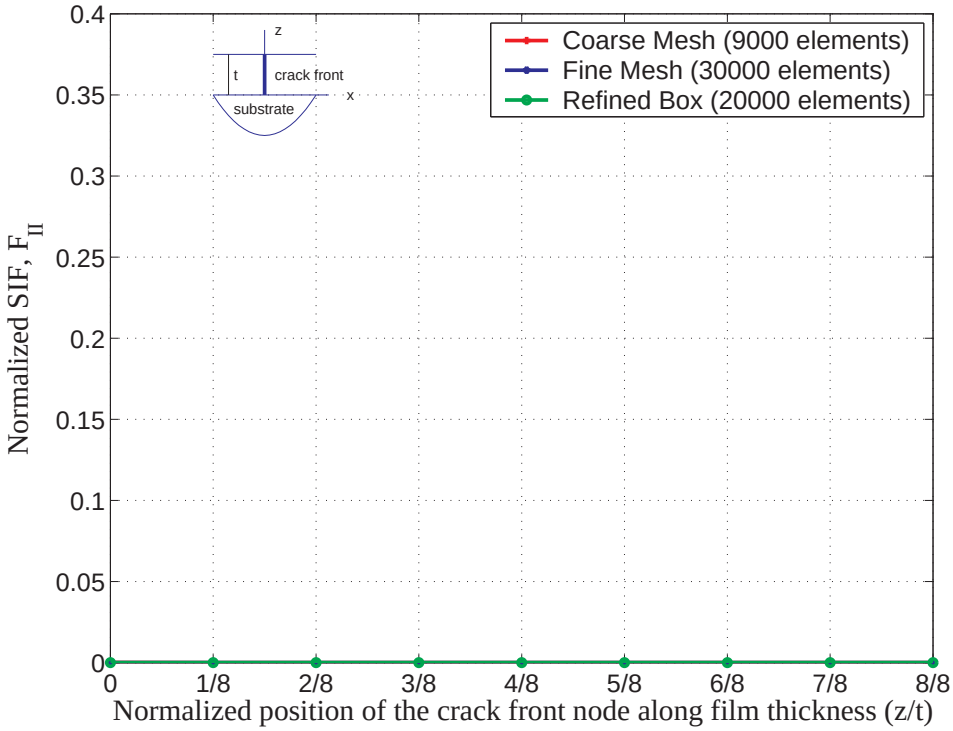

Figure 6.5. Mode-II Stress intensity factor for $a/W = 0.3$, $H/W = 1$, $\beta = 90^o$ (Straight Crack)

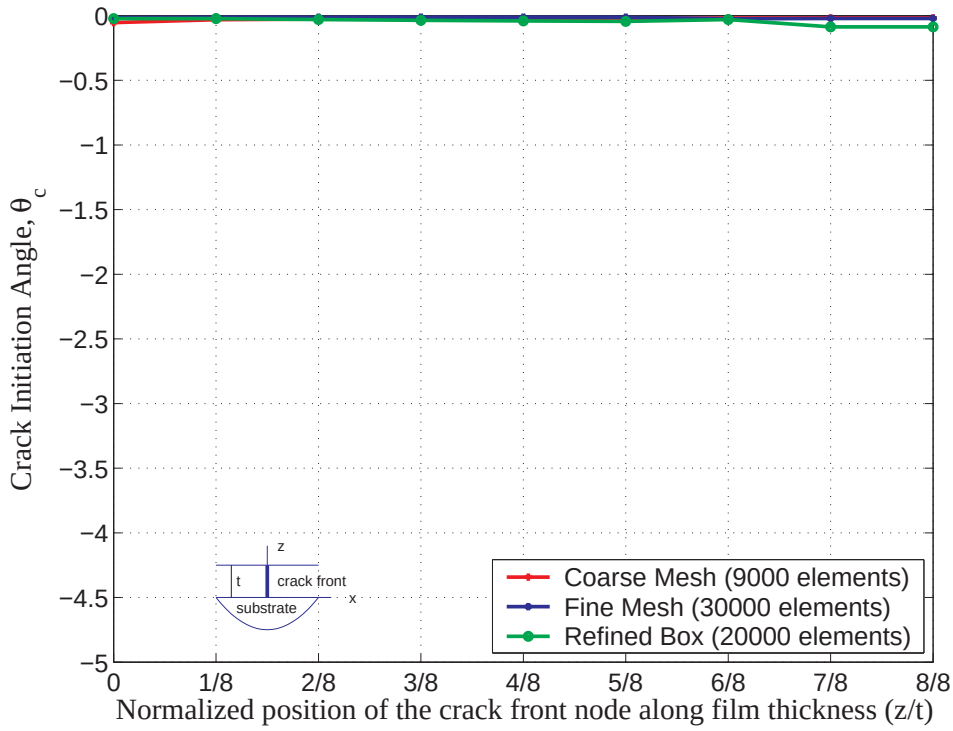

Figure 6.6. Crack initiation angle for $a/W = 0.3$, $H/W = 1$, $\beta = 90^o$ (Straight Crack)

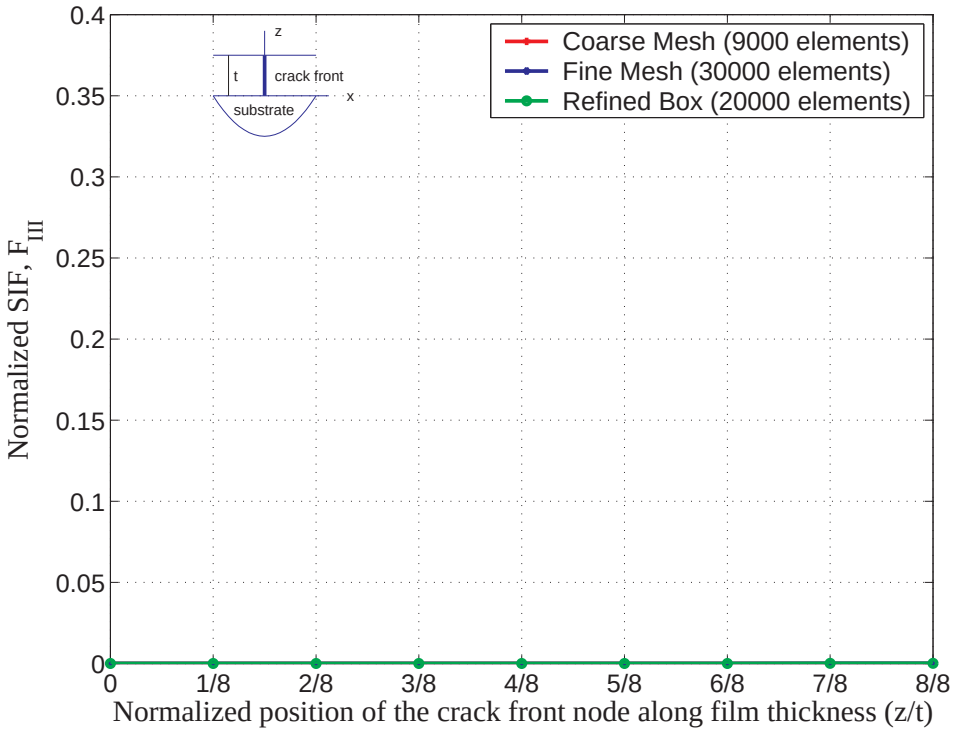

Figure 6.7. Mode-III stress intensity factor for $a/W = 0.3$, $H/W = 1$, $\beta = 90^o$ (Straight Crack)

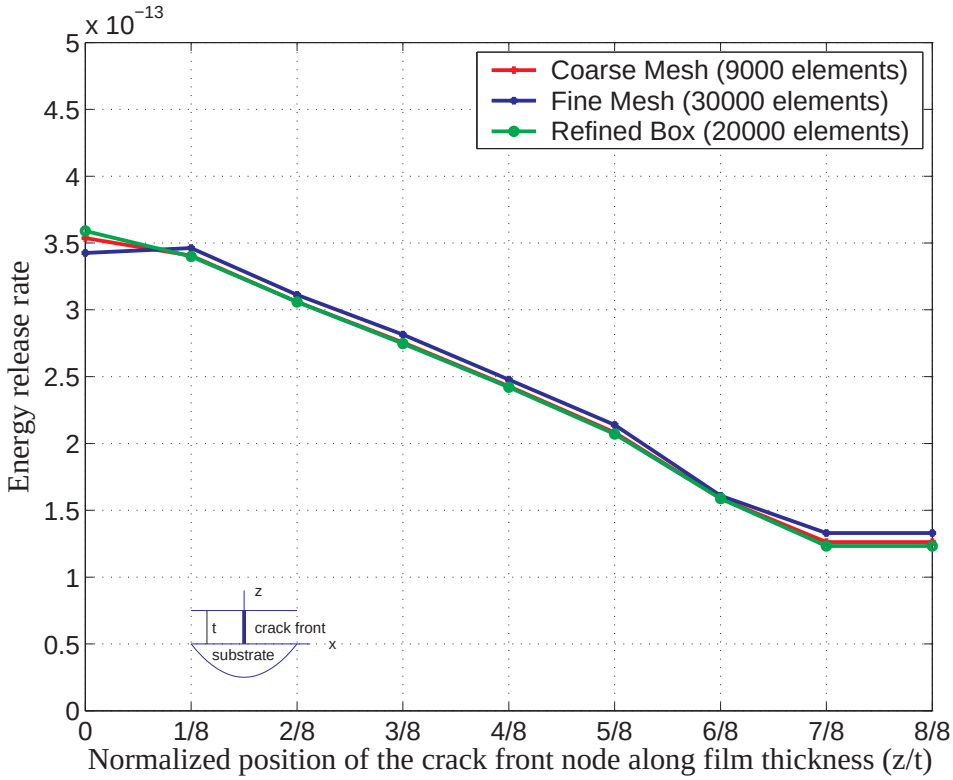

Figure 6.8. Energy release rate for $a/W = 0.3$, $H/W = 1$, $\beta = 90^o$ (Straight Crack)

6.1.2. Effect of thin film geometry on SIF Calculations

Two cases are studied for the effect of geometry: $H/W = 1$ and $H/W = 2$. SIF calculations show that mode-I, mode-II and mode-III SIF's are larger for $H/W = 2$ case than $H/W = 1$ case, as can be seen in figure 6.9. This is partly due to normalization of the stress intensity factors with respect to constant pressure which is applied on the vertical walls of the substrate.

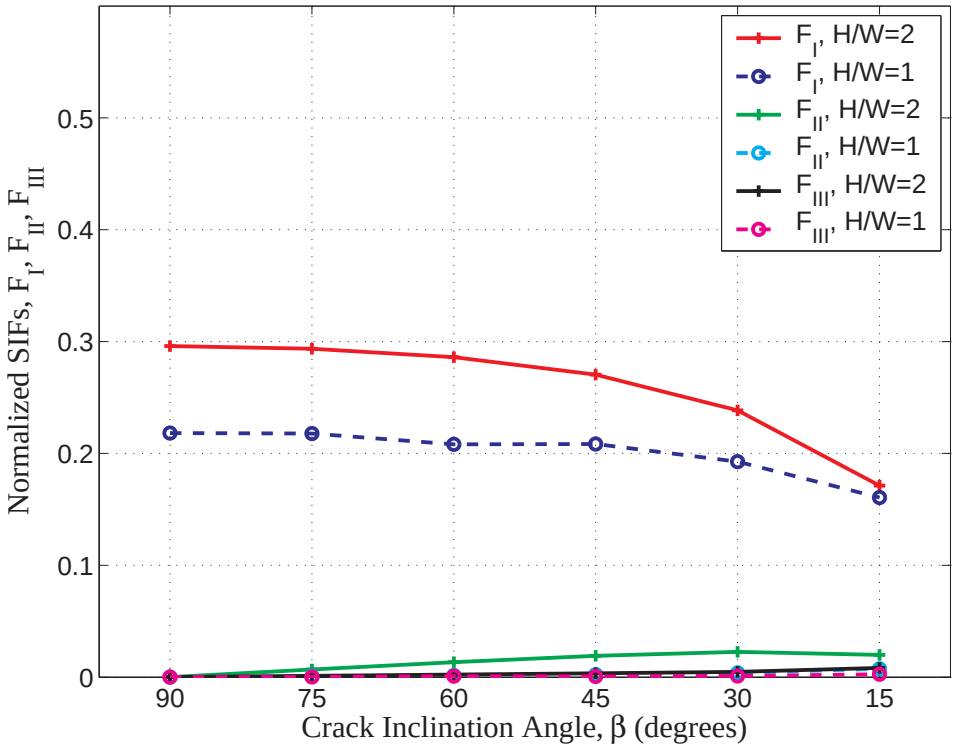

Figure 6.9. Effect of H/W ratios on SIF

However the effect cannot be explained by normalization as crack initiation angles are also different for two different H/W values. Crack initiation angles are found out to be larger for $H/W = 2$ case as presented in figure 6.10. Therefore it may be concluded that geometry is also an important parameter in crack analysis. For modeling real life applications or experimental work, exact geometry of systems should be transferred into finite element model.

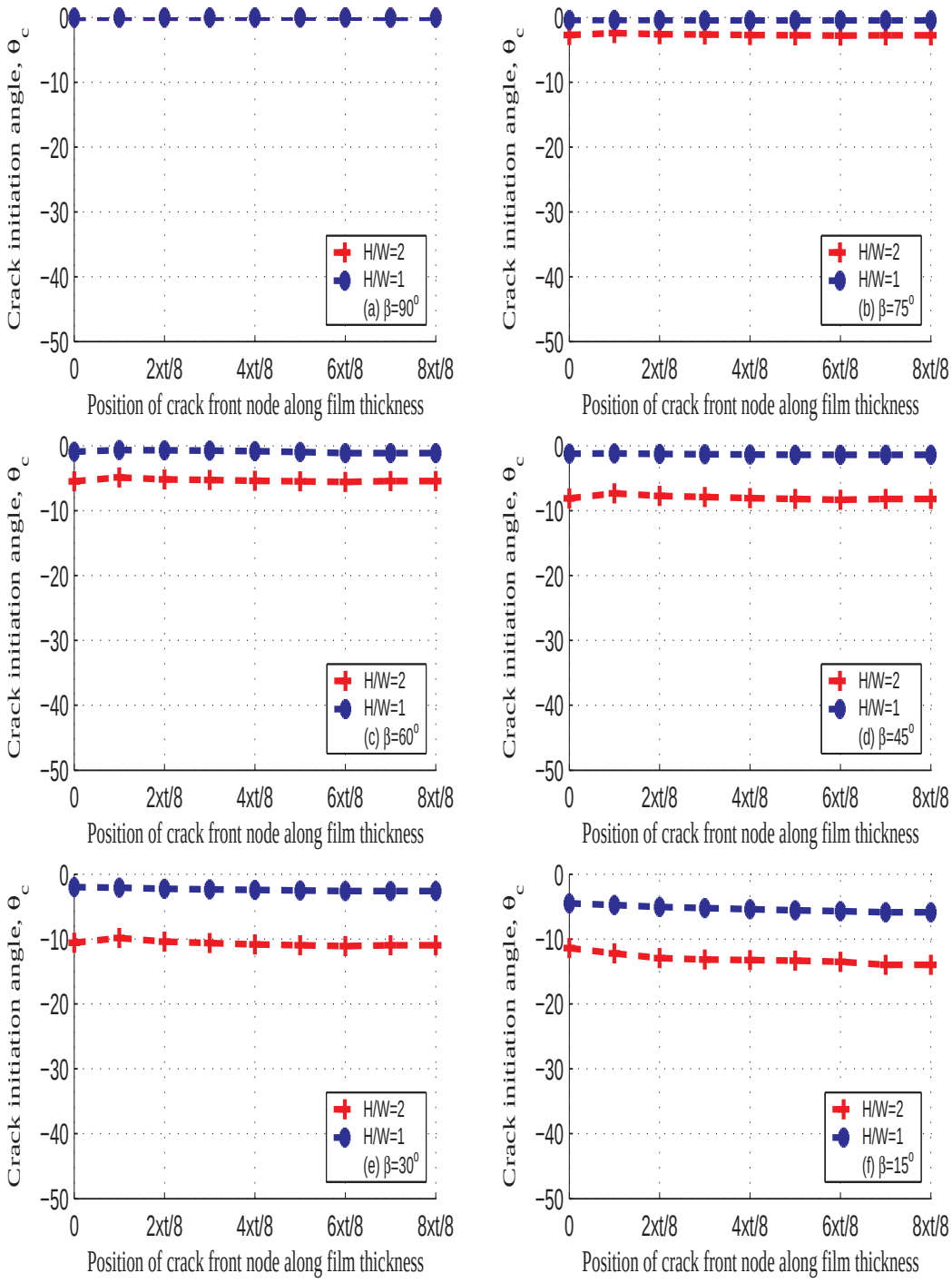

Figure 6.10. Effect of H/W ratios on crack initiation angles

6.2. General Crack Analysis For Thin Film On Substrate

6.2.1. Stress Intensity Factor Calculations

Two different thin film materials are studied for thin film with an edge crack deposited on a substrate to see the effect of elastic mismatch on fracture parameters. Average SIF values calculated for different material systems and are presented in figures 6.11 and 6.12 for several crack inclination angles. It is observed that for AlN thin film, which is more stiff than GaN, all stress intensity factors are higher. With increasing crack length to plate width ratio(a/W), stress intensity factors decrease unlike 2D case where SIFs increase when crack length increase. Decrease in SIFs in thin film systems is due to normalization where the crack length, a, appears in the denominator. However K values increase up to crack lengths of several film thicknesses and reach a steady state case. Steady state cracking will be discussed in following chapters.

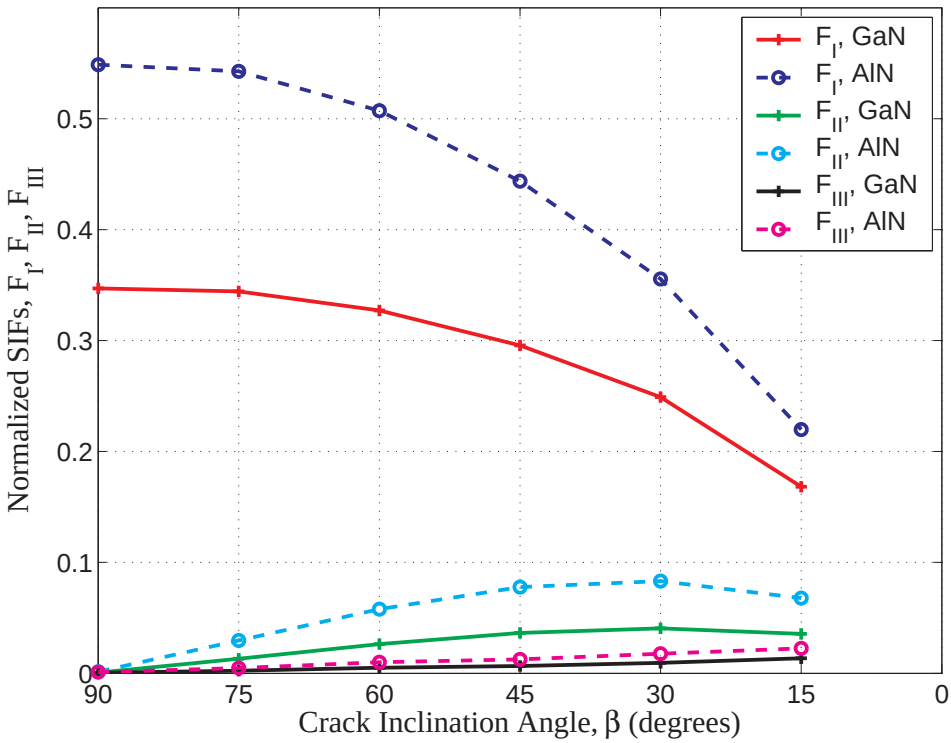

Figure 6.11. Average SIF for $a/W = 0.2$

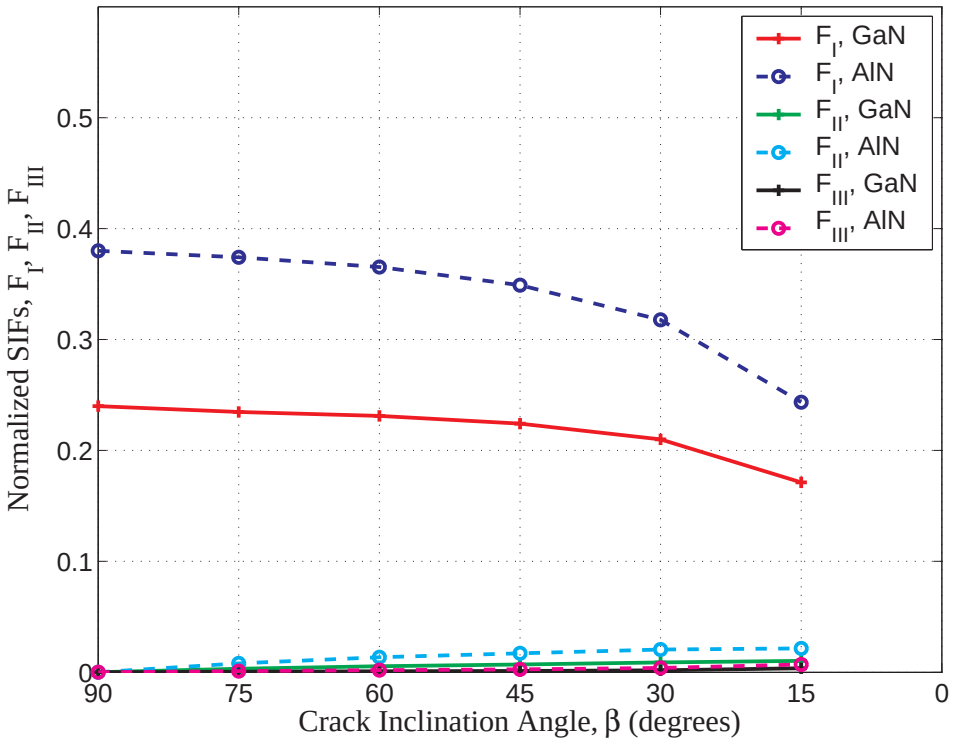

Figure 6.12. Average SIF for $a/W = 0.5$

6.2.2. Crack Initiation Angles

Crack initiation angles for 4 different crack lengths and 6 different initial crack angles are analyzed in this section. The crack initiation angles are found out to be of almost equal value along the thickness for each case. The figures are presented in the following figure 6.13 for $a/W = 0.2$. Similar behavior is observed for $a/W = 0.3, 0.4$ and 0.5.

Crack initiation angles θ_c tend to increase with decreasing initial crack angles β. The amount of increase in crack initiation angle is also effected by elastic mismatch as presented in figure 6.14. AlN-Si thin film and substrate system has higher crack initiation angles for each case than that of GaN-Si. AlN is around two times stiffer than GaN which results in higher shear stress on the thin film - substrate interface. Which in turn relatively higher K_{II} values with respect to K_{II} and higher crack initiation angles.

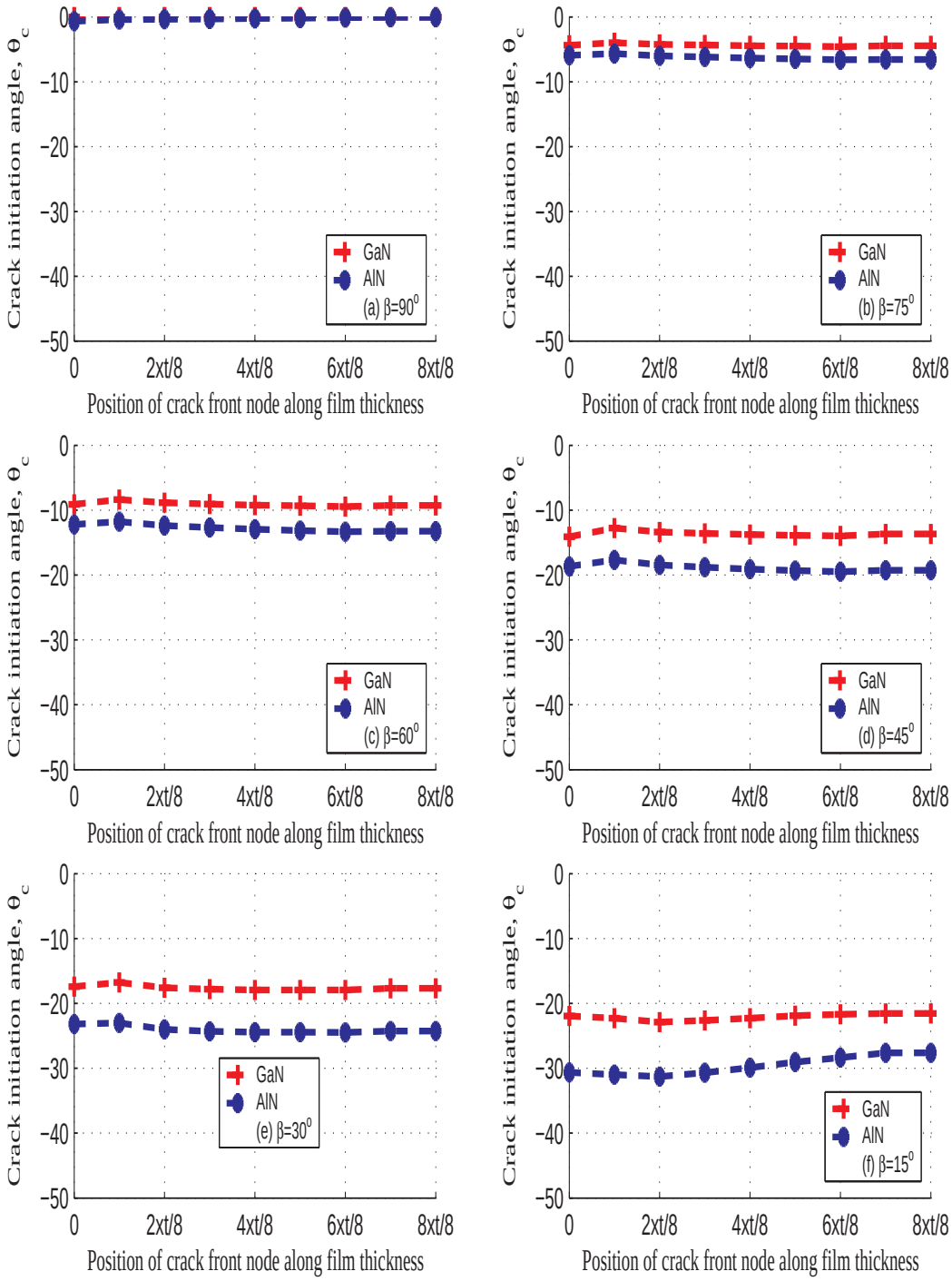

Figure 6.13. Crack initiation angles, θ_p for $a/W = 0.2$

The effect of the crack length on the crack initiation angles is inverse proportional as presented in figure 6.15. For increasing crack length, a/W ratio, crack initiation angles decrease for each initial crack angle.

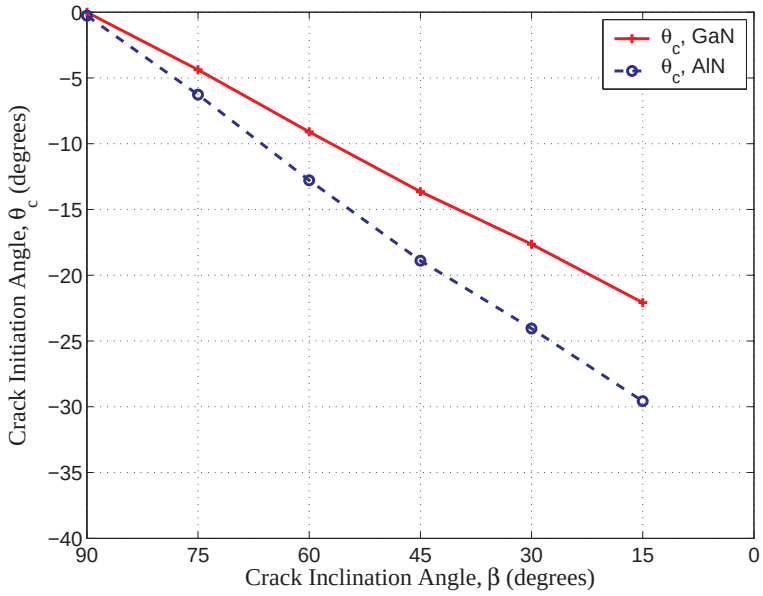

Figure 6.14. Crack initiation angle vs crack inclination angle for $a/W = 0.2$

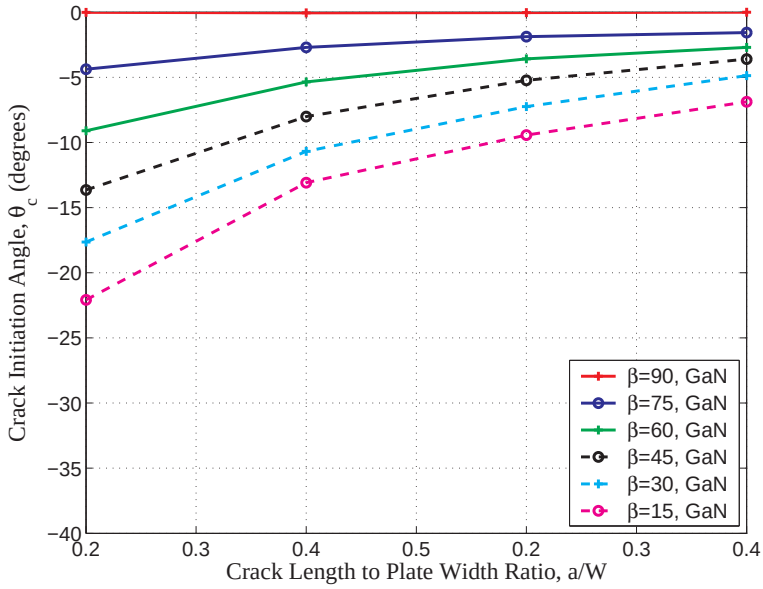

Figure 6.15. Crack initiation angle vs a/W

6.2.3. Energy Release Rate

Crack front moves as a function of the energy release rate due to relative motion of the nodes on each layer of the crack front along film thickness. Energy release rate for $a/W = 0.2$ is presented in figure 6.16 to show the relative next quasi-static time position of the crack front nodes. Energy release rate is found out to be lower at thin film and substrate interface where it is maximum at the free surface position. This is the case for crack length to plate ratios $a/W = 0.3, 0.4$ and 0.5. Energy release rate does not increase with increasing crack length due to steady state cracking phenomenon where cracking energy release rate reaches its steady state value after several film thickness of crack length. As it will be discussed on the following chapters, the steady state crack front shape is also found by successive iterations based on the energy release rate calculations and updated crack front geometry based on the energy release rate of each element layer with respect to average energy release rate of the crack front.

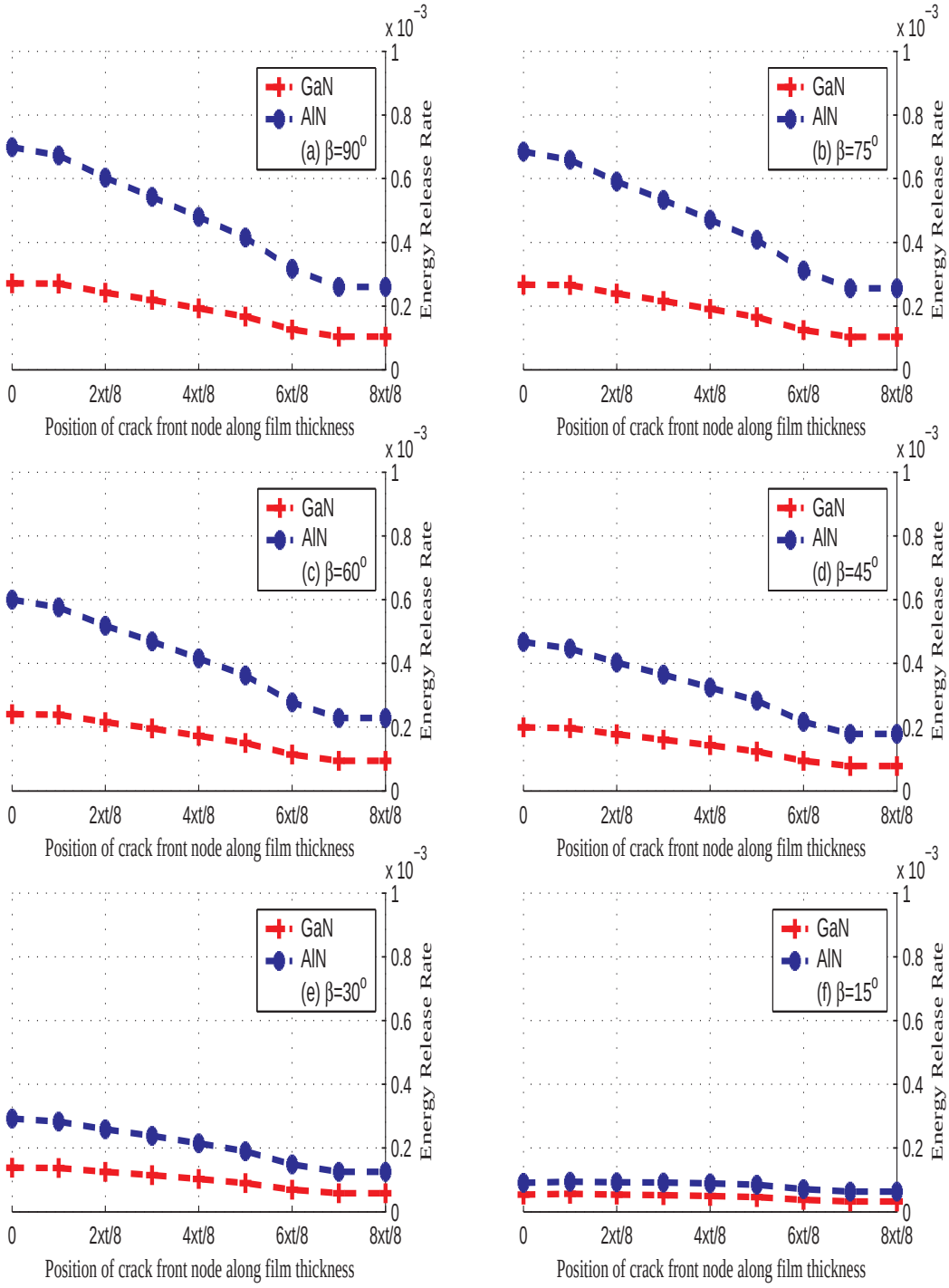

Figure 6.16. Energy release rate along crack front nodes for $a/W = 0.2$

6.2.4. Normal Distribution on Thin Film-Elastic Substrate

Normal stress, σ_{yy}, distribution is also studied along the path, which passes through the tip of the crack at several film thickness positions. The results are presented in figures 6.18 to 6.21 for $H/W = 2$ at $\beta = 90^o$ degrees.

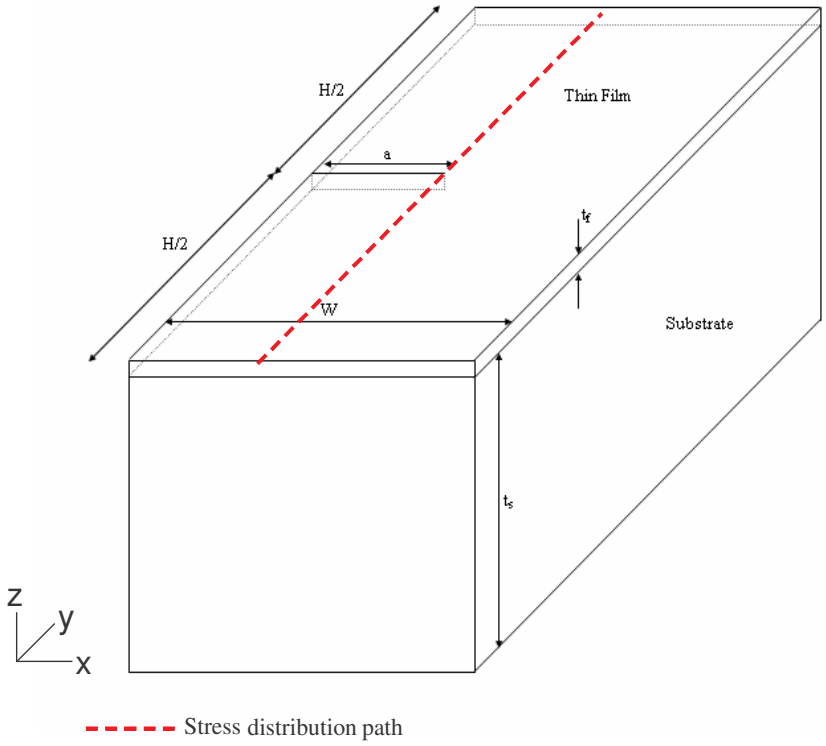

Figure 6.17. Stress distribution path

Normal stress σ_{yy}, drops gradually along film thickness from interface to free surface, in the direction of increasing film thickness. The peak of normal stress occurs at the crack tip.

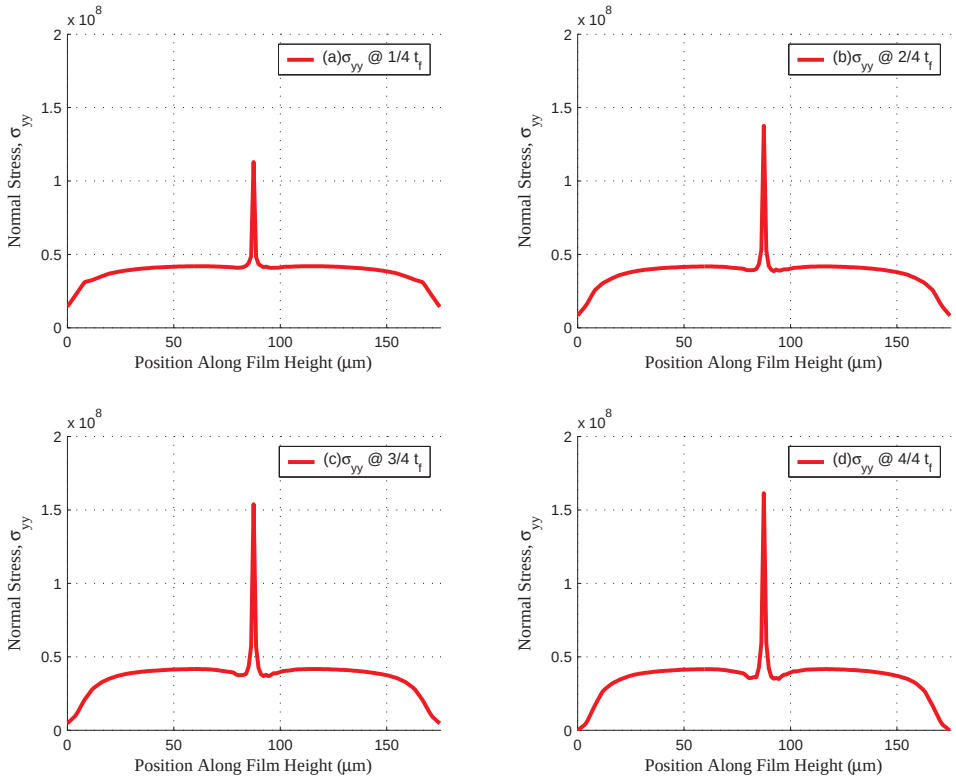

Figure 6.18. Stress distribution along thin film, $a/W = 0.2$

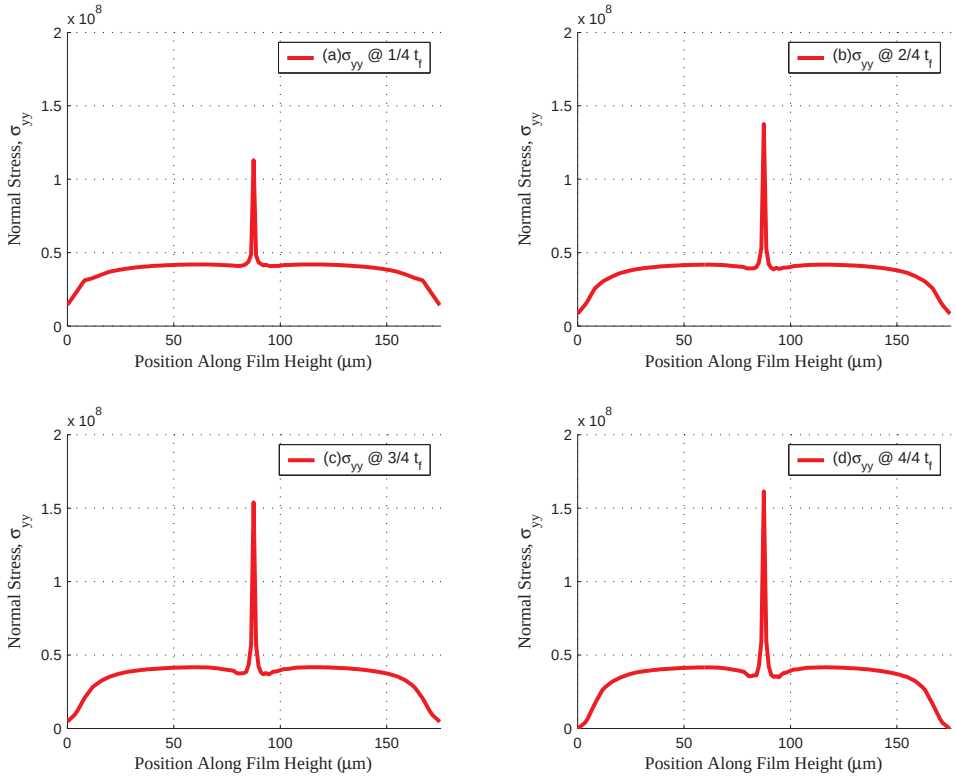

Figure 6.19. Stress distribution along thin film, $a/W = 0.3$

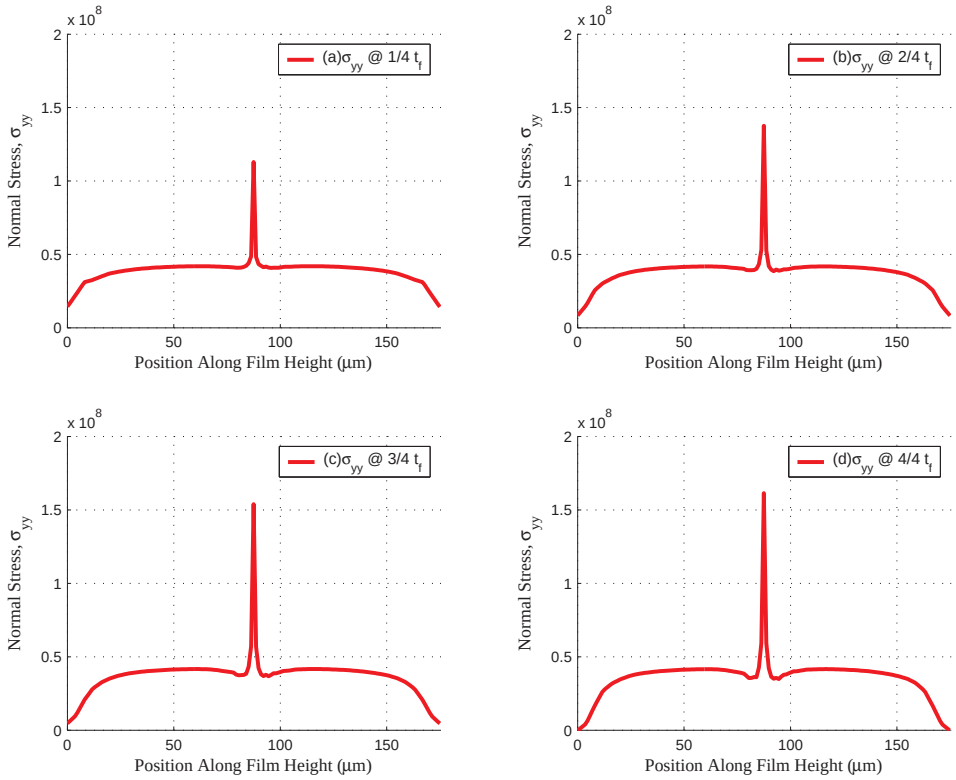

Figure 6.20. Stress distribution along thin film, $a/W = 0.4$

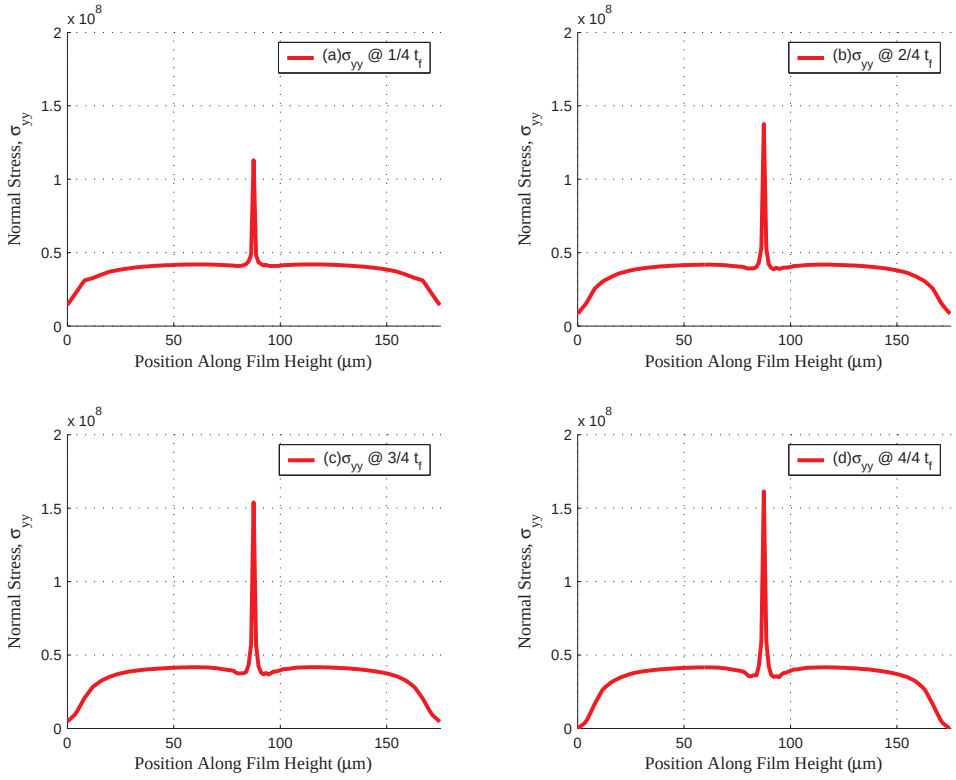

Figure 6.21. Stress distribution along thin film, $a/W = 0.5$

7. 3-D CRACK FRONT SHAPE DETERMINATION AT STEADY STATE CONDITIONS

7.1. Background & Analysis

The aim of this chapter is to analyze the steady state conditions for the channel cracking and to determine the appropriate crack front shape in 3-D for steady state conditions. Examination of the crack front shape is essential at this point as upcoming analysis will depend on the SIF calculations on each film thickness layer.

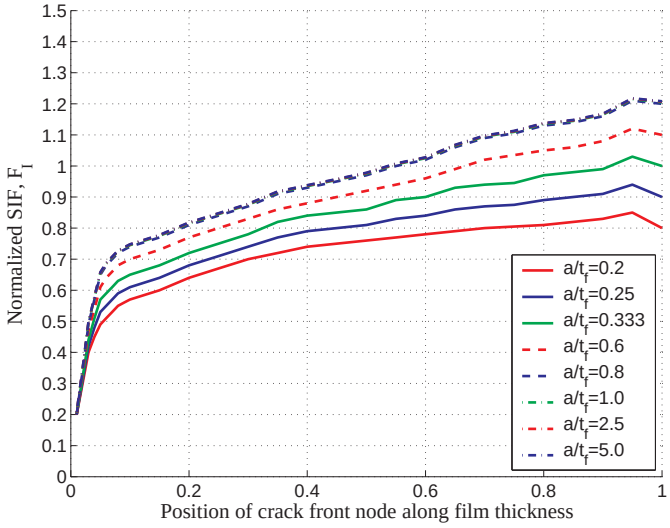

Figure 7.1. Stress intensity factor across the thickness of the film for various crack lengths. (Cross-section of thin film on crack plane is depicted) [10]

Nakamura and Kamath [10] have studied full 3-D steady state crack front shape for rigid substrate-brittle film systems in detail where they showed that the crack front attains steady state conditions once the crack length is approximately twice the film thickness. Mode-I stress intensity factor distribution along crack front is presented in figure 7.1 for several crack lengths. The stress intensity factor distribution does not vary much after crack length a, reaches approximately 2 film thickness value t_f. They showed that the leading crack edge assumes a nearly parabolic shape through the film thickness. Crack front profiles and corresponding stress intensity factor distributions are plotted in figures 7.2 and 7.3. Crack front shape is found by successive FEA iterations of model

to satisfy the constant K_I requirement along the film thickness except two ends of the front. We will use constant G (energy release rate) assumption through out our analysis as we will be dealing with mixed mode problems. The connection between assumption of constant K_I and G is well established since the energy release rate has identical behavior with that of K_I in pure mode-I problems as in case of Nakamura&Kamath's study.

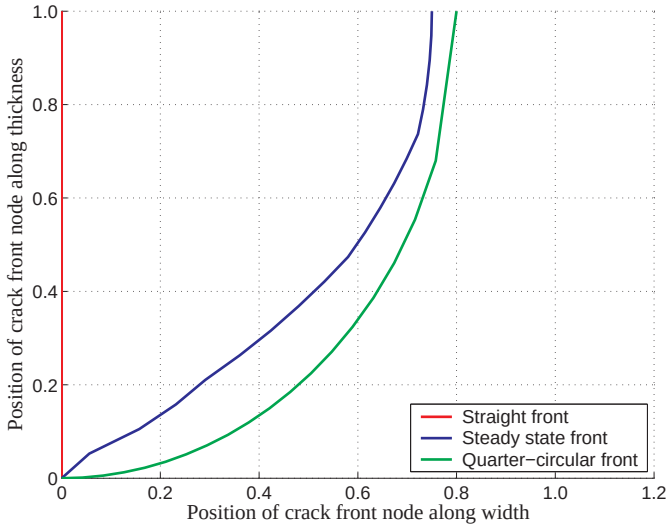

Figure 7.2. Crack front profile of thin-film on rigid substrate

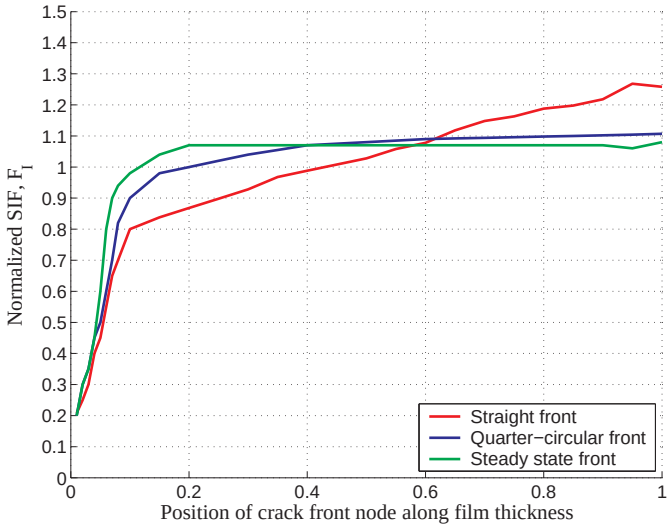

Figure 7.3. SIF of thin-film on rigid substrate

Ambrico and Begley [11] have extended the study of three-dimensional thin film cracking analysis of Nakamura and Kamath by considering the compliant substrates. They have performed fully three-dimensional finite element analysis to determine energy release rates as a function of flaw size for both contained through cracks and edge

cracks intersecting free surfaces. As a result of their studies it is found out that for edge flaws, the crack length required to achieve steady state is significantly larger than the film thickness when the substrate is more compliant than the film.

Mainly Dundurs parameter α determines whether the crack attains steady state conditions or not, where this parameter depends on the elastic mismatch between the thin film and the substrate. Two values are significant: $\alpha = -1$ corresponds to an elastic film on a rigid substrate, $\alpha = 0$ corresponds to a homogenous elastic system.

$$\alpha = \frac{E_f/\left(1-\nu_f^2\right) - E_s/\left(1-\nu_s^2\right)}{E_f/\left(1-\nu_f^2\right) + E_s/\left(1-\nu_s^2\right)} \tag{7.1}$$

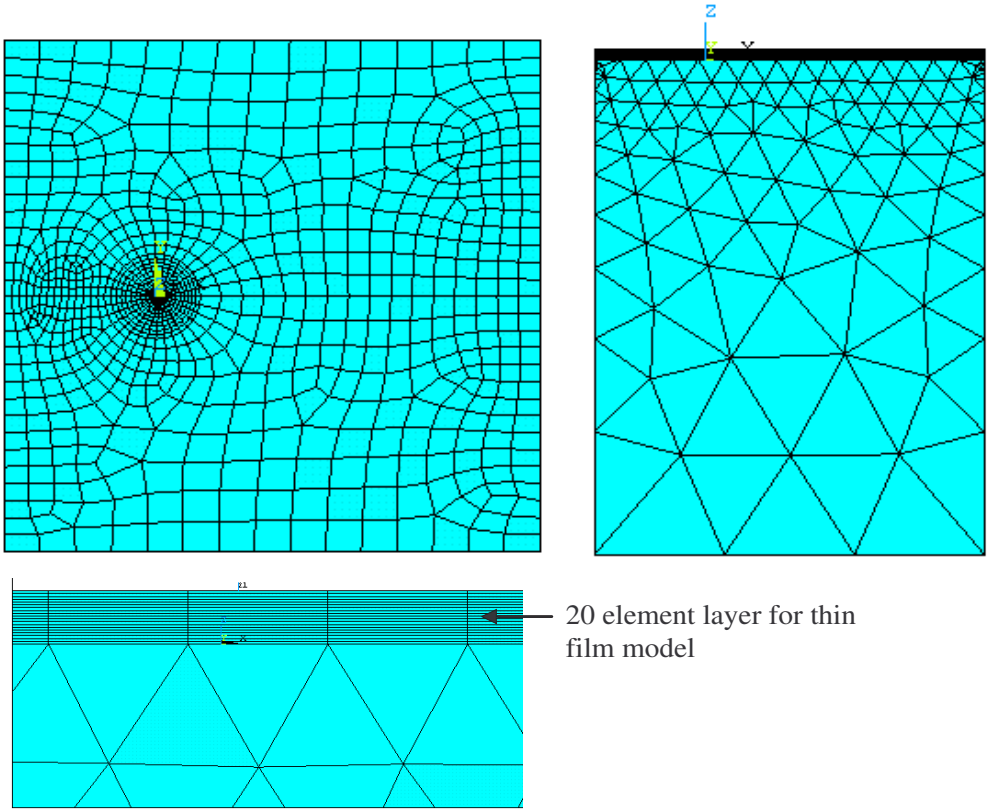

Figure 7.4. FEA mesh for crack front determination analysis

Ambrico and Begley have shown that the steady state is reached in homogeneous elastic systems for edge cracks at $a/t_f \cong 20$. As the compliance of the substrate

Table 7.1. Thin film-substrate systems

	E_f (Young's Modulus - Film)	E_s (Young's Modulus - Substrate)	Dundurs Parameters - α
GaN / Si	181 GPa	131 GPa	0.16
Si / SiC	131 GPa	420 GPa	-0.52

increases, the crack length required to reach steady state increases and decreases for stiffer substrates.

In this study, thin film is modeled with 20-noded brick elements with 20 element layers along the film thickness. Substrate is modeled with 10 node tetrahedral elements of coarse mesh. Pyramid elements are used for transition region from brick to tetrahedral elements. Crack tip is meshed manually by placing singular elements.

Equal amount pressure is applied on substrate vertical walls to attain bi-axial stress state through thin film where the substrate walls are kept in proper boundary conditions to prevent rigid body motion of the model.

We have studied both stiff substrates as well as compliant substrates. Two different thin film-substrate systems were studied as GaN film on Si substrate for compliant substrate case and Si film on SiC substrate for stiff substrate case. The systems have Dundurs parameter α of value 0.16 and -0.52 respectively. Si/SiC system is expected to give results similar to as of Nakamura and Kamath as $\alpha = -0.52$ is more near to rigid substrate value of $\alpha = -1$.

For channeling crack analysis, the analysis will give more robust solutions for stiffer substrates as steady state is reached on shorter edge crack lengths. This will restrict the concern region to the gray area shown in figure 7.5 of Energy release rate for elastic cracks vs. channeling crack length presented by Ambrico and Begley.

The crack front shape corresponding to nearly constant energy release rate (G) across the thickness is determined using an iterative remeshing of the finite element

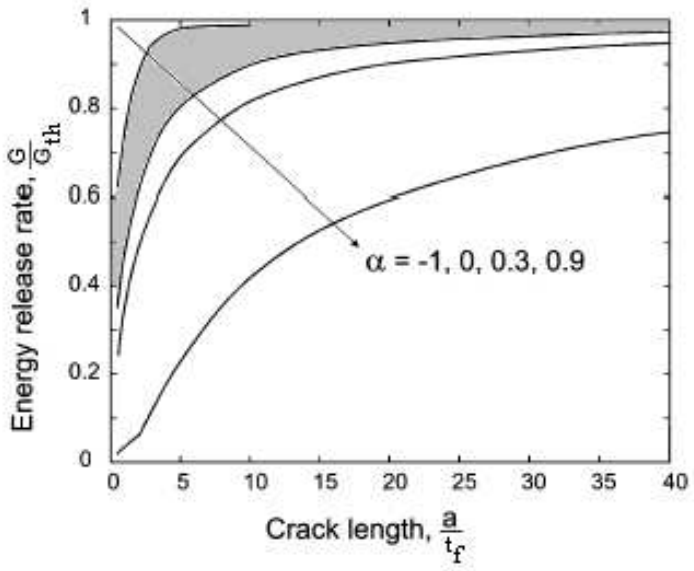

Figure 7.5. Energy release rate for elastic cracks vs. channeling crack length [11]

model. During the remeshing, the crack front nodes are shifted in the crack direction (x-dir in this case) based on the difference between plain strain energy release rate calculated at a node and the average plain strain energy release rate for the entire crack front(G_{ave}). For example, if G at a node is higher than G_{ave}, then its x coordinate is increased proportional to the normalized difference $(G - G_{ave})/G_{ave}$. The process is carried out for all crack front nodes and repeated for several iterations.

The iterative algorithm is as shown in figure 7.6. The steady state crack front shape obtained as a result of the iterative analysis can then be used in the subsequent crack propagation analysis as the increasing crack length guarantees the steady state nature of the crack propagation (a/t_f ratio increases on each successive propagation step).

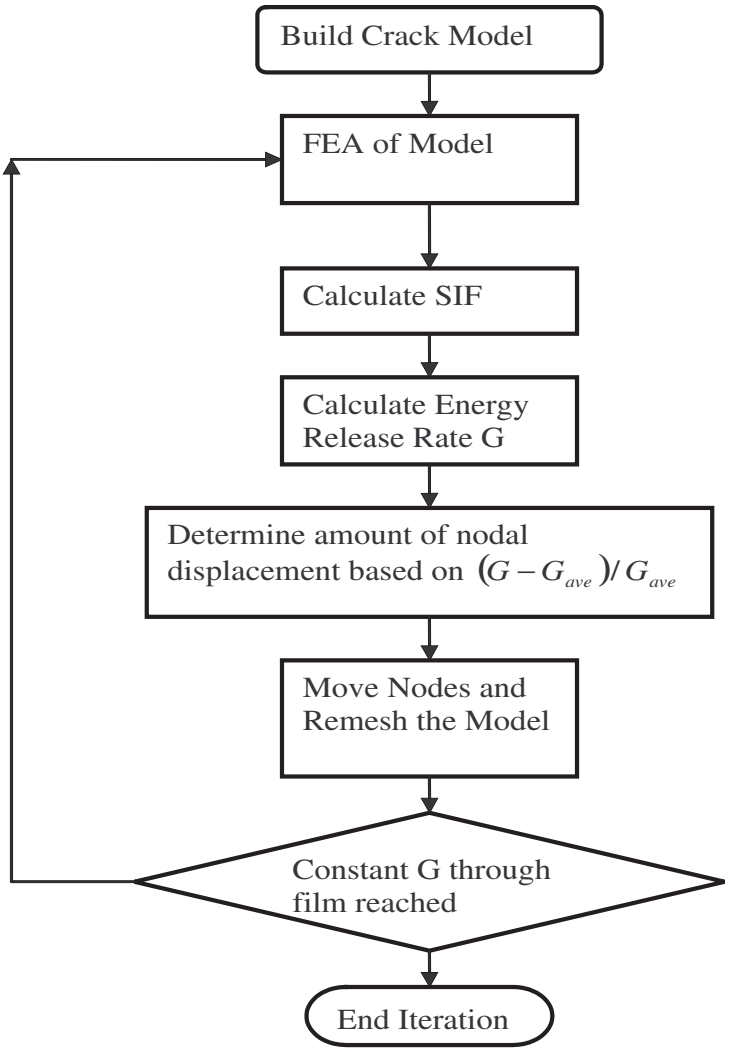

Figure 7.6. Crack front shape determination algorithm

The proposed study is applied for an initial crack having straight crack front. The results of the analysis performed by assuming straight crack front as initial profile are in good agreement with Nakamura and Kamath and are presented in figures .

From the iterative analysis results, it is found out that for a/W ratio 0.3 and a/t_f ratio 11.25 the SIF and crack front profile does not depend highly on the Dundur's parameter α. The value of the SIF is higher on compliant substrate case as the strain transferred from substrate to film is higher. The SIF profile tends to have more of equal value on each successive iteration; as it can be observed in figures 7.7 through 7.10.

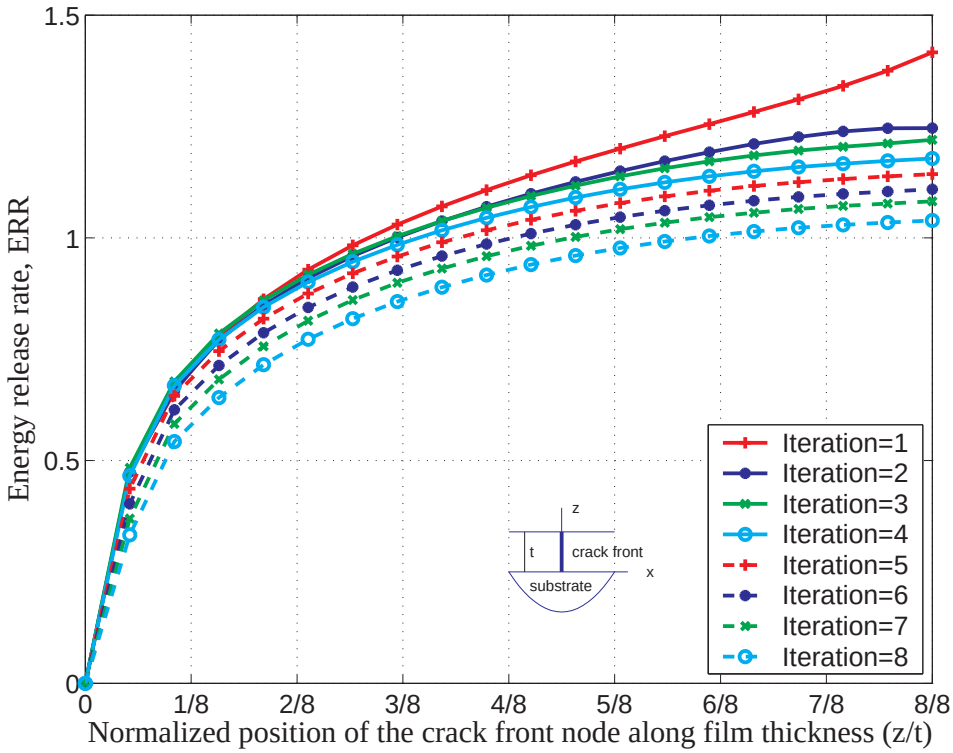

Figure 7.7. SIF along film thickness for compliant ($\alpha = 0.16$) substrate - Straight line as initial profile

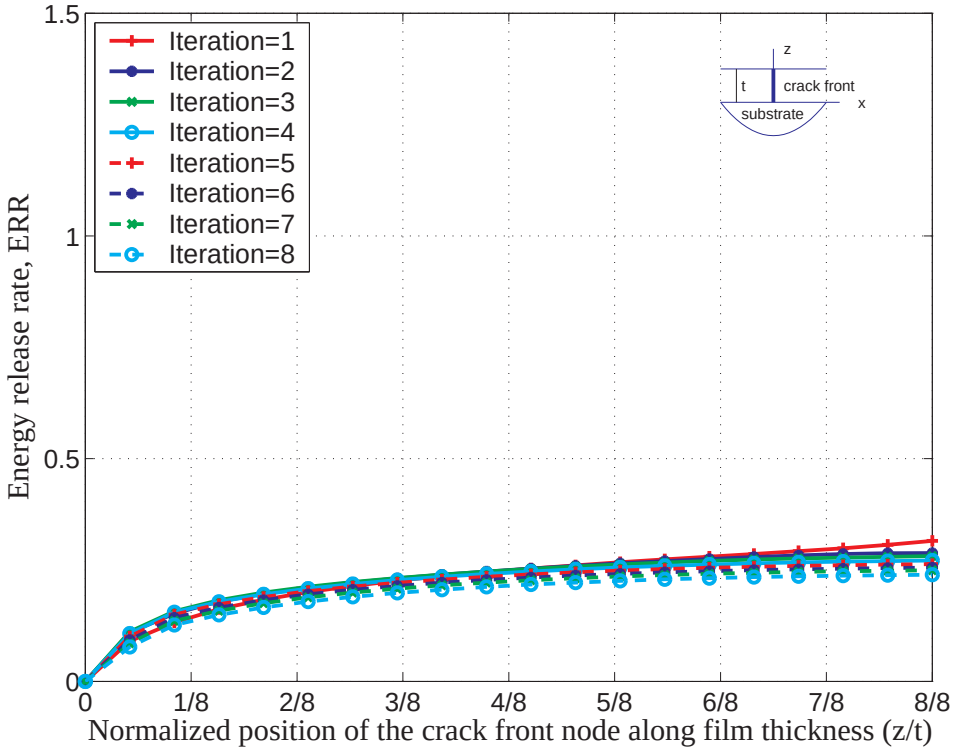

Figure 7.8. SIF along film thickness for stiffer ($\alpha = -0.52$) substrate - Straight line as initial profile

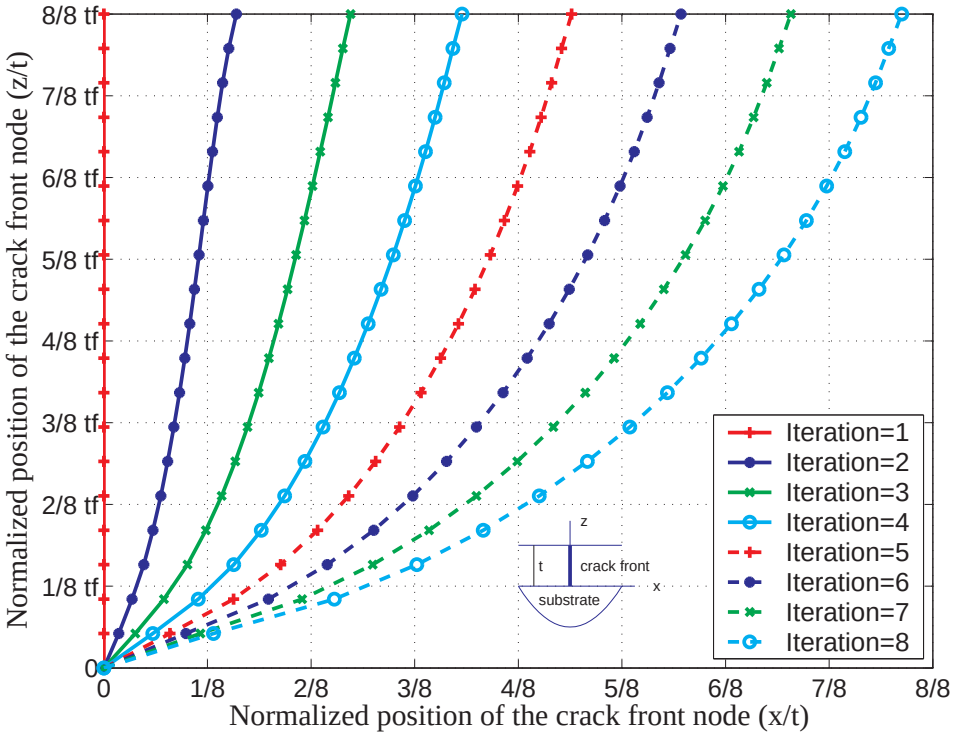

Figure 7.9. Crack front shape for compliant ($\alpha = 0.16$) substrate - Straight line as initial profile

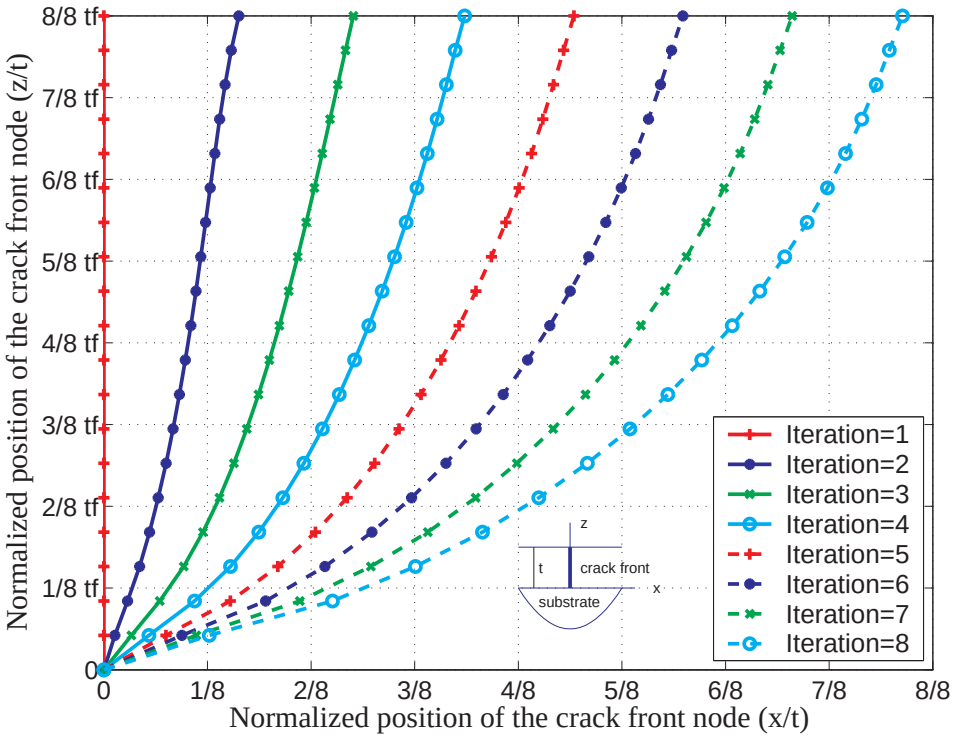

Figure 7.10. Crack front shape for stiffer ($\alpha = -0.52$) substrate - Straight line as initial profile

8. CRACK PROPAGATION ANALYSIS OF SQUARE PLATE THIN FILM-SUBSTRATE SYSTEM WITH A CUT EDGE

8.1. Background & Analysis

Crack propagation in three-dimensional thin film and substrate systems are studied in this chapter for square plate. Figure 8.1 shows the problem geometry where the one corner of the square film is cut. The elastic substrate is under equal biaxial loading. The crack propagation is investigated for 4 different cut lengths. The effect of interface is studied by performing the analysis with and without interface. A nonlinear (bilinear) material model is used for the investigation of interface effect on crack propagation path.

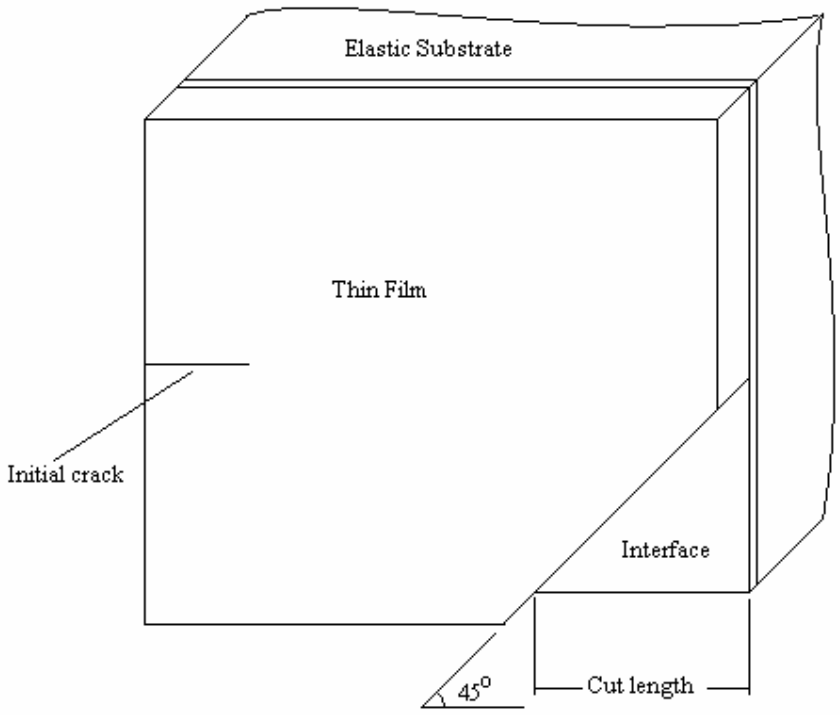

Figure 8.1. Square plate crack propagation geometry

The study of Liang et. al. [4] includes a background to square plate with a cut edge analysis. They have presented analysis of mud crack pattern. They have showed that the crack tips intersect crack lines at right angles. This phenomenon is important for the parallel crack interactions also where sequential crack propagation is studied. In addition, it is observed that two crack tips approaching each other will bypass each other and then be attracted to each other to form a small cell. However, the two crack tips traveling parallel to each other tend to repel. Same type of interactions is expected to be observed for crack tip to approach the cut face at right angle.

Finite element model includes both tetrahedral and hexahedral elements for the elastic substrate and the thin film. Figure 8.2 shows the finite element mesh constructed for the square thin film-substrate analysis.

There are 10 layers along the film thickness with the same pattern at each element layer. The interface is modeled with the transitional elements from hexahedral to tetrahedral. The material properties are taken to be as of the elastic substrate for no interface effect case.

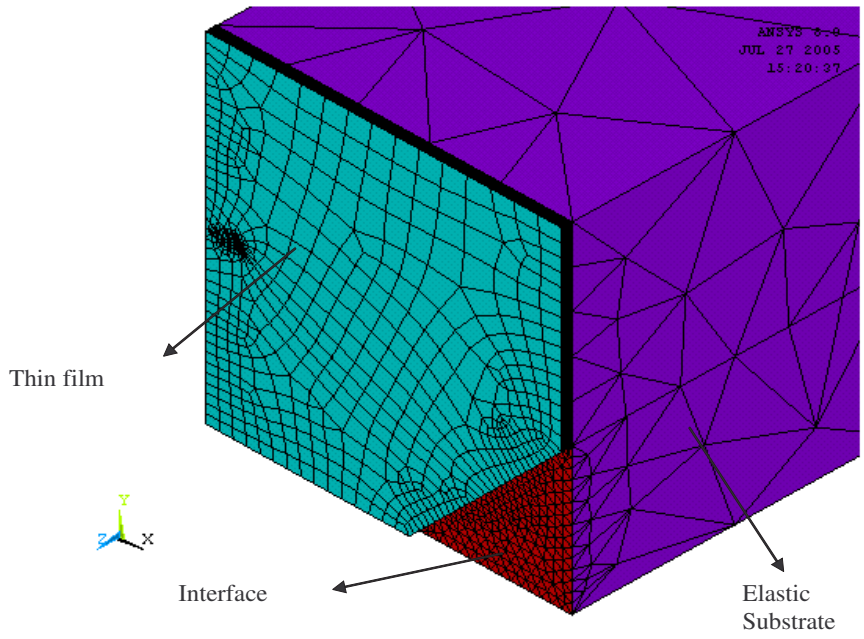

Figure 8.2. Finite element model for square thin plate and substrate analysis

8.2. Curved Crack Front vs. Straight Crack Front

Square thin film substrate system with an edge crack and a cut edge on opposite side is studied by imposing straight crack front and using steady state curved crack front. It is found out that the crack propagation paths for straight crack front and curved crack front are very similar. Therefore one can deduce that the crack front shape does not play a major role in the determination of crack interactions and prediction of crack propagation paths. Based on this outcome for meshing purposes straight crack front will be used. The propagation paths for curved and straight crack fronts are presented in the following three figures, 8.3 to 8.5.

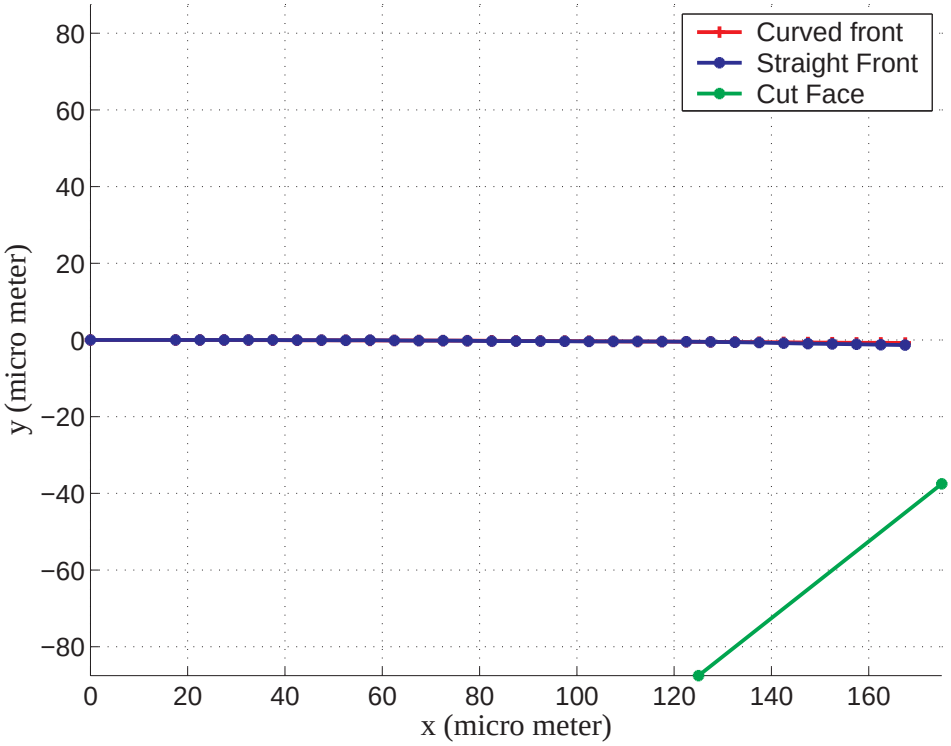

Figure 8.3. Crack propagation on a square plate with a corner cut; Curved vs. straight crack front, cut length = 50/175

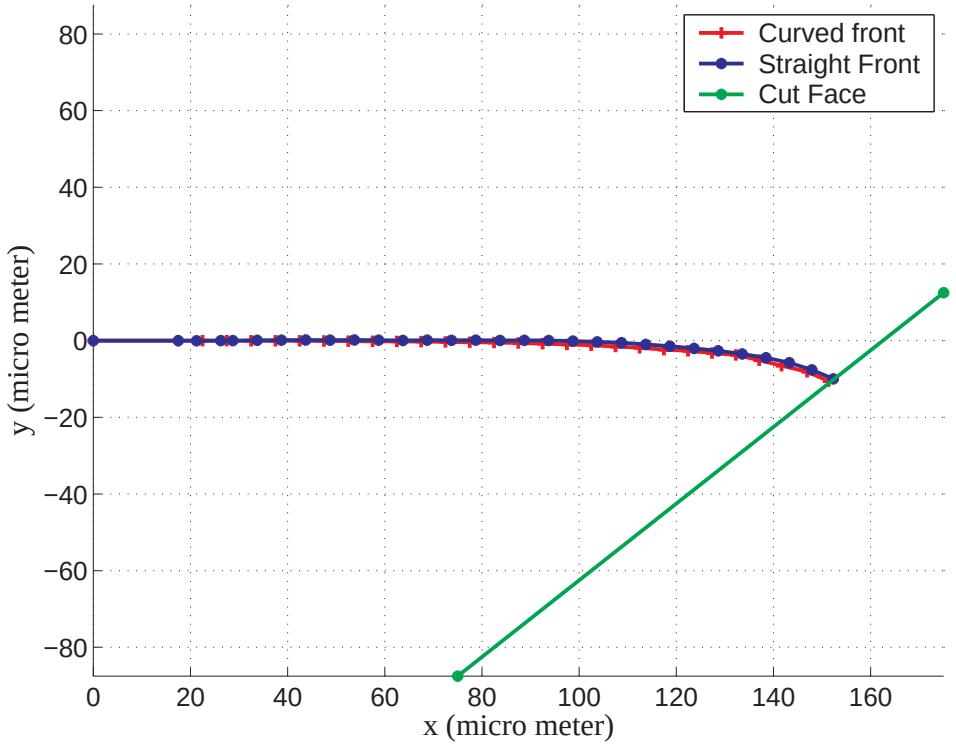

Figure 8.4. Crack propagation on a square plate with a corner cut; Curved vs. straight crack front, cut length = 100/175

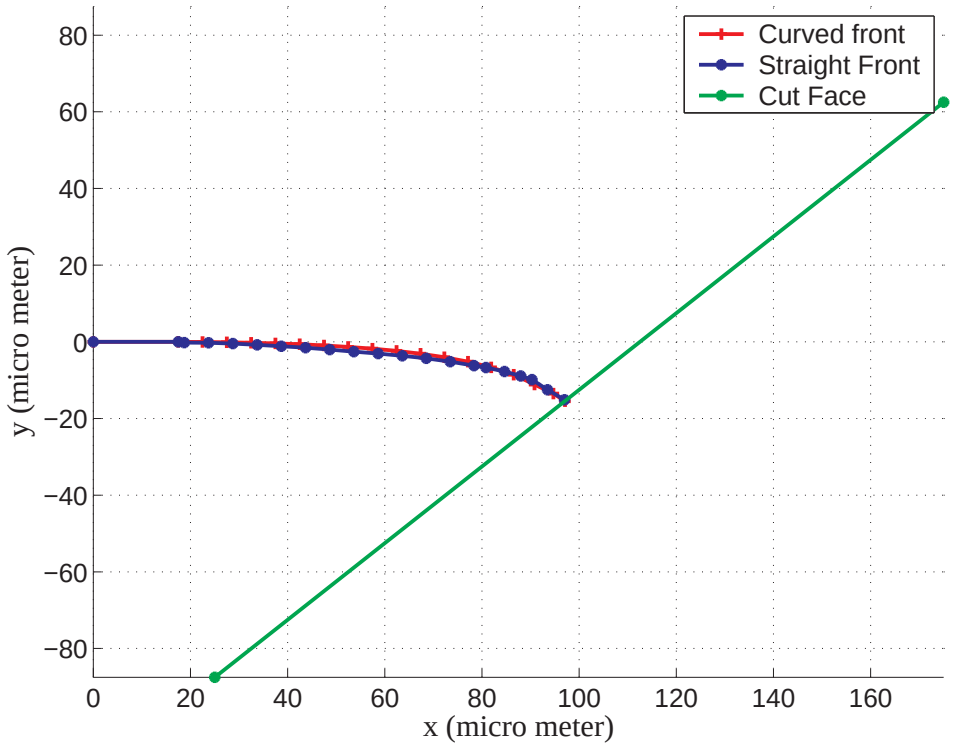

Figure 8.5. Crack propagation on a square plate with a corner cut; Curved vs. straight crack front, cut length = 150/175

8.3. Effect of Interface

8.3.1. Interface Modeling by Bilinear Material

Interface effect on crack propagation path is studied by modeling interface layer as a separate layer between thin film and substrate. Interface thickness is taken to be 1/5 of film thickness t_f. Interface material is taken to be nonlinear. A bilinear model is used for modeling the interface effect. Bilinear isotropic hardening ($BISO$) option uses the Von Mises yield criteria coupled with an isotropic work hardening assumption. The material behavior is described by a bilinear stress-strain curve(figure 8.6) starting at the origin with positive stress and strain values. The initial slope of the curve is taken as the elastic modulus of the substrate material. At the specified yield stress (σ_y), the curve continues along the second slope defined by the tangent modulus C (having the same units as the elastic modulus). C is taken to be 0 for further analysis, which is a model of elastic perfectly plastic material. Two different values of σ_y, 50MPa and 75Mpa is used to study the effect of interface.

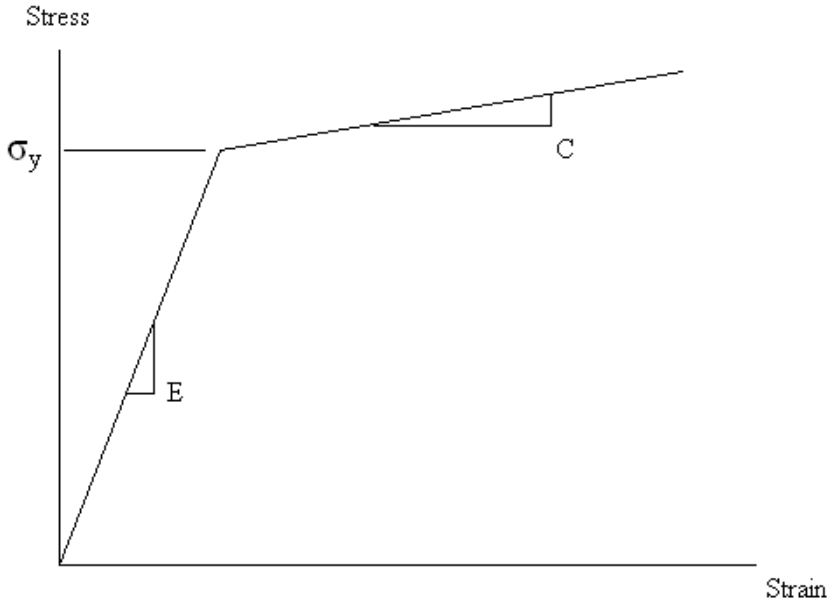

Figure 8.6. Bilinear isotropic hardening, nonlinear material model for interface

The Von Mises stresses and the plastic deformation of the interface layer is plotted in figures 8.7 and 8.8 respectively for the case of cut length equal to 50 microns and

σ_y equal to 50 MPa. It is seen that most of the film is subject to plastic deformation to some amount, especially near crack tip. Those elements plastically deformed can be treated as failed elements as elastic-perfectly plastic material model is used.

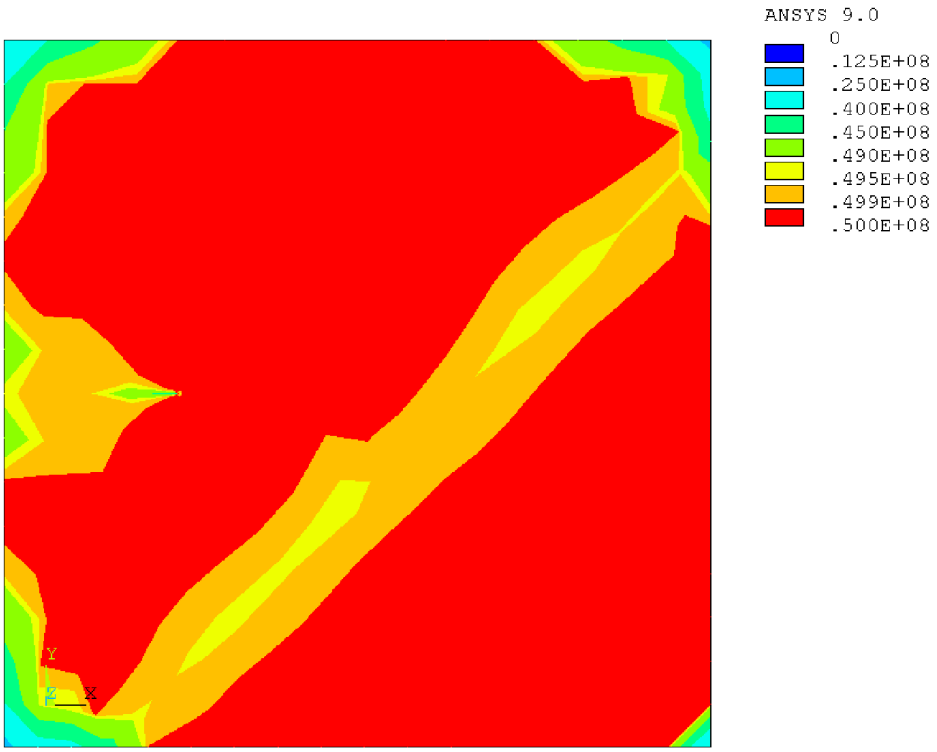

Figure 8.7. Von Mises stress distribution of interface layer-Cut length = 50/175 x film width, σ_y=50 MPa

Crack propagation paths are presented in figures 8.9 through 8.11 for interface and no interface cases. For square crack propagation analysis it is seen that the crack tip approaches to cut edge about 90^o , except the smallest cut length, which is 50/175 times the film width. The propagation path is found out to be similar for interface and no interface cases. It can be concluded that presence of an interface layer has minimum effect on crack propagation paths.

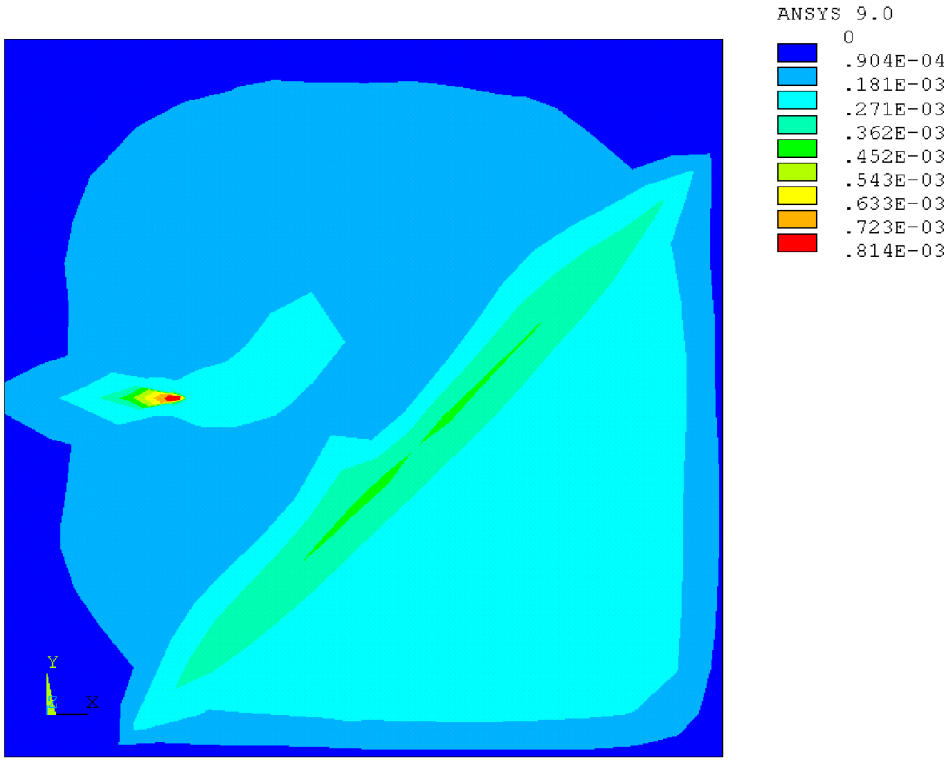

Figure 8.8. Plastic deformation of interface layer-Cut length = 50/175 x film width, σ_y=50 MPa

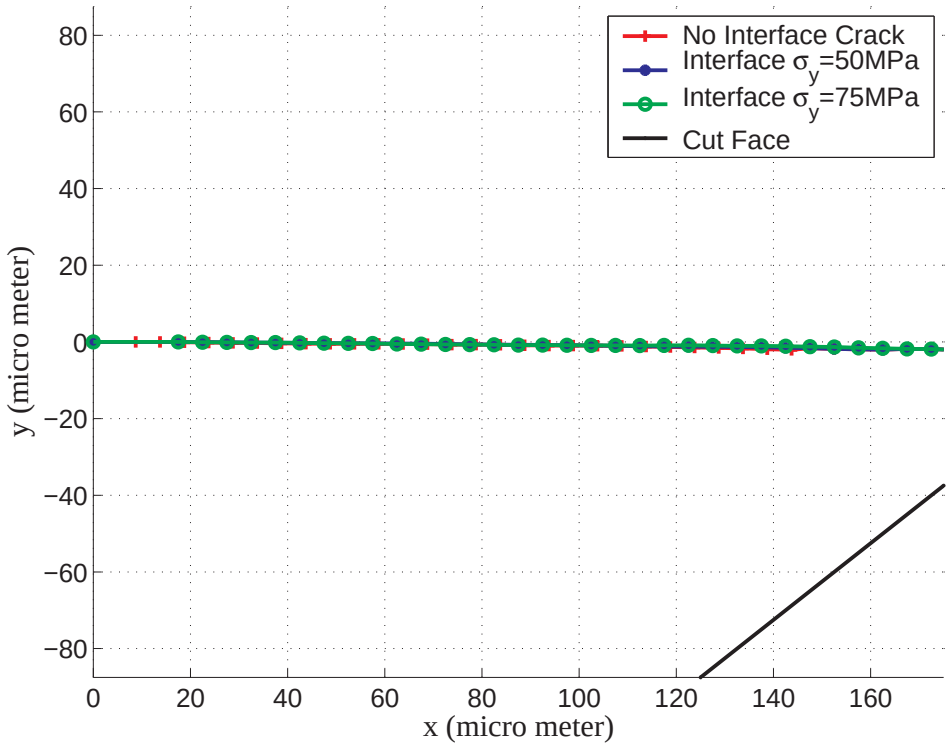

Figure 8.9. Square plate analysis for interface and no interface case-Cut length = 50/175 x film width

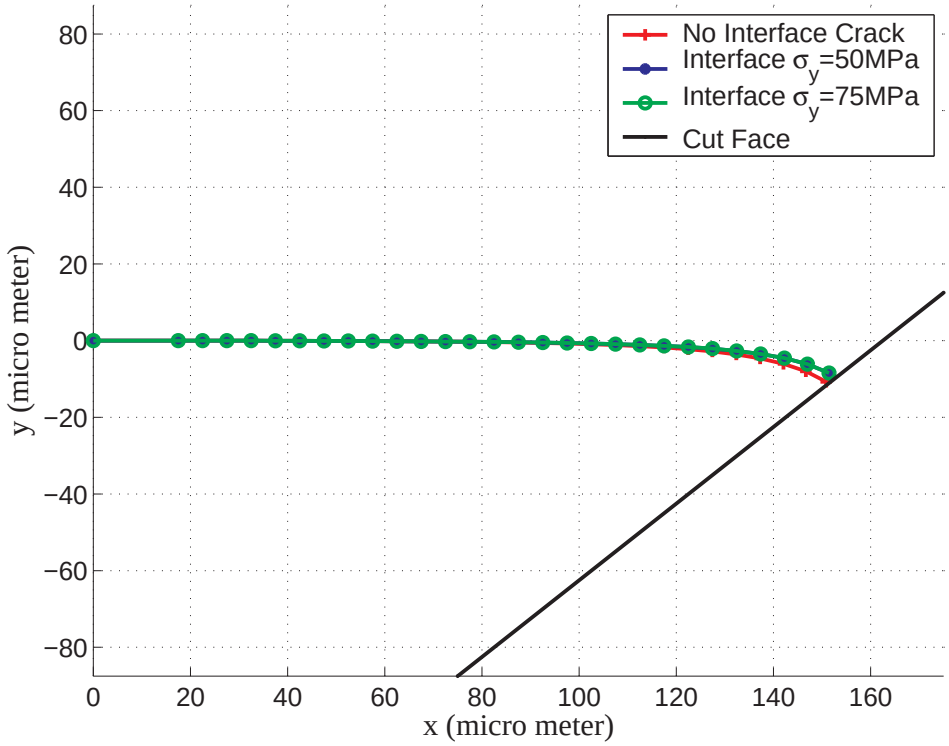

Figure 8.10. Square plate analysis for interface and no interface case-Cut length = 100/175 x film width

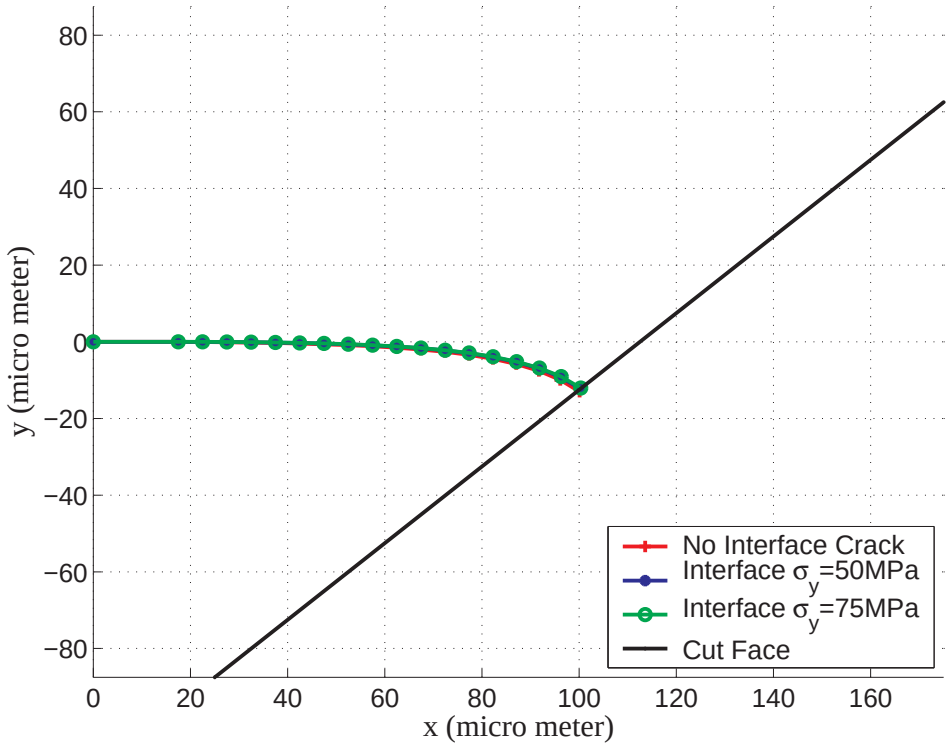

Figure 8.11. Square plate analysis for interface and no interface case-Cut length = 150/175 x film width

Table 8.1. Crack propagation path for no interface case list-Cut length = 150/175 x film width

Propagation step	X (micron)	Y (micron)	θ_c (degrees)
1	0.00	0.00	0.00
2	17.50	0.00	0.00
3	22.50	-0.04	-0.47
4	27.50	-0.10	-0.69
5	32.50	-0.19	-1.02
6	37.50	-0.30	-1.32
7	42.50	-0.45	-1.64
8	47.49	-0.64	-2.22
9	52.49	-0.88	-2.72
10	57.48	-1.17	-3.30
11	62.46	-1.52	-4.10
12	67.44	-1.99	-5.30
13	72.41	-2.59	-6.96
14	77.35	-3.37	-8.99
15	82.24	-4.39	-11.75
16	87.06	-5.74	-15.63
17	91.73	-7.52	-20.84
18	96.12	-9.90	-28.49
19	100.10	-12.94	-37.36

Table 8.2. Crack initiation angles for last propagation step-Cut length = 150/175 x film width

Node location (z/t_f	θ_c (degrees)	Averaged θ_c (degrees)
1/10	-6.46	-9.46
2/10	-7.50	-9.46
3/10	-8.33	-9.46
4/10	-9.06	-9.46
5/10	-9.67	-9.46
6/10	-10.16	-9.46
7/10	-10.55	-9.46
8/10	-10.82	-9.46
9/10	-10.98	-9.46
10/10	-11.03	-9.46

Crack propagation path is listed in table 8.1 with the crack initiation angles. It is seen that the free edge approach angle is approximately -37^o, where it should be -45^o for a 90 degree approach. This is due to incremental propagation step size and averaging of the crack initiation angles along the crack front. The last line is actually a calculated value from the previous step, meaning it is not analyzed. As it can be seen from the table, there is an decrease trend in crack initiation angle at each successive propagation step. Therefore it is expected for the crack tip to reach the free surface at a lower angle (more near to 90^o) than calculated -37^o. In addition, when the crack initiation angle distribution is investigated, it can be seen (table 8.2) that the top free surface nodes face lower crack initiation angles. So average value is not much but a higher value. So the visible top node of the crack front actually approaches to the free edge almost at right angles.

8.3.2. Interface Modeling by Cohesive Zone Material

Interface between thin film and substrate is modeled also using cohesive zone material model which directly introduces fracture mechanism by adopting softening relationships between traction and the separation. This type of modeling introduces a critical fracture energy that is also the energy required to break apart the interface surfaces. Cohesive zone model consists of a constitutive relation between the traction T acting on the interface and the corresponding interfacial separation δ (displacement jump across the interface) [29].

The interfacial separation is defined as the displacement jump, δ, i.e., the difference of the displacements of the adjacent interface surfaces:

$$\delta = u^{TOP} - u^{BOTTOM} = interfacial\ separation \tag{8.1}$$

The definition of the separation is based on local element coordinate system, figure 8.12. The normal of the interface is denoted as local direction n, and the local tangent direction is denoted as t. Thus:

$$\delta_n = n.\delta = normal\ separation \tag{8.2}$$

$$\delta_t = t.\delta = tangential(shear)\ separation \tag{8.3}$$

An exponential form of the cohesive zone model, originally proposed by Xu and Needleman [30], uses a surface potential:

$$\phi(\delta) = e\sigma_{max}\overline{\delta}_n \left[1 - (1 + \Delta_n) e^{-\Delta_n} e^{-\Delta_n^2}\right] \tag{8.4}$$

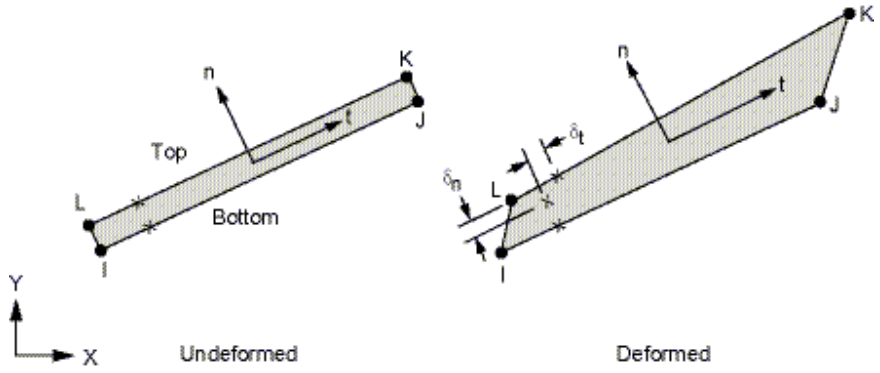

Figure 8.12. Schematic of interface elements

where:

$\phi(\delta)$ = surface potential

σ_{max} = maximum normal traction at the interface

$\overline{\delta}_n$ = normal separation across the interface where the maximum normal traction is attained with δ_t=0

$\overline{\delta}_t$ = shear separation where the maximum shear traction is attained at $\delta_t = \frac{\sqrt{2}}{2}\overline{\delta}_t$

$\Delta_n = \frac{\delta_n}{\overline{\delta}_n}$

$\Delta_t = \frac{\delta_t}{\overline{\delta}_t}$

The traction is defined as:

$$T = \frac{\partial \phi(\delta)}{\partial \delta} \tag{8.5}$$

or

$$T_n = \frac{\partial \phi(\delta)}{\partial \delta_n} \tag{8.6}$$

and

$$T_t = \frac{\partial \phi(\delta)}{\partial \delta_t} \tag{8.7}$$

16-noded interface elements are used to model cohesive zone interface between thin film and substrate. Maximum normal traction is taken to be 50MPa and 75MPa and corresponding crack propagation paths are plotted in figures 8.13 to 8.15. It is seen that the effect of interface strength is minimal and can be ignored.

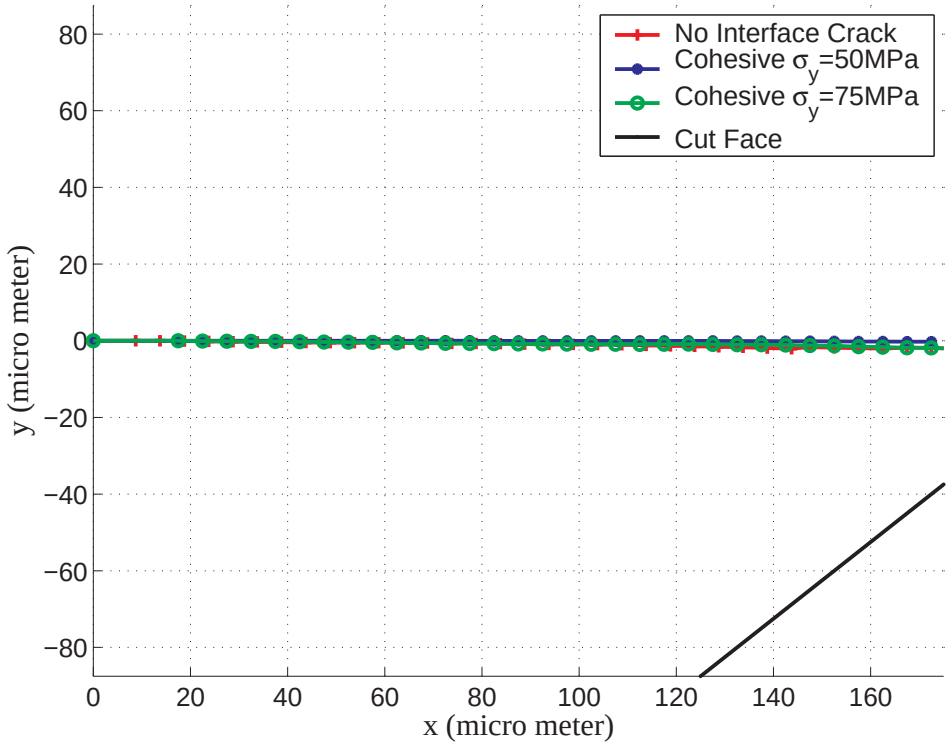

Figure 8.13. Square plate analysis for interface and no interface case-Cut length = 50/175 x film width

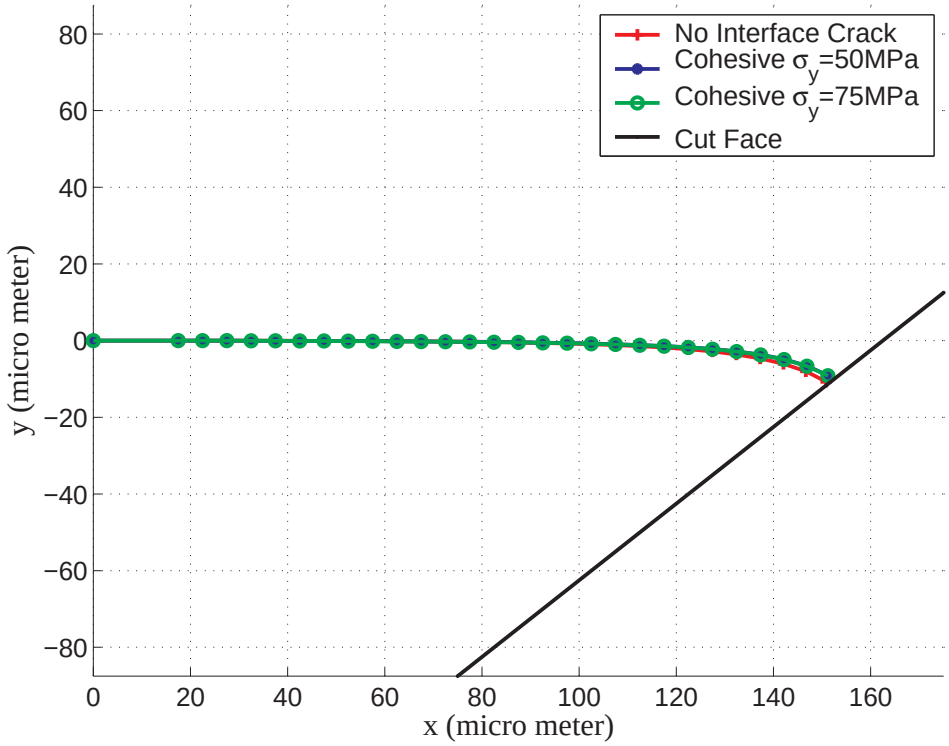

Figure 8.14. Square plate analysis for interface and no interface case-Cut length = 100/175 x film width

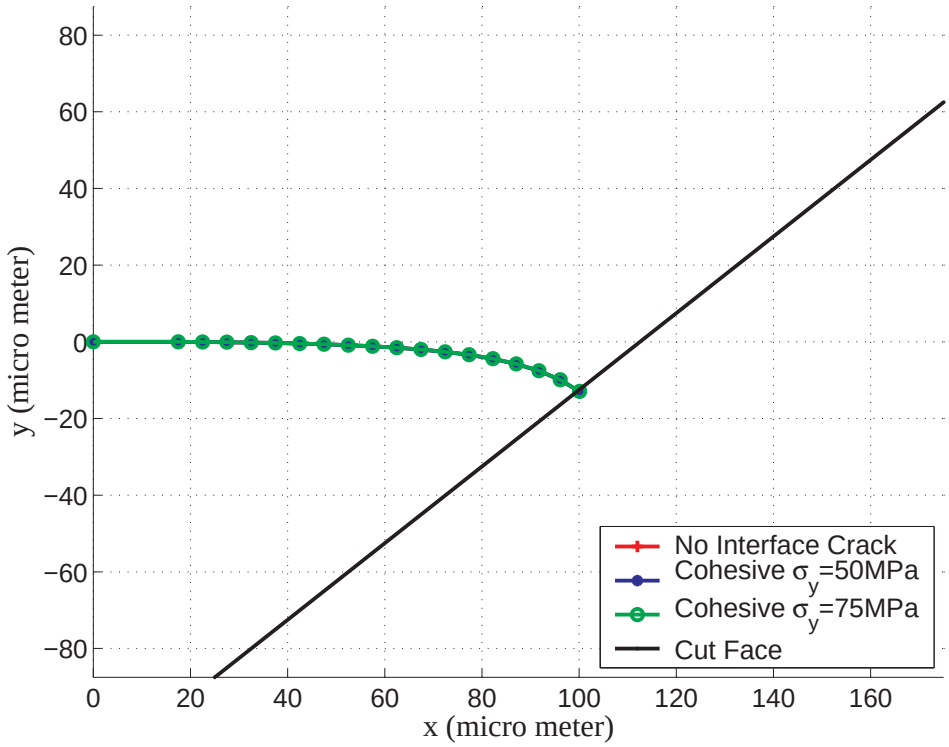

Figure 8.15. Square plate analysis for interface and no interface case-Cut length = 150/175 x film width

8.4. Effect of Elastic Mismatch

Crack propagation analysis in square thin film-substrate system with an edge crack is also performed with three different material systems corresponding to $\alpha = -0.36$, $\alpha = 0.36$ and $\alpha = 0.79$. As shown by Xia and Hutchinson [3], it is expected to observe earlier turn of cracks with more compliant substrates, that is with higher α values. Crack propagation paths are plotted in figures 8.16 to 8.18. As expected, for $\alpha = 0.79$ case, crack turns to cut edge before than the two stiffer substrate systems.

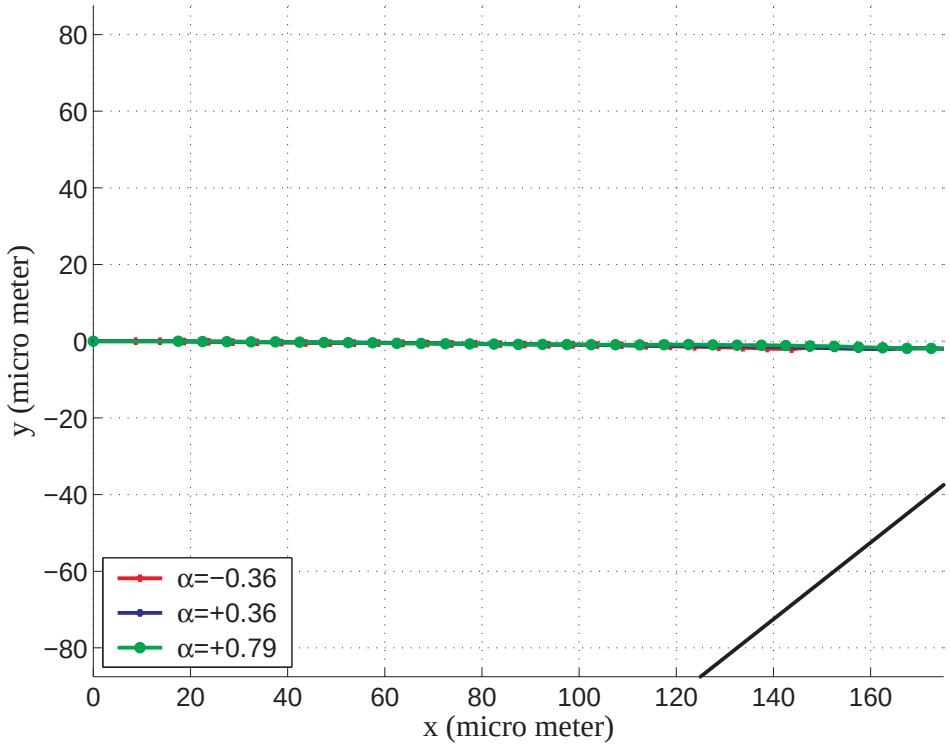

Figure 8.16. Crack propagation on a square plate with a corner cut; Elastic mismatch effect, cut length = 50/175

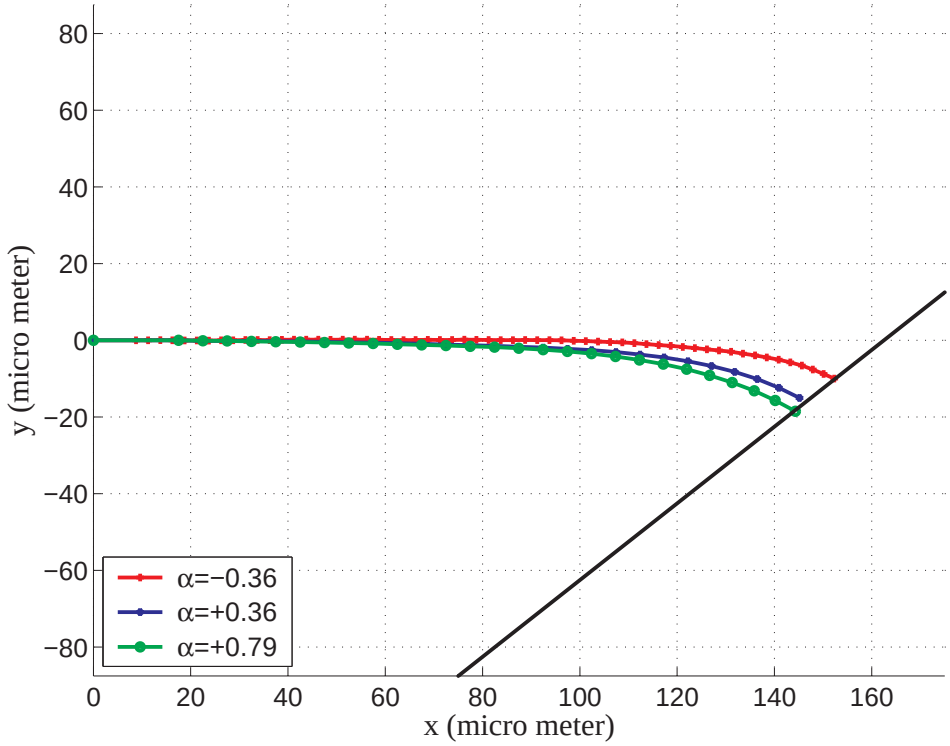

Figure 8.17. Crack propagation on a square plate with a corner cut; Elastic mismatch effect, cut length = 100/175

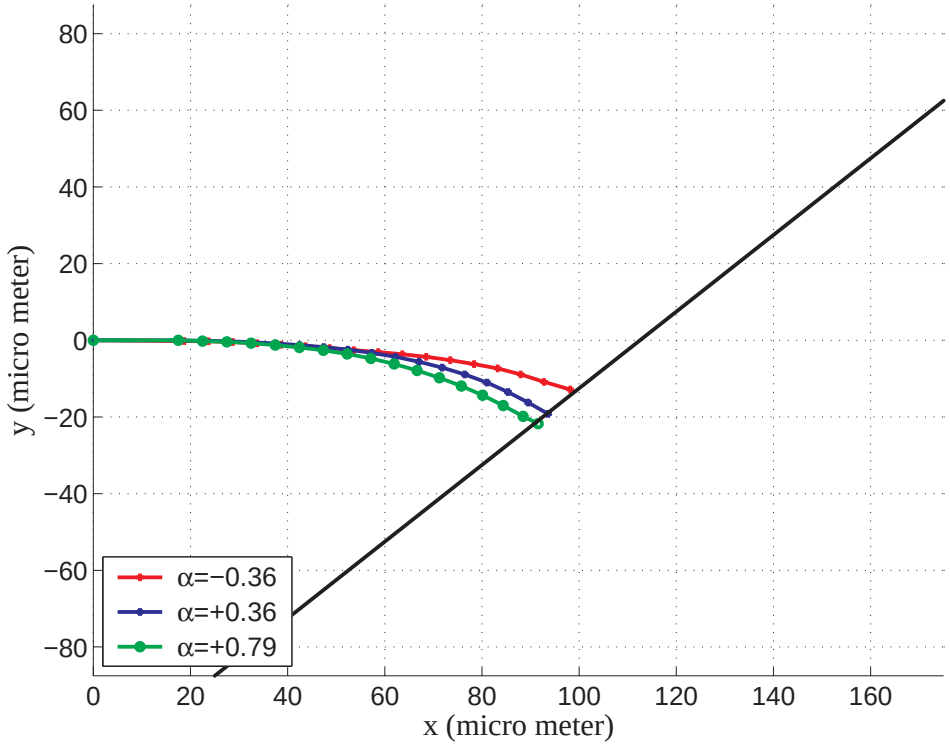

Figure 8.18. Crack propagation on a square plate with a corner cut; Elastic mismatch effect, cut length = 150/175

8.5. Effect of Orthotropic Material Properties

Orthotropic material properties of the substrate is modeled in this section for the substrate as some materials like silicon present orthotropic mechanical properties. 4 different shear modulus values are used to model silicon substrate keeping the previously used elastic modulus and Poisson ratio. This way the effect of orthotropic mechanical properties of substrate on thin film crack propagation can be observed. An orthotropic material can be defined with 3 material constants at least with compliance matrix S:

$$[S] = \begin{pmatrix} S_{11} & S_{12} & S_{12} & 0 & 0 & 0 \\ S_{12} & S_{11} & S_{12} & 0 & 0 & 0 \\ S_{12} & S_{12} & S_{11} & 0 & 0 & 0 \\ 0 & 0 & 0 & S_{44} & 0 & 0 \\ 0 & 0 & 0 & 0 & S_{44} & 0 \\ 0 & 0 & 0 & 0 & 0 & S_{44} \end{pmatrix}$$

where

$$S_{11} = \frac{1}{E}$$
$$S_{12} = -\frac{\nu}{E}$$
$$S_{44} = \frac{1}{G}$$

Crack propagation paths are presented in figure 8.19. For shear modulus values less than the isotropic materials crack tends to feel presence of the facing free surface earlier and reaches the free surface at a lower location than those of higher shear modulus values. However very low shear modulus values are not valid for silicon, in fact it is slightly higher than the isotropic case. As the difference between isotropic and orthotropic shear modulus values of silicon does not differ much, crack propagation path is not affected much compared to studied cases.

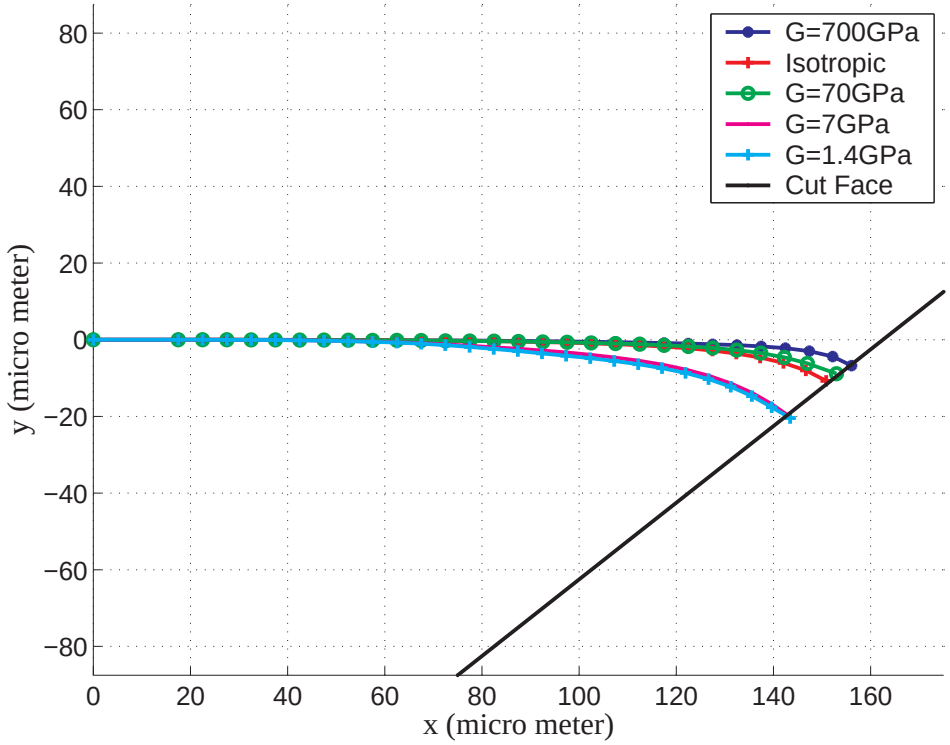

Figure 8.19. Crack propagation on a square plate with a corner cut; Orthotropic material effect, cut length = 100/175

9. 3-D ANALYSIS OF CRACK INTERACTIONS OF THIN FILM-SUBSTRATE SYSTEMS

The aim of this chapter is to present the fracture parameters of an edge crack in a thin film-substrate systems by considering the effect of another stationary adjacent crack. The adjacent crack distance to concern crack is varied and its effect is observed by plotting the stress intensity factors and the crack initiation angles. The crack propagation paths will be discussed in the following chapter.

A comprehensive study by Liang et. al. [4] covers the crack interactions of edge cracks in a thin film-substrate system. The crack interactions were studied in the sub-section of "Multiple cracks of different lengths moving in a blanket film". They have showed that parallel cracks of equal length repel each other and follow a divergent path. Also smaller cracks are trapped in the wake of propagating longer cracks. We will concentrate on one crack and analyze interactions with another parallel stationary crack.

9.1. 3D Stationary Crack Analysis In Thin Film-Substrate Systems

Up to this section, we have concentrated on the fracture analysis of single crack of certain length on a thin film with and without the effect of substrate. In this section we will stick to a predetermined crack length whereas we will be performing analysis by varying the adjacent crack distance p to concern crack and its length. We will consider the near to rigid and more compliant substrate - thin film configurations of Si thin film laying on the SiC substrate where the Dundurs parameter $\alpha = -0.52$. Loading condition is taken to be biaxial and mode-I as two different cases. Thin film and substrate interface is taken to be rigidly bonded to each other, i.e. interface effects are not studied in the analysis.

Crack length is kept constant at $a/W = 0.3$, a being the concern crack length and W being the film width. The film width and height is taken to be equal. The

adjacent crack length is going to be studied for a longer adjacent crack with respect to concern crack length. The substrate thickness is chosen to be 50 times of the thin film. Adjacent crack distance is varied for 8 equal increments of 2 sections, one is the coarse region far from the concern crack and one is the fine region, which covers the very near region around the concern crack. Transition from coarse region to fine region is taken as nine percent of half the film height, which is based on the SIF trend calculations and the meshing strategy.

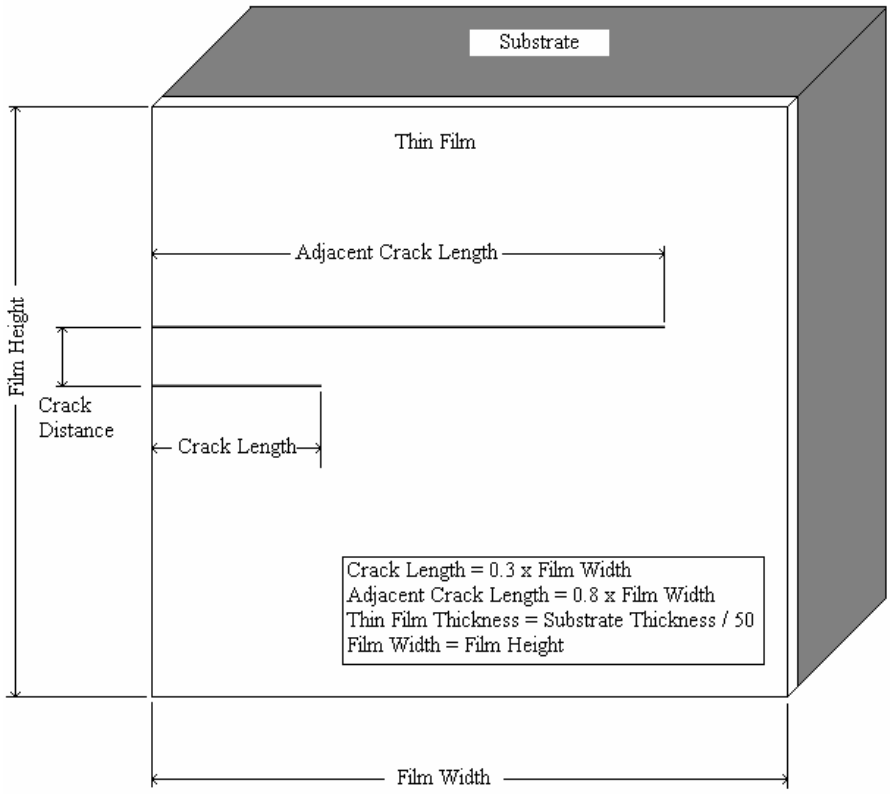

Figure 9.1. Crack interaction analysis geometry

Bi-Axial analysis results are examined for two important parameters, mode-I normalized stress intensity factor F_I and the crack initiation angle θ_c. Problem geometry is presented in figure 9.1.

9.1.1. Biaxial loading - Long Adjacent Crack

Results presented on the following figures are all non-dimensional. The film height is taken to be equal to film width. Pressure applied on the substrate vertical walls is 100 MPa. F_I trend for the biaxial loading case for the coarse region is shown on figure 9.2, where the values are very near to each other after adjacent crack distance $3.6t_f$. Therefore we can expect to see the crack interaction affects below this threshold region, which is also our transition value from coarse analysis region to fine analysis region. The effect zone can be calculated from figure 3.8 by reading the reference length value l for $\alpha = -0.52$. $l \approx 1.75t_f$ which is almost in the calculated region $1.8t_f - 3.6t_f$.

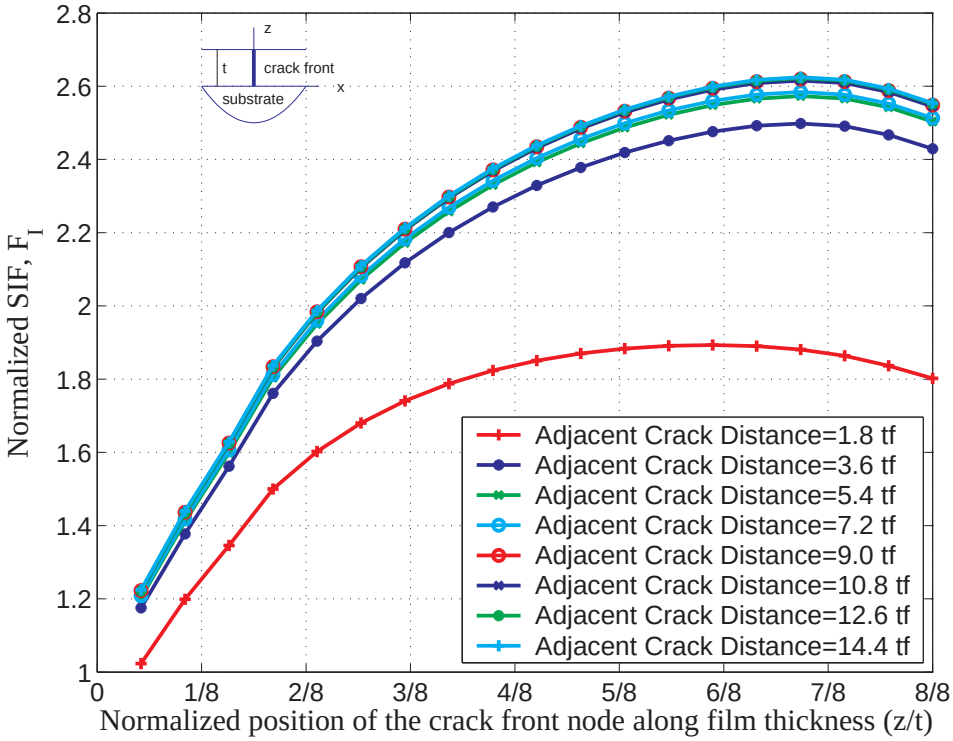

Figure 9.2. Effect of long adjacent cracks on F_I under biaxial loading (coarse region)

Fine region SIFs, as shown in figure 9.3, reveal the effect of the adjacent crack increases with the decreasing distance between concern crack and adjacent crack. F_I decreases monotonically and reach zero value at the free surface, meaning that the concern crack is trapped and will not propagate in the current configuration.

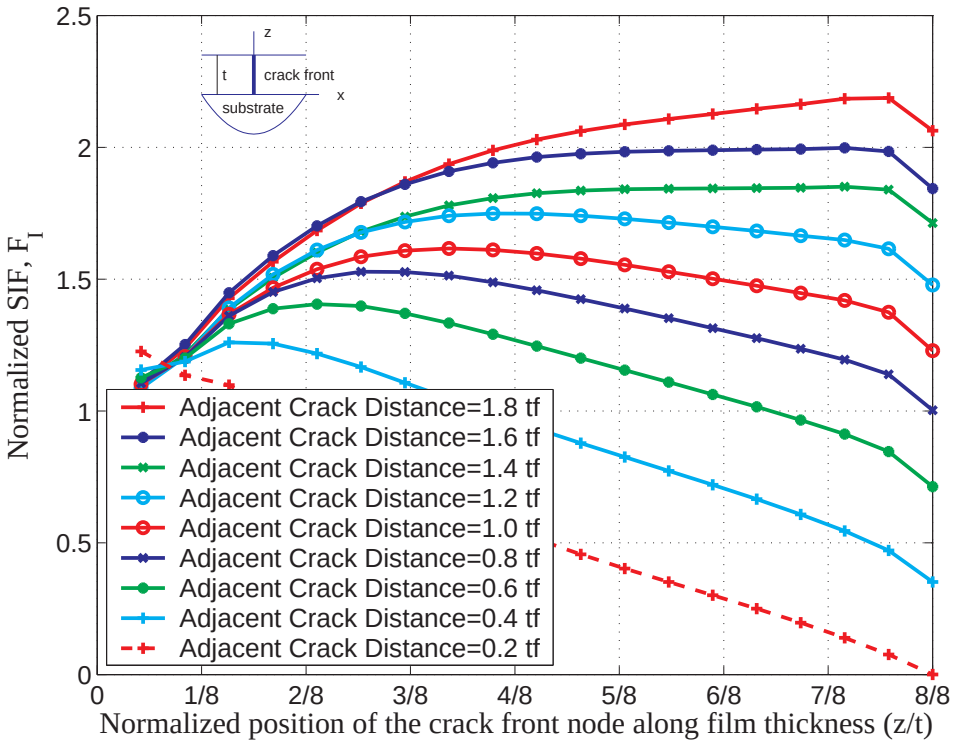

Figure 9.3. Effect of long adjacent cracks on F_I under biaxial loading (fine region)

Crack propagation angles are calculated using the formula;

$$\theta_c = 2tan^{-1}\left[\frac{K_I}{4K_I} - \frac{1}{4}\sqrt{\left(\frac{K_I}{K_{II}}\right)^2 + 8}\right] \tag{9.1}$$

which is derived using the maximum hoop stress criteria.

The coarse region crack propagation angles are very near to zero value. The effect of the adjacent crack becomes important on the crack propagation angles in the fine region. Propagation angle is not constant along the film thickness as well with the decreasing adjacent crack distance. However the increasing crack propagation angle should not be regarded as a sign of turn on the propagation path because of the decreasing value of the mode-I SIF.

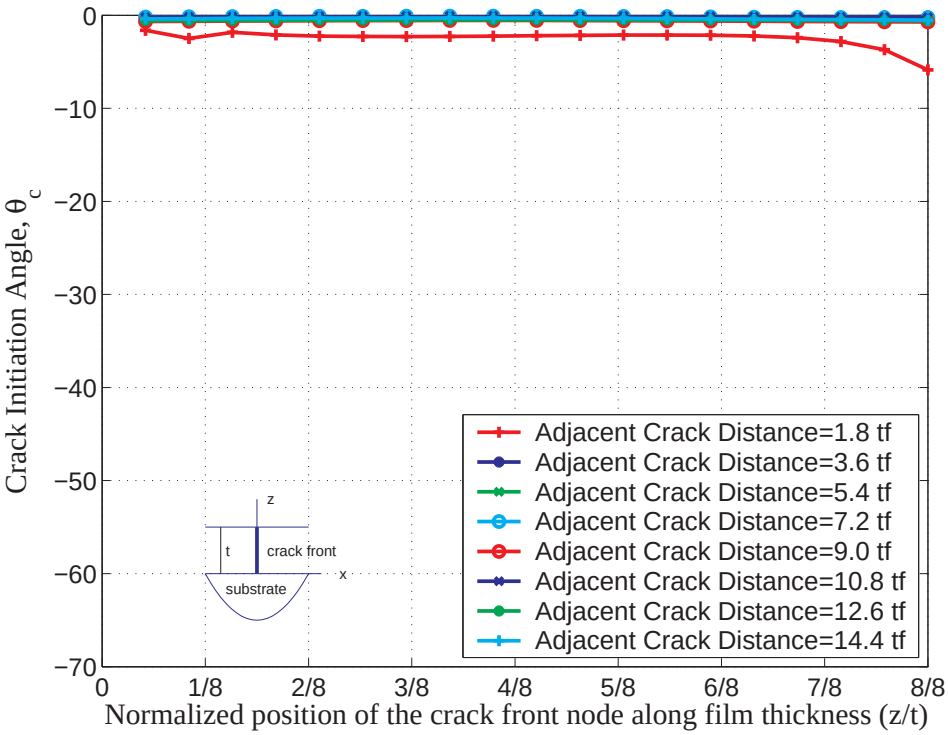

Figure 9.4. Effect of long adjacent crack on θ_c under biaxial loading (coarse region)

Mode-II SIF trend for the fine region is plotted on figure 9.6 where it is seen that the values does not differ from each other on successive adjacent crack distances. The values tends to increase a bit on the thin film surface which in turn results in high crack initiation angles as F_I decreases on the thin film surface with the decreasing adjacent crack distance.

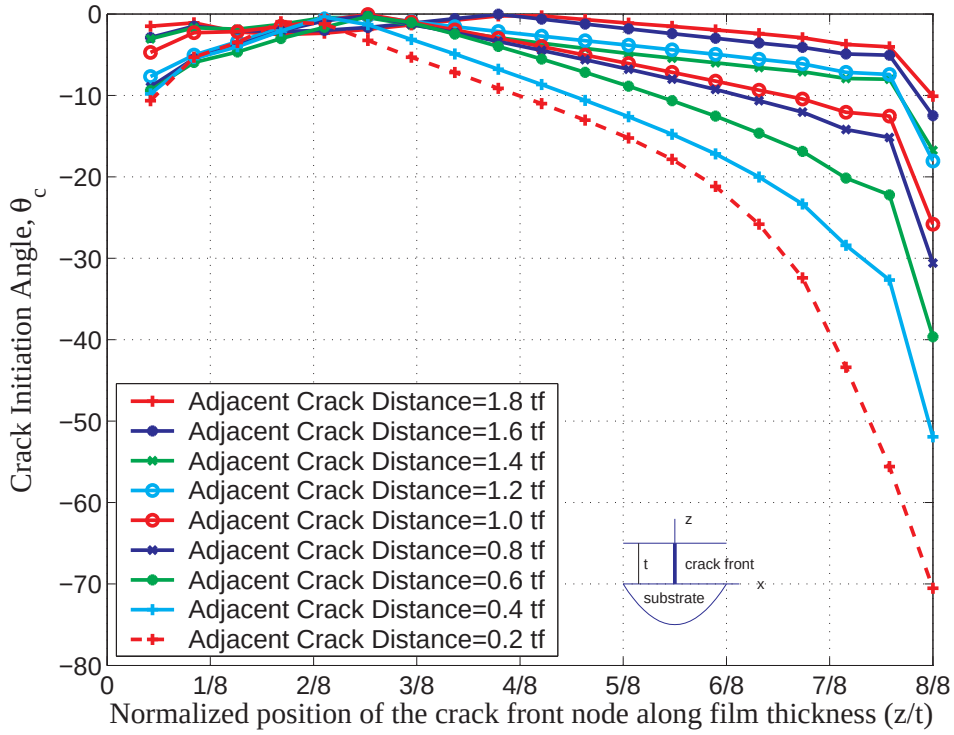

Figure 9.5. Effect of long adjacent crack on θ_c under biaxial loading (fine region)

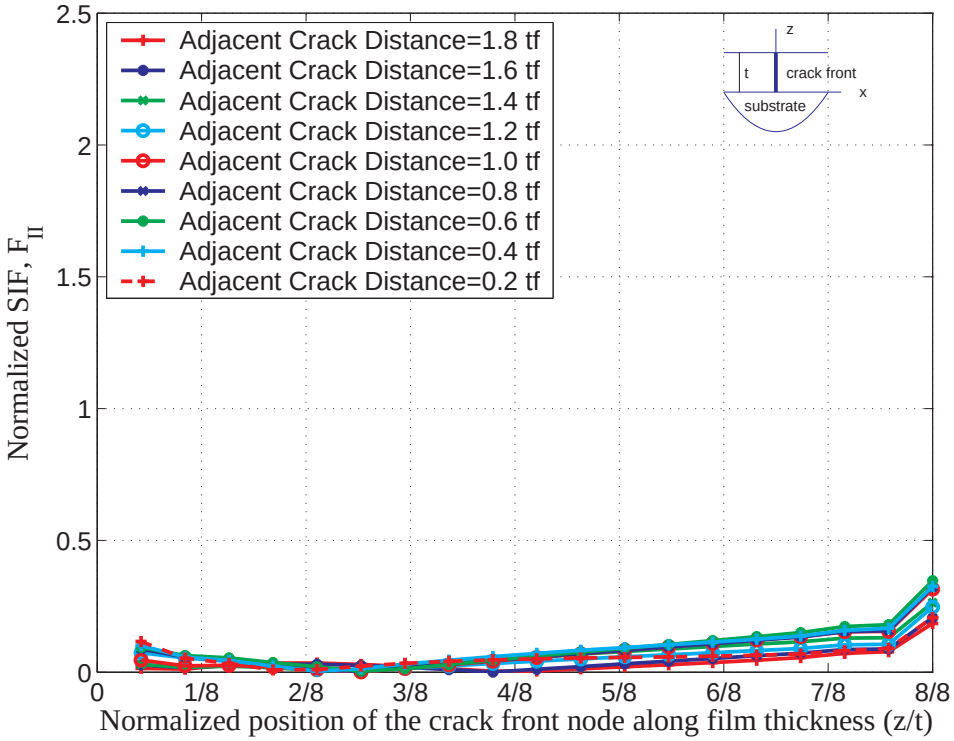

Figure 9.6. Effect of long adjacent cracks on F_{II} under biaxial loading (fine region)

9.1.2. Mode-I loading - Long Adjacent Crack

Analysis are repeated for pure mode-I loading to observe any effect of loading. The results are presented in figures 9.7 to 9.10. It is observed that there is no major difference between biaxial and pure mode-I loading. Effect zone is found out to be between $1.8t_f$ and $3.6t_f$ for pure mode-I loading as in the case of biaxial loading.

Stress distribution along the path which starts from bottom edge of thin film-substrate system, passes through crack tip and end at top edge is plotted in figure 9.11 for 4 cases. Crack tip is recognized in the middle where stress makes peak. In presence of adjacent crack which is $1.8t_f$ apart, stress field around the crack tip is effected. However for $7.2t_f$ and $14.4t_f$ far adjacent cracks stress field is not disturbed.

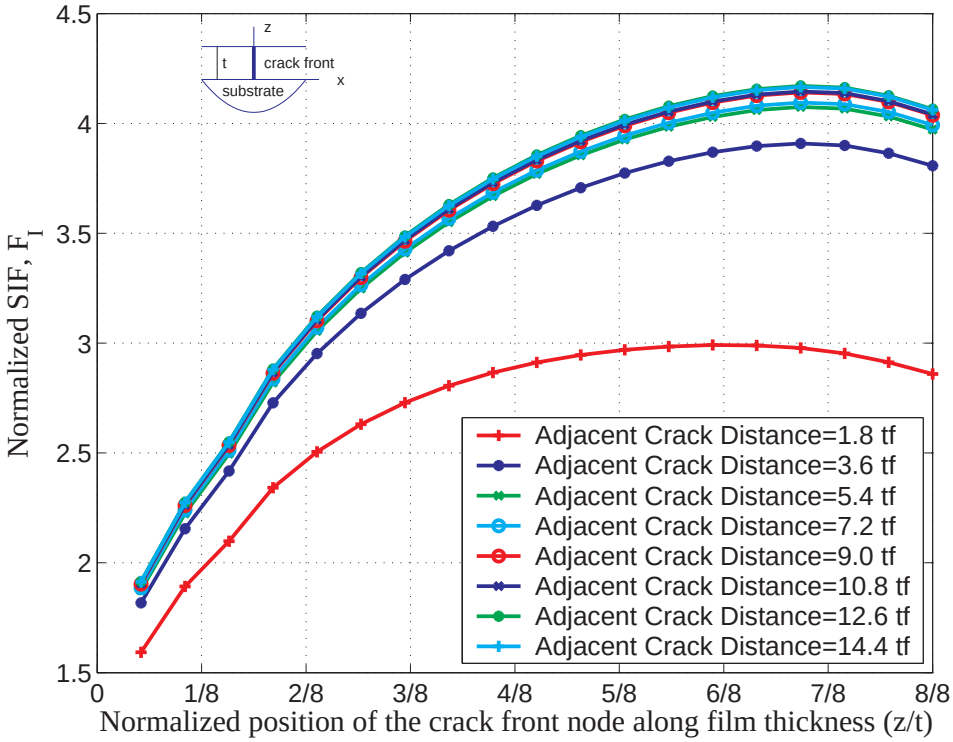

Figure 9.7. Effect of long adjacent cracks on F_I under mode-I loading (coarse Region)

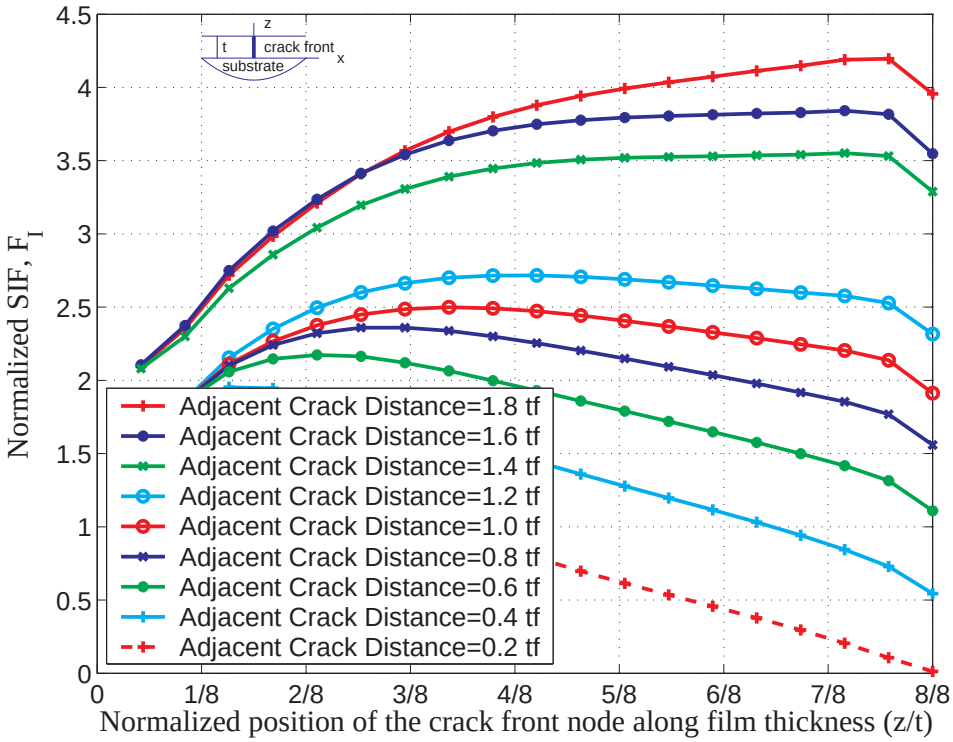

Figure 9.8. Effect of long adjacent cracks on F_I under mode-I loading (fine Region)

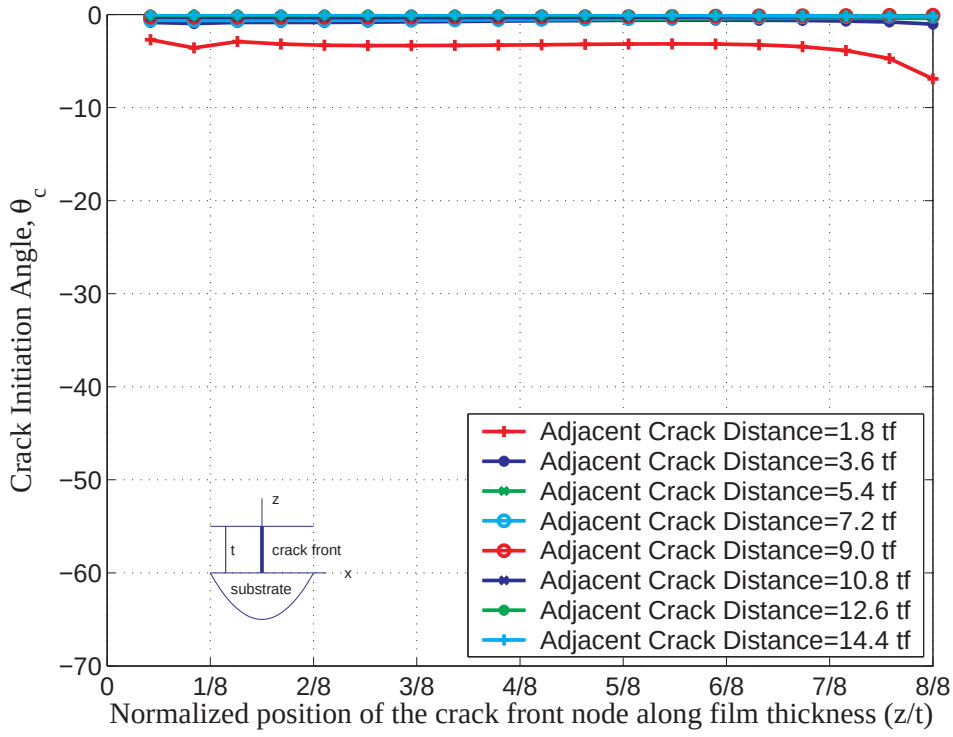

Figure 9.9. Effect of long adjacent cracks on θ_c under mode-I loading (coarse Region)

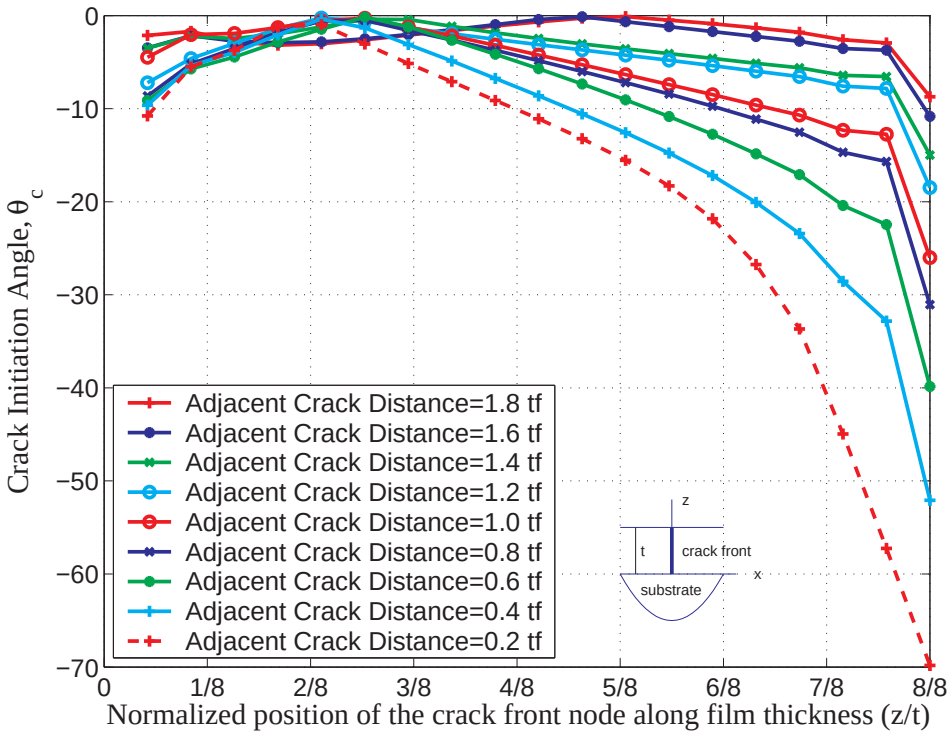

Figure 9.10. Effect of long adjacent cracks on θ_c under mode-I loading (fine Region)

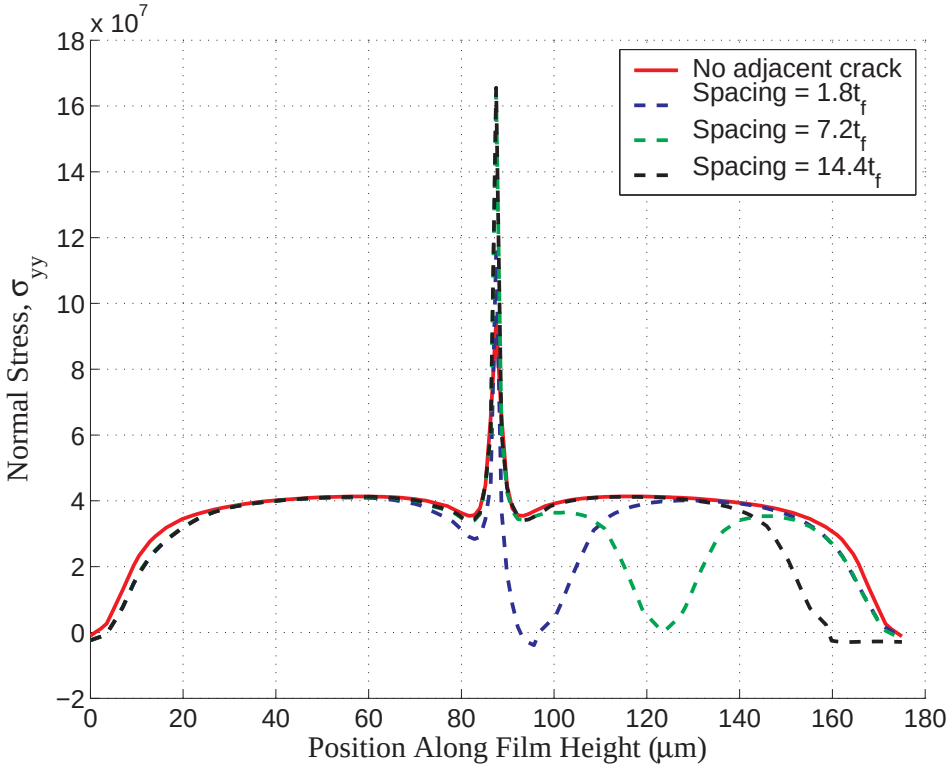

Figure 9.11. Normal stress(σ_{yy}) distribution along thin film (Coarse Region)

9.2. 3D Edge Crack Propagation In Thin Film-Substrate Systems

Crack interactions in three-dimensional thin film and substrate systems are studied in this section with propagation and including interface effects. Figure 9.12 shows the problem geometry where one propagating crack is studied with another stationary adjacent crack on the three layer thin film, interface and elastic substrate system.

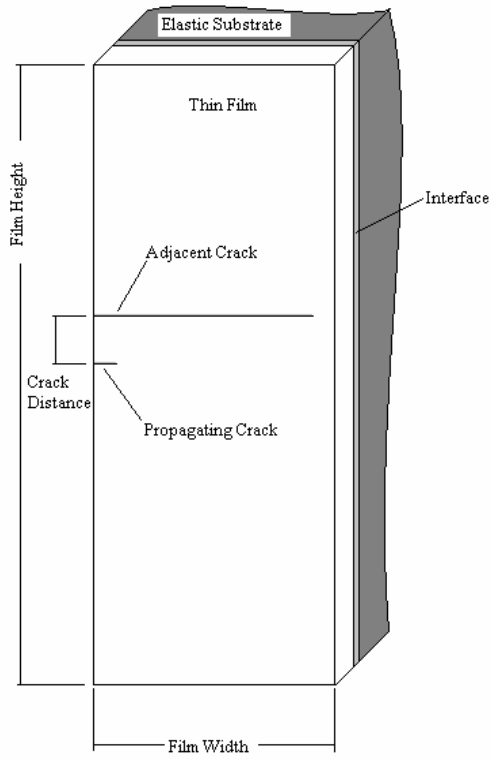

Figure 9.12. Parallel crack interactions geometry

The elastic substrate is under equal biaxial loading. The crack propagation is investigated for 3 different crack spacing of 2, 4 and 10 times the film thickness. The effect of interface is studied by performing the analysis with and without interface. A nonlinear (bilinear) material model is used for the investigation of interface effect on crack propagation path. The propagation path and the effect of the adjacent crack on the path is presented.

Finite element model includes both tetrahedral and hexahedral elements for the elastic substrate and the thin film. Figure 9.13 shows the finite element mesh constructed for the square thin film-substrate analysis.

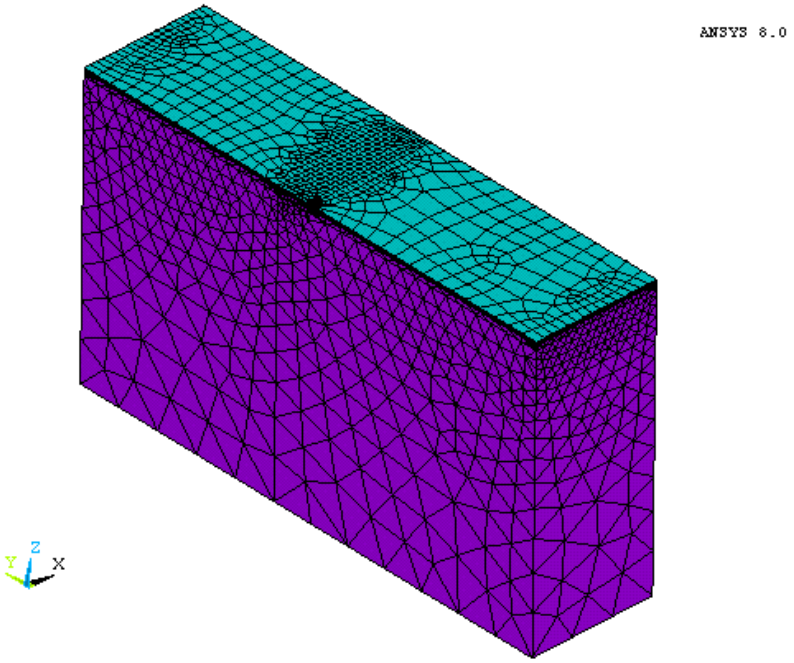

Figure 9.13. Finite element model for parallel crack interactions analysis

9.2.1. Effect of Interface

Interface effect on parallel crack interactions are studied by using a separate interface layer and cohesive zone material models as in case of square plate with a corner cut. As presented in previous chapter, interface is modeled by a thin layer, where material model is taken to be elastic perfectly plastic. And cohesive zone modeling is as in case of square plate with corner cut case.

Results are presented in figures 9.14 through 9.20 for interface and no interface cases. Figure 9.14 shows the case of no adjacent crack, where the crack propagates on a straight path till it reaches the far end as expected. For adjacent crack spacing equal to $2t_f$, it is seen that the propagating crack turns to adjacent crack. However it is seen that in presence of interface, crack turns earlier than no interface case, as well with decreasing interface strength. But again the effect of interface is minimal and can be ignored. Propagating crack does not turn to adjacent long crack when crack spacing is equal to $4t_f$ and $10t_f$ for both interface and no interface cases. This was also expected for no interface case, as the crack interaction analysis revealed that the effect zone was between $1.8t_f - 3.6t_f$.

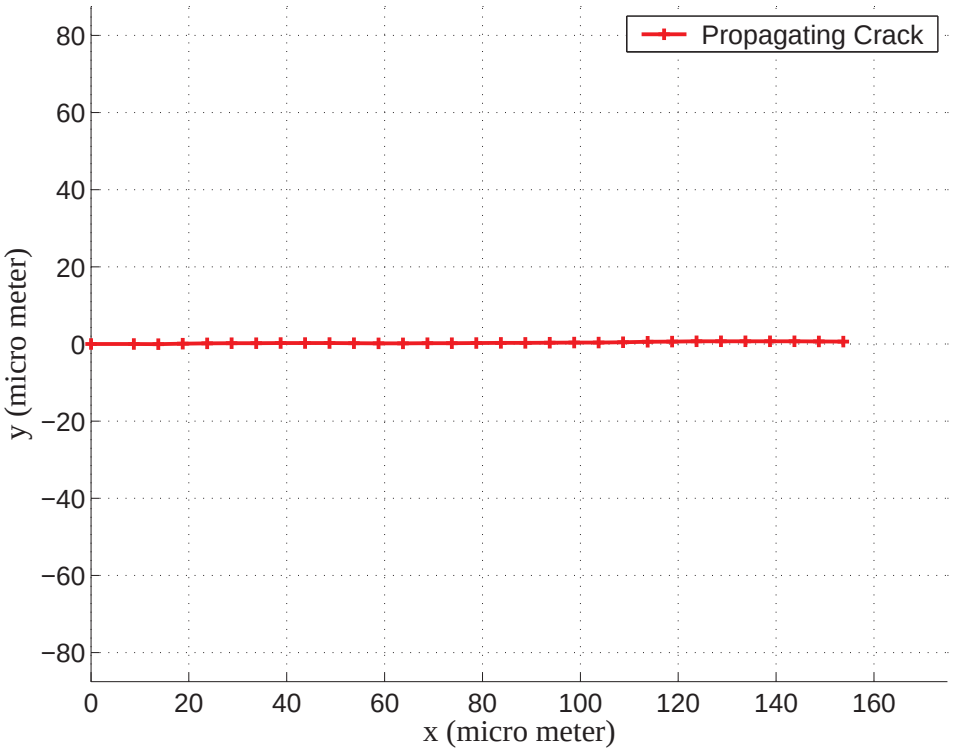

Figure 9.14. Crack propagation path; no adjacent crack

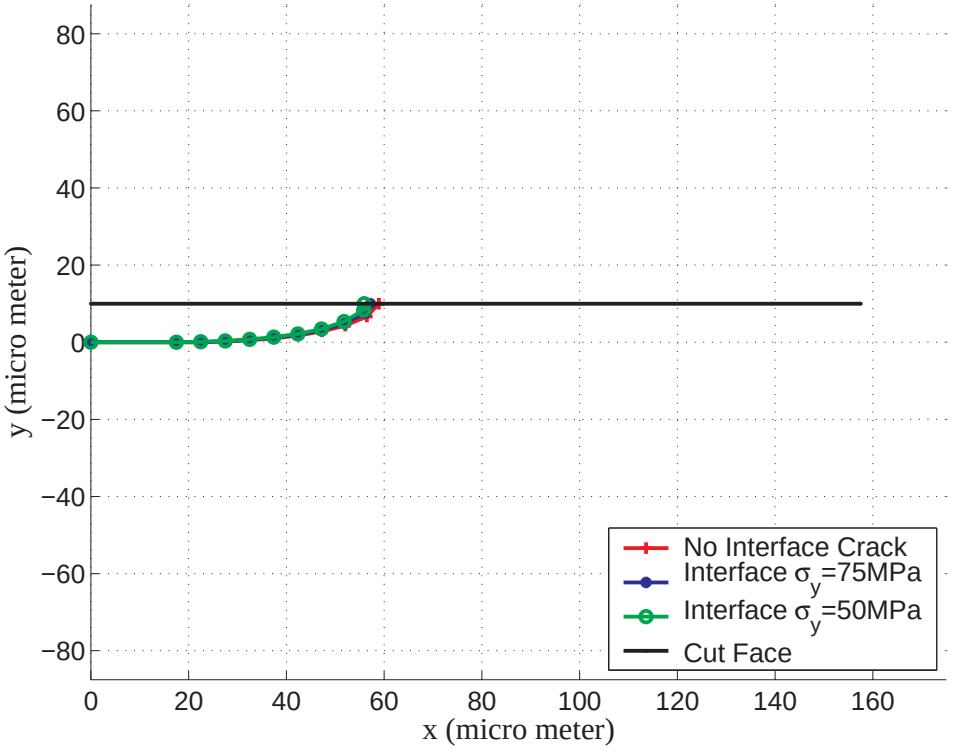

Figure 9.15. Crack propagation path; adjacent crack distance = 2 x film thickness (BISO modeling)

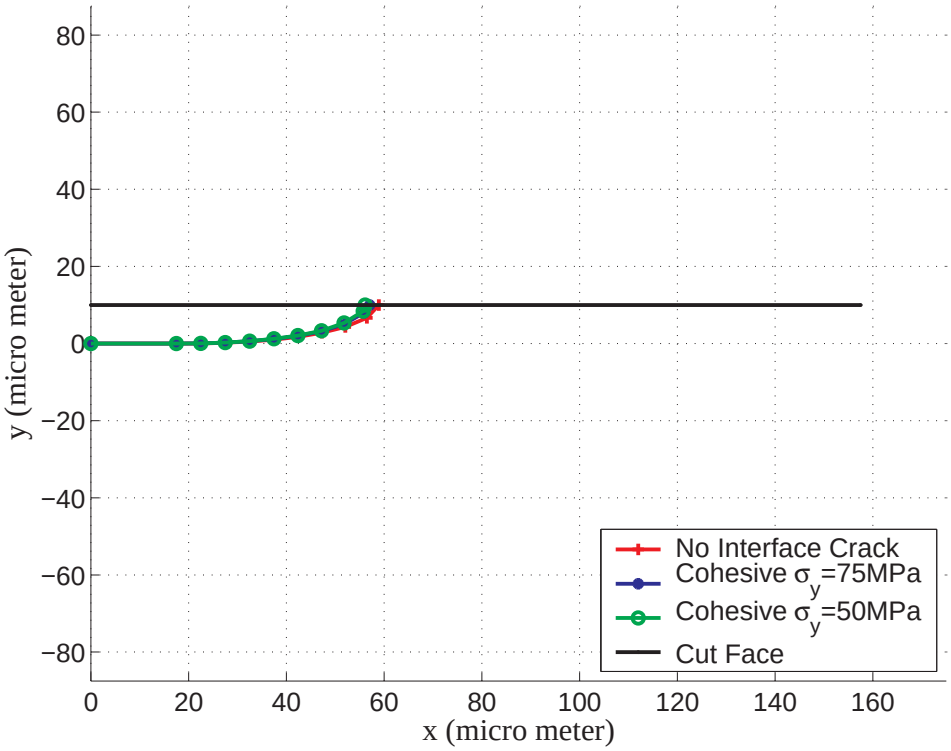

Figure 9.16. Crack propagation path; adjacent crack distance = 2 x film thickness (Cohesive zone modeling)

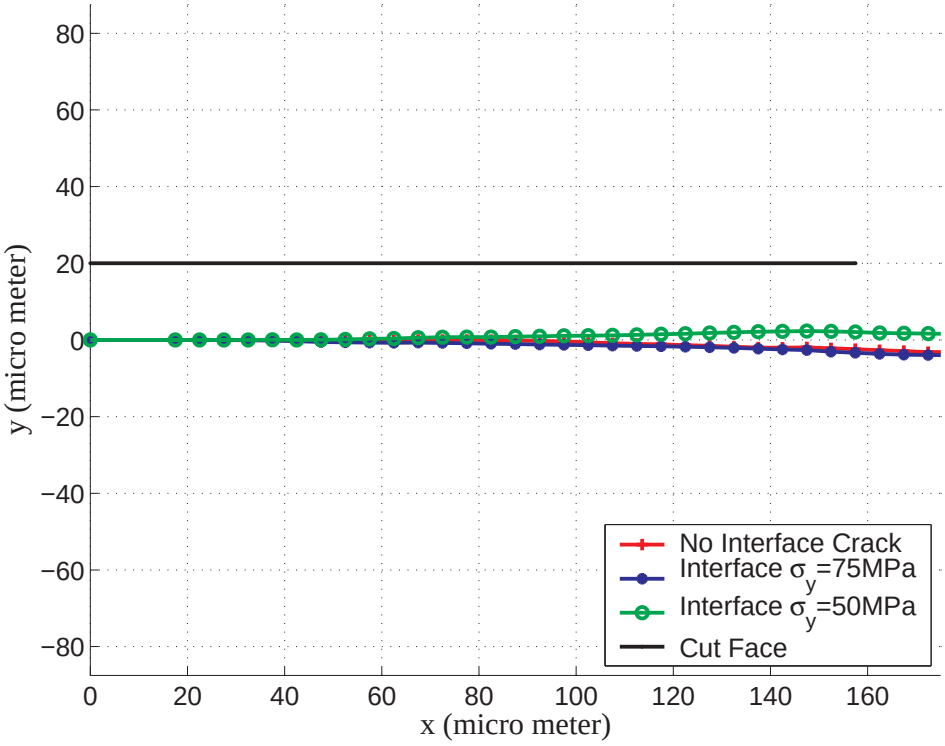

Figure 9.17. Crack propagation path; adjacent crack distance = 4 x film thickness (BISO modeling)

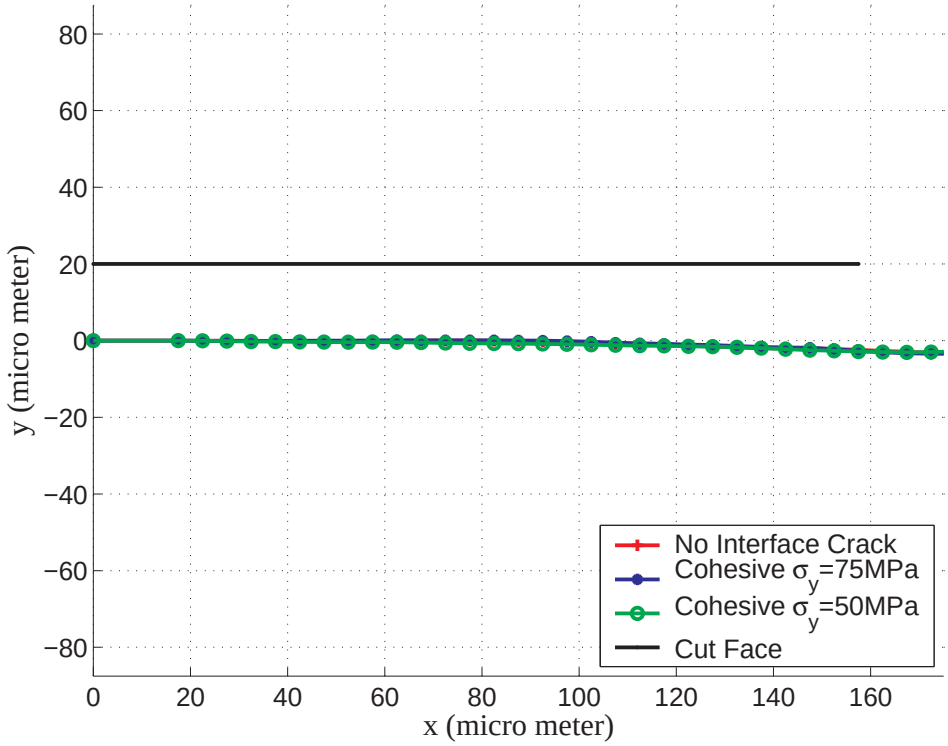

Figure 9.18. Crack propagation path; adjacent crack distance = 4 x film thickness (Cohesive zone modeling)

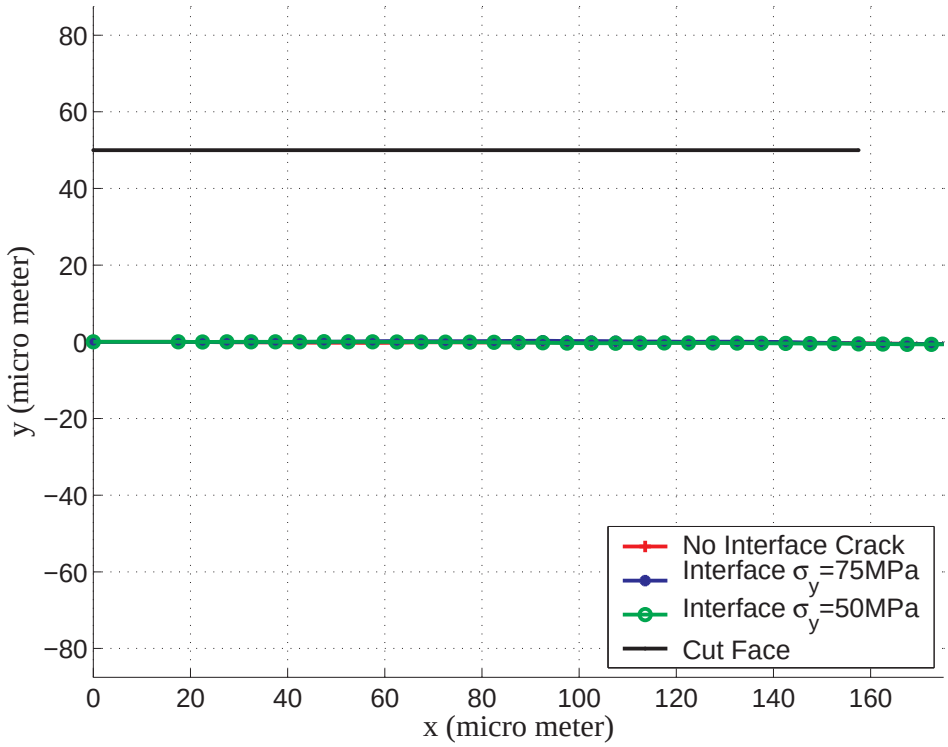

Figure 9.19. Crack propagation path; adjacent crack distance = 10 x film thickness (BISO modeling)

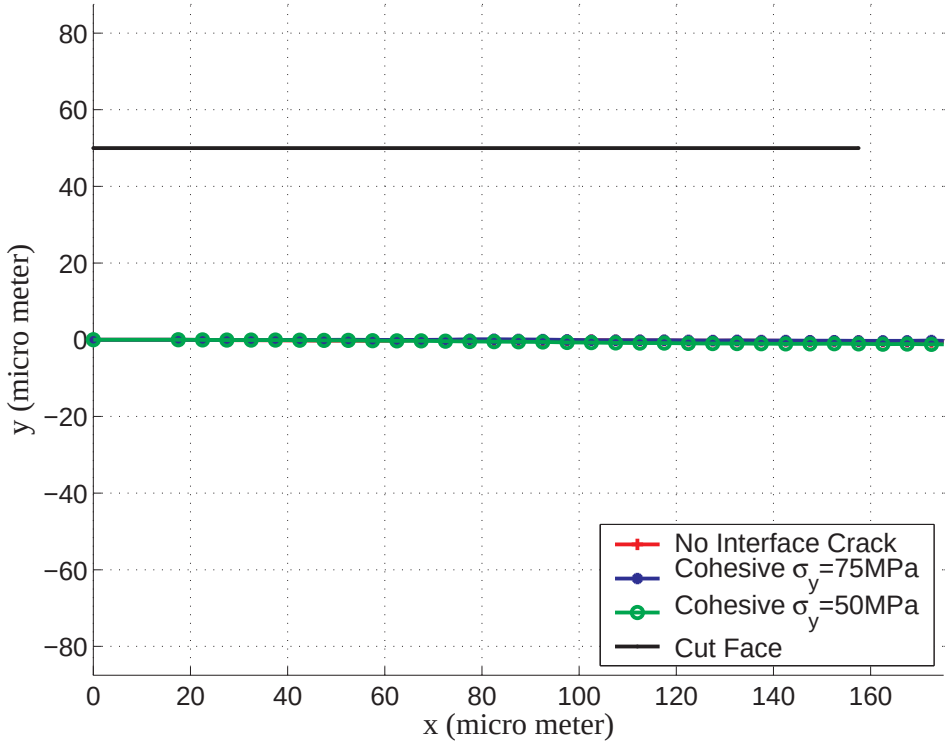

Figure 9.20. Crack propagation path; adjacent crack distance = 10 x film thickness (Cohesive zone modeling)

9.2.2. Effect of Elastic Mismatch

Effect of elastic mismatch on parallel cracks are studied for three different values: $\alpha = -0.36$, $\alpha = 0.36$ and $\alpha = 0.79$. Propagation paths are plotted in figures 9.21 to 9.23. It was observed that propagating crack turns to adjacent one quicker in case of more compliant substrate when the adjacent crack distance is $2 \times t_f$. When adjacent crack spacing is increased to $4 \times t_f$, propagating crack feels the presence of adjacent crack in case of $\alpha = 0.79$. At $10 \times t_f$ adjacent crack spacing, propagating crack does not turn to free surface of the adjacent crack.

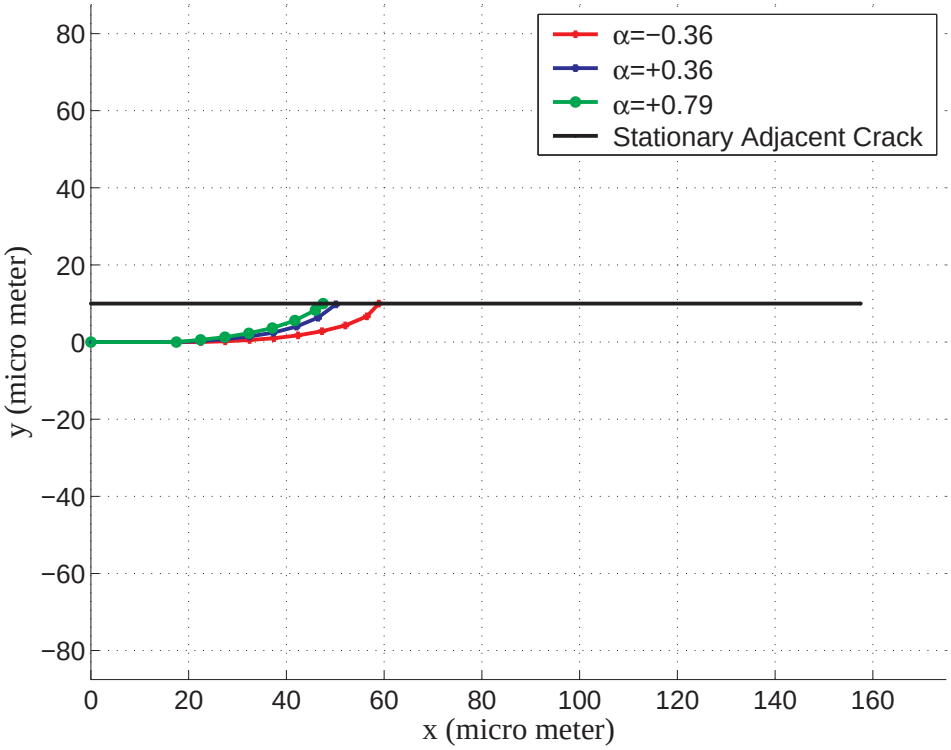

Figure 9.21. Interactions, no interface layer; adjacent crack distance = 2 x film thickness

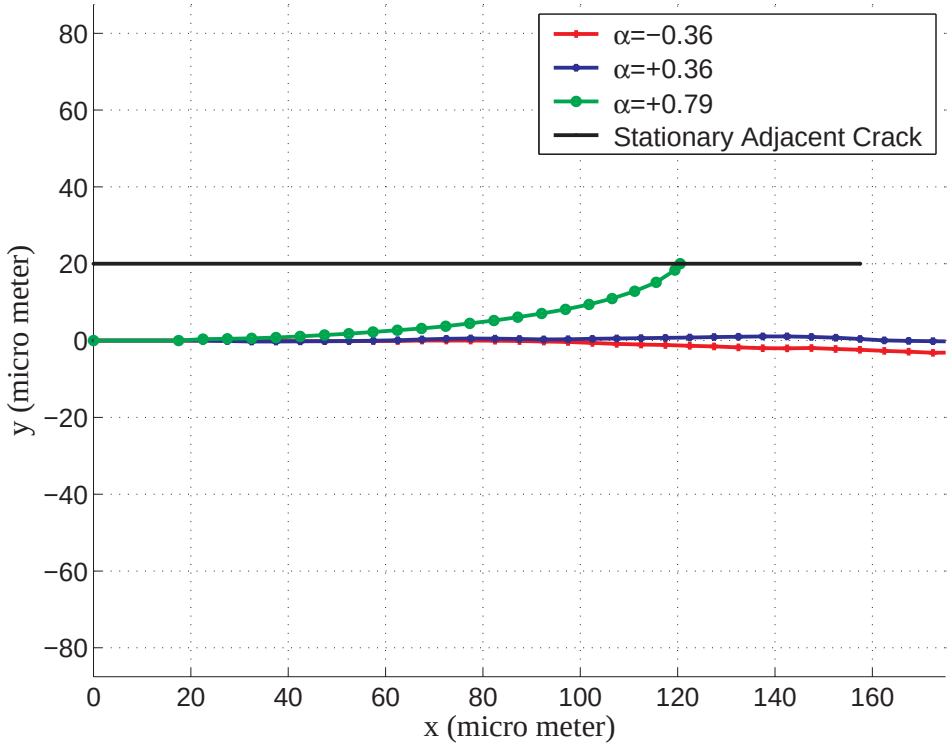

Figure 9.22. Interactions, no interface layer; adjacent crack distance = 4 x film thickness

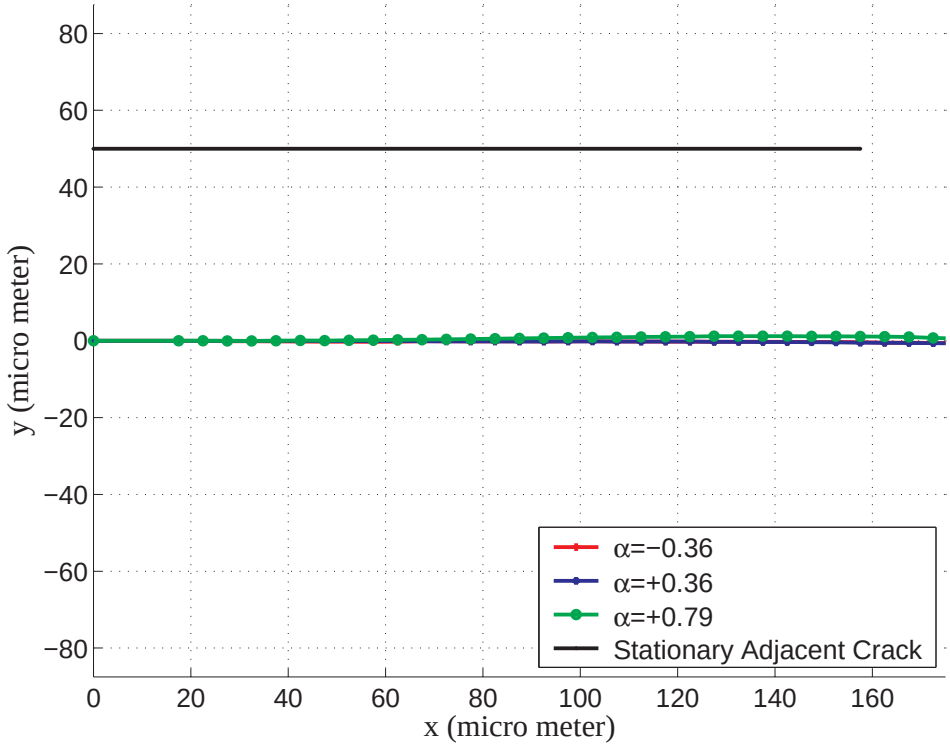

Figure 9.23. Interactions, no interface layer; adjacent crack distance = 10 x film thickness

Stress distribution along crack tip is shown in figure 9.24. It is seen that exponential decay region is larger for higher α values, which also explains the interaction between parallel cracks. Xia and Hutchinson [3] introduced the reference length l, characterizing the exponential decay of the changes transverse to the crack. l has been plotted for Dundurs parameters between -1 and 1 in figure 3.8. In absence of any elastic mismatch between film and the substrate ($\alpha = 0$)), $l = 1.98$. l exceed the film thickness t_f when the film is very stiff compared to the substrate ($\alpha \approx 1$) and will be of the order of t_f when the film is very compliant relative to the substrate ($\alpha \approx -1$). Reference values for $\alpha = -0.36, 0.36$ and 0.79 are read as 1.75, 2.75 and $5.75 \times t_f$ respectively from figure 3.8. The crack tip is at position y=87.5 microns in figure 9.24 and the decay of the stress field is more steep for relatively compliant substrates (increasing α value).

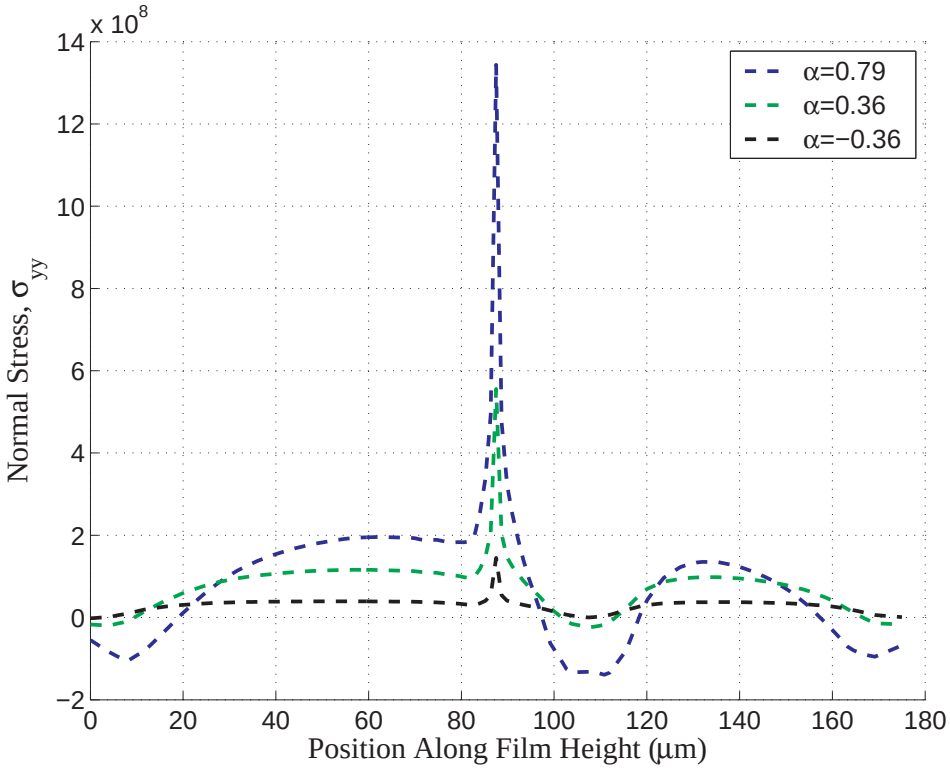

Figure 9.24. Normal stress distribution along thin film

10. CONCLUSIONS

The aim of this study was to determine the crack interactions and crack propagations using finite element method.

Study of 2D edge crack in a rectangular plate was performed as a first step to validate the finite element method. Calculated values of stress intensity factors and crack initiation angles are compared with available literature data of Fett [24, 25] and Sih [23]. Errors below 1% validated robustness of the method used.

Following the 2D edge crack analysis, 3D edge crack analysis in a thin film is carried out by using straight crack front. Stress intensity factors, crack initiation angles and energy release rates. Results are again compared to available data presented by Sih [23] and Murakami [26].

Thin film and substrate systems were examined for several different material groups and geometry. Stress intensity factors, crack initiation angles and energy release rates were calculated. Energy release rates are then used to determine the steady state profile of crack front, which was formerly performed by Nakamura and Kamath [10] by using mode-I stress intensity factor only. The crack front profile was found out to be parabolic curved shape. Effect of using straight or curved front on crack propagation analysis was examined with a case study of square thin film-substrate geometry with an edge cut. The similarity crack propagation paths obtained by using straight and curved crack front revealed that the crack front profile is not a major parameter in crack propagation studies of thin film-substrate systems.

Effect of elastic mismatch and interface was studied again performing analysis in square thin film-substrate system with an edge crack. For the case of varying elastic mismatch, Dundurs parameter α, was chosen to take three different values. It was observed that propagating crack tends to feel the presence of cut edge from further when the substrate is more compliant than the thin film. Effect of interface is studied by

employing two different material models namely elastic-perfectly plastic and cohesive zone material models. Interface strength is studied by assigning different values of yield strength and maximum traction stress for elastic-perfectly plastic and cohesive zone materials respectively. It was observed that crack propagation paths of a edge crack on a rectangular plate with an edge cut does not effected by interface strength much. Orthotropic materials properties, effect of shear modulus value of substrate is also studied by comparison of crack propagation paths. In case of lower values of substrate shear modulus (with same elastic modulus), crack tends to turn to free surface earlier and its effect can be observed.

Crack interactions between parallel cracks were investigated for different elastic mismatch values and effect of an interface strength. It was found out that parallel cracks interact with each other at certain crack spacing which depends mostly on elastic mismatch between the thin film. With more compliant substrates, propagating crack turned to adjacent crack in shorter distance. Similar behavior could not be observed in case of interface layer, where again elastic-perfectly plastic and cohesive zone materials models are employed. Therefore it is concluded that effect of interface strength on thin film crack propagation paths is not of major importance and can be ignored for most of the practices.

Numerical examples can be verified with experimental studies for future studies.

REFERENCES

1. Shenoy, V. B., A. F. Schwartz and L. Freund, "Crack patterns in brittle films", *Int. J. Fracture*, Vol. 103, pp. 1–17, 2000.

2. Schulze, G. and F. Erdogan, "Periodic cracking of elastic coatings", *Int. J. Solids Structures*, Vol. 35, No. 8-29, pp. 3615–3634, 1998.

3. Xia, Z. and J. Hutchinson, "Crack patterns in thin films", *J. Mech. Phys. Solids*, Vol. 48, pp. 1107–1131, 2000.

4. Liang, J., R. Huang, J. H. Prevost and Z. Suo, "Evolving crack patterns in thin films with the extended finite element method", *Int. J. Solids Structures*, Vol. 40, pp. 2343–2354, 2003.

5. Chakravarthy, S. S., E. H. Jordan and W. K. S. Chiu, "Thin film and substrate cracking under the influence of externally applied loads", *Engineering Fracture Mechanics*, Vol. 72, pp. 1286–1298, 2005.

6. Hutchinson, J. W. and Z. Suo, "Mixed mode cracking in layered materials", *Advances in Applied Mechanics*, Vol. 29, pp. 10–35, 2000.

7. Mishnaevsky, L. L. and D. Gross, "Micromechanisms and mechanics of damage and fracture in thin film/substrate systems", *Int. Applied Mech.*, Vol. 40, pp. 140–155, 2004.

8. Zak, A. R. and M. L. Williams, "Crack point singularities at a bimaterial interface", *Journal of Applied Mechanics*, Vol. 30, pp. 142–143, 1963.

9. Beuth, J. L., "Cracking of thin bonded films in residual tension", *Int. J. Solids Struct.*, Vol. 29, No. 13, pp. 1657–1675, 1992.

10. Nakamura, T. and S. M. Kamath, "Three-dimensional effects in thin film fracture

mechanics", *Mechanics of Materials*, Vol. 13, pp. 67–77, 1992.

11. Ambrico, J. M. and M. R. Begley, "The role of initial flaw size, elastic compliance and plasticity in channel cracking of thin films", *Thin Solid Films*, Vol. 419, pp. 144–153, 2002.

12. Huang, R., J. Prevost, Z. Huang and Z. Suo, "Channel-cracking of thin films with the extended finite element method", *Engineering Fracture Mechanics*, Vol. 70, pp. 2513–2526, 2003.

13. Copur, H., *Crack initiation in statically loaded functionally graded materials*, MS Thesis, Bogazici University, Istanbul, Turkey, Jun 2004.

14. Erdogan, F. and G. C. Sih, "On the crack extension in plates under plane loading and transverse shear", *J Basic Eng.*, Vol. 85, pp. 519–527, 1963.

15. Westergaard, H. M., "Bearing pressures and cracks", *Journal of Applied Mechanics*, Vol. 6, pp. 49–53, 1939.

16. Williams, M. L., "On the stress distribution at the base of a stationary crack", *Journal of Applied Mechanics*, Vol. 24, pp. 109–114, 1957.

17. Madenci, E. and I. Guven, *The finite element method and application in engineering using ANSYS*, Springer, The University of Arizona, 2006.

18. Henshell, R. D. and K. G. Shaw, "Crack tip finite elements are unnecessary", *International Journal for Numerical Methods in Engineering*, Vol. 9, pp. 495–507, 1975.

19. Barsoum, R. S., "On the use of isoparametric finite elements in linear fracture mechanics", *International Journal for Numerical Methods in Engineering*, Vol. 10, pp. 25–37, 1976.

20. Barsoum, R. S., "Triangular quarter-point elements as elastic and perfectly plastic

crack tip elements", *International Journal for Numerical Methods in Engineering*, Vol. 11, pp. 85–98, 1977.

21. ANSYS, *ANSYS Manual*, ANSYS Inc., 8.0 edn., 2003, see also URL http://www.ansys.com.

22. Paris, P. C. and G. C. Sih, "Stress analysis of cracks", *ASTM STP*, Vol. 381, pp. 30–80, 1965.

23. Sih, G. C., *Handbook of stress-intensity factors : stress-intensity factor solutions and formulas for reference*, ASTM, 1973-4.

24. Fett, T., "Mixed-mode stress intensity factors for the obliqued edge crack in rectangular specimens", *International Journal of Fracture*, Vol. 61, pp. 3–10, 1993.

25. Fett, T., "Stress intensity factors for edge-cracked plates under arbitrary loading", *Fatigue fracture engineering material structure*, Vol. 22, pp. 301–305, 1998.

26. Murakami, Y., *Stress intensity factors handbook*, Pergamon Press, 1976.

27. Liu, Q., P. Hamel, W. Hu, P. K. Sharp, A. Lahousse and G. Clark, "Modeling of stable tearing in aircraft structures", *Platforms Sciences Laboratory*, pp. 1–94, 2005.

28. Tetelman, A. S. and A. J. McEvily, *Fracture of structural materials*, John Wiley and Sons, Inc., 1967.

29. ANSYS, *ANSYS Manual*, ANSYS Inc., 10.0 edn., 2005, see also URL http://www.ansys.com.

30. Xu, X. P. and A. Needleman, "Numerical simulations of fast crack growth in brittle solids", *Journal of the Mechanics and Physics of Solids*, Vol. 42, pp. 1397–1434, 1994.